CONFIDENTIAL

# Small Scale Fluid Power Transmission for the Delft Offshore Turbine

## Design, Modeling, Construction and Testing of a Small Scale Fluid Power Transmission

A.S. Kempenaar

Master of Science Thesis

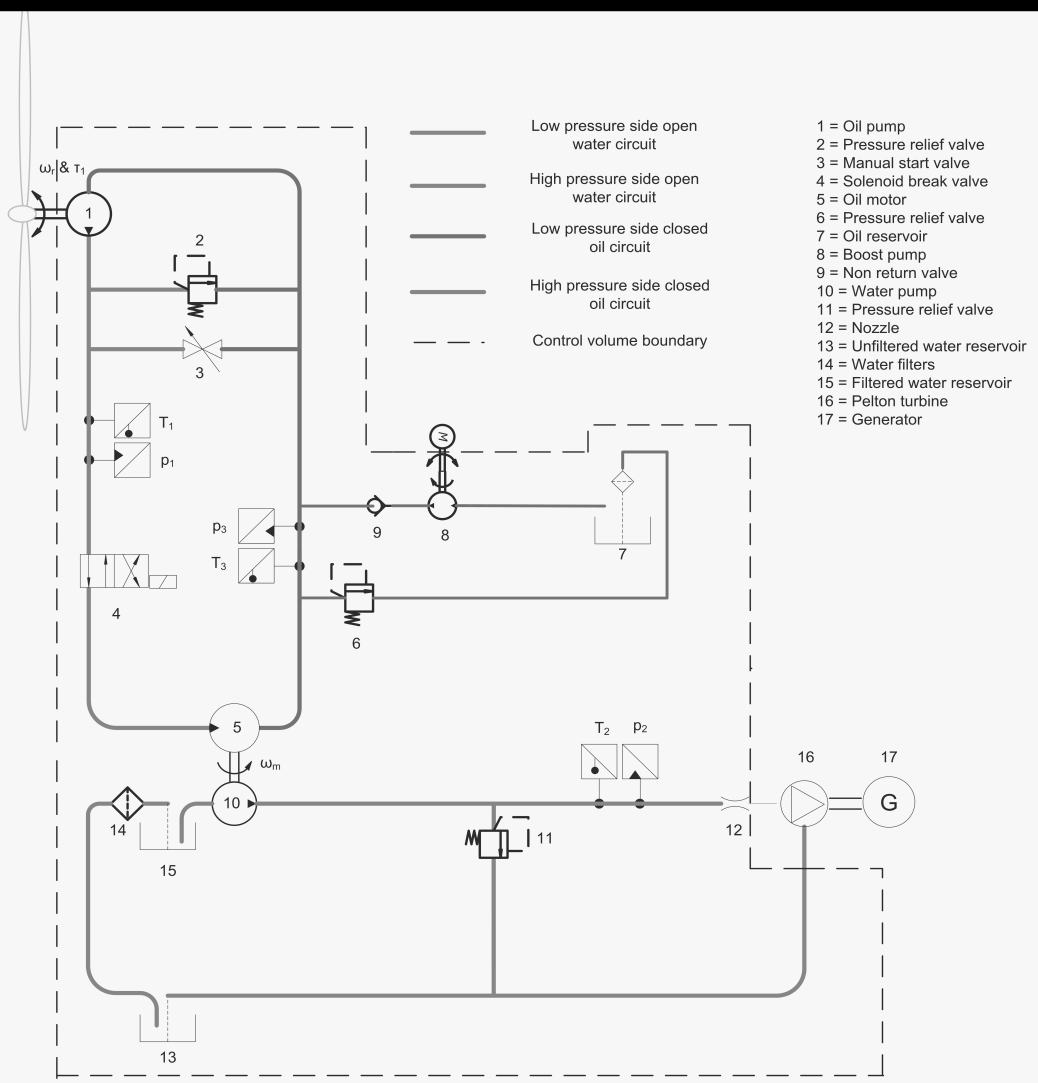


TU Delft Delft University of Technology

CONFIDENTIAL

# Small Scale Fluid Power Transmission for the Delft Offshore Turbine

## Design, Modeling, Construction and Testing of a Small Scale Fluid Power Transmission

Master of Science Thesis

For the degree of Master of Science in Sustainable Energy Technology
at Delft University of Technology

A.S. Kempenaar

March 14, 2012

Faculty of Applied Physics · Delft University of Technology

TU Delft Delft University of Technology
All rights reserved.

Copyright © Offshore Engineering (OE)

Delft University of Technology
Department of
Offshore Engineering (oe)

The undersigned hereby certify that they have read and recommend to the Faculty of Applied Physics for acceptance a thesis entitled

# Small Scale Fluid Power Transmission for the Delft Offshore Turbine

by

A.S. Kempenaar

in partial fulfillment of the requirements for the degree of

Master of Science Sustainable Energy Technology

Dated: March 14, 2012

Supervisor(s):

prof.dr. G.J.W. van Bussel

ir. N.F.B. Diepeveen

ir. P.S. Albers

Reader(s):

ir. A. Jarquin Laguna

dr.ir. J.W. van Wingerden

# Summary

The Delft Offshore Turbine (DOT) project is a research project within the Delft University Wind Energy Research Institute (DUWIND). The main objective of the DOT research project is to make offshore wind energy a competitive energy source.

One of the research lines in the DOT project is considering the centralization of electricity generation within a wind farm. The complete process of wind energy extraction up to the connection with the electrical grid must be taken into account in order to develop an optimal technology to generate electricity from offshore wind energy. The DOT project thus approaches the design of a wind farm by regarding the entire farm as one system instead of a collection of systems. For this purpose a renewed wind farm concept was developed within the DOT project. A unique aspect of the DOT concept are the fluid power transmission systems used to transfer the energy of single turbines to a central platform for electricity generation.

The main objective of this thesis is to prove the functionality of the DOT transmission concept. To prove the functionality of this concept a small scale demonstration set-up of the DOT transmission was designed, constructed and tested.

Prior to the start of the design process the design objectives and requirements were identified. The transmission is designed for a specific 10kW rotor. The rotor speed needs to be controlled close to its optimal tip speed ratio in order to maximize the energy extraction from the wind. This is achieved by using a passive control strategy together with accurately sized components in the transmission. A dynamic model of the transmission was developed to increase the physical understanding of the transmission and to assist in the design process.

The demonstration set-up was constructed in the water laboratory at the faculty of Civil Engineering and Geosciences of the TU Delft. In the demonstration set-up the rotor is simulated by an electric motor with a controllable speed. The dynamic model was validated successfully with experiments in steady state and dynamic conditions. The functionality of the transmission was analyzed by simulations with the validated transmission model and a simplified rotor model. The following conclusions are drawn from the experiment and simulation results:

- For constant wind speed conditions above 4.7m/s the passive control method controls the rotor speed at an almost constant tip speed ratio. With the available 5.96mm nozzle diameter the rotor operates at 90% of the maximum power coefficient $C_{P,max}$.

To operate the rotor at its optimal tip speed ratio (100% of $C_{P,max}$) the nozzle diameter is the only parameter that needs to be adjusted.

- Simulations with turbulent wind speeds show that the tip speed ratio variation is much larger in these conditions than in steady state conditions. In these conditions the rotor operates between 75% and 90% of the maximum power coefficient. The relatively slow response to fluctuations in the transmission cause the larger variations in tip speed ratio in turbulent wind speed conditions.
- The total efficiency of the transmission is between 43% and 48% at wind speeds above 4.7m/s.
- The estimated required wind speed to start the transmission is between 4 and 6m/s.
- The complete system of rotor and transmission is strongly damped. Therefore no problems are expected when the system is excited at one of its natural frequencies.

The experiment and simulation results prove the functionality of the developed transmission. In the near future experiments with the transmission and a 10 kW rotor are planned at a test facility of the Energy research centre of The Netherlands (ECN). Based on the results of this thesis project no problems are expected during these experiments with rotor.

The simplicity of the passive control strategy is a great advantage of this control method. An in-depth research of the suitability of this method for large single turbines or wind farms is recommended. Based on the analysis in this thesis, the main concern for large scale application is the slow response of the transmission to fluctuations in the wind speed. The response time will increase due to the reduced stiffness caused by longer pipelines with larger diameters.

# Table of Contents

# Acknowledgments

I would like to thank all my supervisors for their great supervision and good advice in all the practical challenges encountered during my thesis project. I would especially like to thank my daily supervisor Niels Diepeveen for his great dedication and support to help complete this thesis project and report successfully.

The internal departments within the TU Delft that contributed to the project are:

- The Water Laboratory personal; All the support and expertise of the Water Laboratory personal was of grate value during the project. I would especially like to thank S. de Vree for his great support and patience in the different challenges we experienced throughout the project.
- Electronic and Mechanical Support Division (DEMO); Several components used in the demonstration set-up were developed by DEMO.

The external parties who contributed into making this a successful project are:

- Bosch Rexroth Group; Supplied many of the used components in the demonstration set-up. I would like to thank P. Weitering and M. van der Hurk in particular for their advice in the design phase.
- Water hydraulics Co. Ltd; Supplied one of their water pumps at cost price to the project.
- Energy research Center of the Netherlands (ECN); Supplied the data of the 10 kW Aircon turbine.

Delft, University of Technology A.S. Kempenaar
March 14, 2012

# Chapter 1

# Introduction

## 1-1 Background

Offshore wind energy is a very young industry with an enormous potential. The first ever large scale offshore wind farm was built in 2001 of the coast of Denmark; the Horns Rev wind farm with a power capacity of 160MW. With the current offshore wind farm technology 65% of the total estimated European electricity demand in 2020 could be supplied by offshore wind energy from European coastal areas [1]. However, offshore wind energy is currently still one of the most expensive energy sources. To achieve this potential the offshore wind energy price must become competitive.

The current used turbines in offshore wind farms are adapted onshore turbines. The onshore turbines were optimized in the past decades specifically for onshore application. Much of the technology used in these turbines is still based on onshore application. These turbines each have a generator that converts the wind energy into electricity. The electricity is then transferred to the shore via a transformer platform. The two major differences between onshore and offshore wind farms are:

- The size of the offshore wind farms is much larger in the order of several 100 MW and still increasing
- The environment in which the wind farm is installed, maintained and operated

Onshore turbines adjusted for offshore application are not necessarily the optimal technology to generate electricity from offshore wind energy. With this statement in mind, the Delft Offshore Turbine (DOT) project was launched in 2008 by Delft University Wind Energy Research Institute (DUWIND). The main objective of the DOT research project is to make offshore wind energy a competitive energy source.

One of the research lines in the DOT project is considering the centralization of electricity generation within a wind farm. The complete process of wind energy extraction up to the

connection with the electrical grid must be taken into account in order to develop an optimal technology to generate electricity from offshore wind energy. The DOT project thus approaches the design of a wind farm by regarding the entire farm as one system instead of a collection of systems.

The initial design concept consists of wind turbines that transfer their energy using fluid power transmissions to a central platform where the electricity is generated, see figure 1-1. Compared to the conventional wind farms this concept will result an enormous reduction in the number of required generators and other power electronic components. Other main drives while developing this concept were:

- Minimizing number of components
- Simplifying the system as much as possible

In this concept fluid power transmissions are used to transfer the energy from the wind turbine rotors to the central generator platform. Fluid power transmissions are used in several industries and are found to be a proven and reliable method to transmit power [2]. The application of these transmission is however relatively new in the wind turbine industry. The high power density and reliability are the main reasons to choose for a fluid power transmission system. Another advantage is the good controllability of fluid power transmissions [2].

Hydraulic turbines are used in this concept to generate electricity from the supplied fluid power. It is a proven technology that is mainly applied in hydro power plants. Hydraulic turbines also have the highest operating efficiencies of all the power generation systems [3].

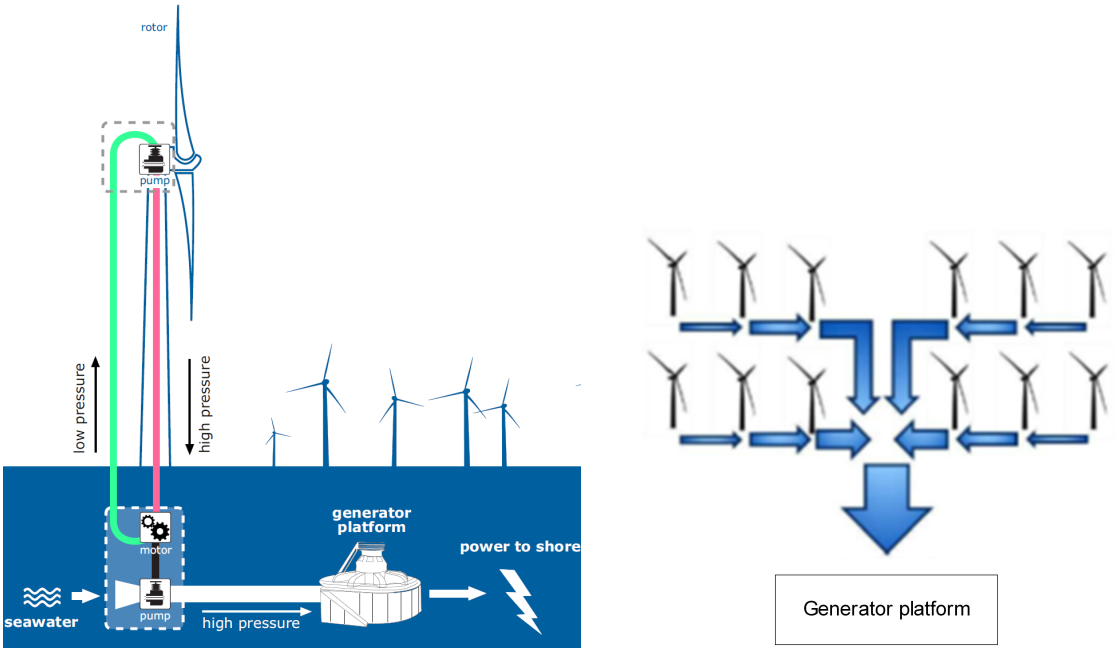


(a) Single turbine [4]

(b) Multiple turbines [3]

**Figure 1-1:** Delft Offshore Turbine (DOT) concept for a single turbine and multiple turbines

The complete DOT wind farm concept consists of four systems, see figure 1-1. A brief description of these systems is given next:

1. The wind turbine rotor extracts wind energy and converts it into mechanical energy. The used rotor in the concept is a 2 bladed rotor. Compared to the current used 3 bladed rotor it requires less components. The 2 bladed rotor will also reduce the installation time and costs.
2. The closed-loop oil circuit transfers the energy from the rotor to the base of the turbine. This is done in 2 steps. The first steps is the conversion of mechanical energy into hydraulic energy by a pump that is directly driven by the rotor. The hydraulic energy is then transferred to the base of the turbine tower by pipelines or hoses in a closed oil circuit. At the base of the turbine the hydraulic energy is converted back into mechanical energy by a hydraulic motor.
3. The open-loop water circuit transfers the energy from the base of the turbine to a central platform in the wind farm. The mechanical energy at the tower base is first converted into hydraulic energy by a sea water pump. The hydraulic energy is then transferred by a single seawater pipeline to the generator platform.
4. The generator platform converts the hydraulic energy of multiple turbines into electrical energy. The hydraulic energy is first converted into mechanical energy by a hydraulic turbine. The electrical generator then converts the mechanical energy into electricity. The electricity is finally transferred to the onshore grid from the platform.

The performance of the DOT wind farm concept has been researched for a single turbine in steady state conditions. It was estimated that the total electrical energy production of this turbine is 2% less than for a turbine with a conventional transmission. Thus, the success of the DOT concept will depend on the potential reduction of the wind farm costs [3].

## 1-2 Thesis Objective

The next step into realizing the above proposed concept, is to prove the functionality of this wind farm concept. The main objective of this thesis project is to prove the functionality of the fluid power transmission used in the DOT concept. From this main objective the following main research question was defined:

> How to design a fluid power transmission for a 10kW rotor using the DOT transmission concept?

Fluid power transmission refers to the closed-loop oil circuit and the open-loop water circuit systems as explained above. This covers the required systems for the energy transfer from the turbine to the generator platform. Some attention is also paid to the rotor and the generator platform. The main research question was subdivided into the following sub research questions:

- What is the main function of the transmission?

- What are the objectives and requirements for the transmission?
- What tools need to be used or developed to assist in the design process?
- How to prove the functionality of the transmission?

To finally prove the functionality of this transmission concept a laboratory demonstration set-up was designed and constructed. The demonstration set-up was built in the water laboratory at the faculty of Civil Engineering and Geosciences of the TU Delft. The main functions of this demonstration set-up were to:

- Demonstrate the functionality of the DOT concept
- Apply theory into practice, and learn from this process
- Use the experiment results for validation of the dynamic model

## 1-3 Approach

The thesis project was divided into five main phases:

1. Design a transmission suitable for a 10kW rotor using the DOT concept; CH 2
2. Develop a dynamic model of the transmission; CH 3 & CH 4
3. Construction of the transmission demonstration set-up in the laboratory; CH 5
4. Run experiments with the demonstration set-up and validate the model with these experiments; CH 6
5. Prove the functionality of the transmission for a 10 kW rotor; CH 7

The design process of the transmission was an iterative process where there was interaction between the different phases. This is also visualized in the flowchart of the project approach, see Figure 1-2.

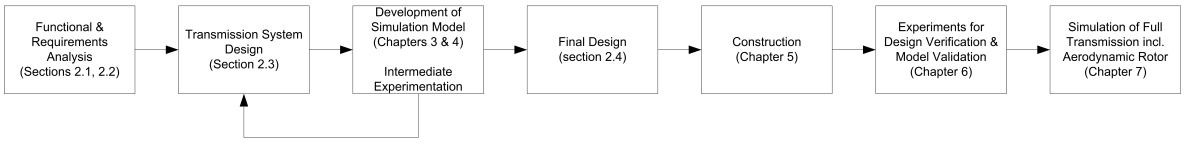


**Figure 1-2:** Project approach flowchart

In the near future experiments with the developed transmission and a 10 kW rotor are planned at a test facility of the Energy research Center of The Netherlands (ECN). The transmission will therefore be designed for this specific rotor.

## 1-4 Report Structure

The flowchart of the project approach also indicates the chapters in which the different phases of the thesis are described, see Figure 1-2. First, the design objectives and requirements were defined. With these defined the design process was started. To assist in the design process a dynamic model of the transmission together with a simplified rotor model was developed. In addition to that several intermediate experiments were carried out to assist in the design process.

After finalizing the design the demonstration set-up was constructed in the laboratory. Several experiments were run with this demonstration set-up in order to validate the dynamic model. As a result of these experiments some modifications were made to the dynamic model. Finally the last step was to prove the functionality of the transmission concept for wind turbines. This was done by running simulations with a complete model that contained the validated transmission model and a simple rotor model.

# Chapter 2

# Design of the Fluid Power Transmission

## 2-1 Introduction

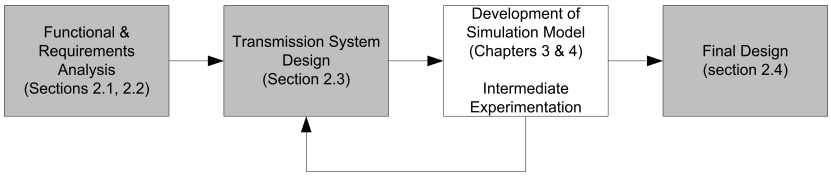


**Figure 2-1:** Chapter 2 highlighted in project approach flow chart

This chapter describes the design process and final design of the small scale transmission developed for this thesis project, see figure 2-1. The main function of the transmission is to transport energy from a wind turbine rotor to the generator platform, see figure 2-2. In this report the transmission refers to all the systems required for the energy transfer between the rotor and the generator platform. The transmission is designed for a predefined rotor.

Like for the design of all systems, the design process of the transmission was an iterative procedure. Before starting this iterative design process the design objectives and requirements were defined, see section 2-2. This included requirements to the power characteristics at the boundaries of the transmission. The required power characteristics at the transmission input and output are determined by respectively the wind turbine rotor and the hydraulic turbine on the generator platform. Therefore, a brief explanation is given on the required power characteristics for an optimal operating rotor and a hydraulic turbine. After having defined the final design objectives and requirements a design approach was developed, see section 2-3. This design approach functioned as a guide line for the iterative design process. A description of the different steps in the design process is given next. This includes the motivations for all the main design choices made during the design process. The developed dynamic model and the simulations that were carried out to assist in the design process are described in chapter 3 and 4. This chapter concludes with the final transmission design in section 2-4.

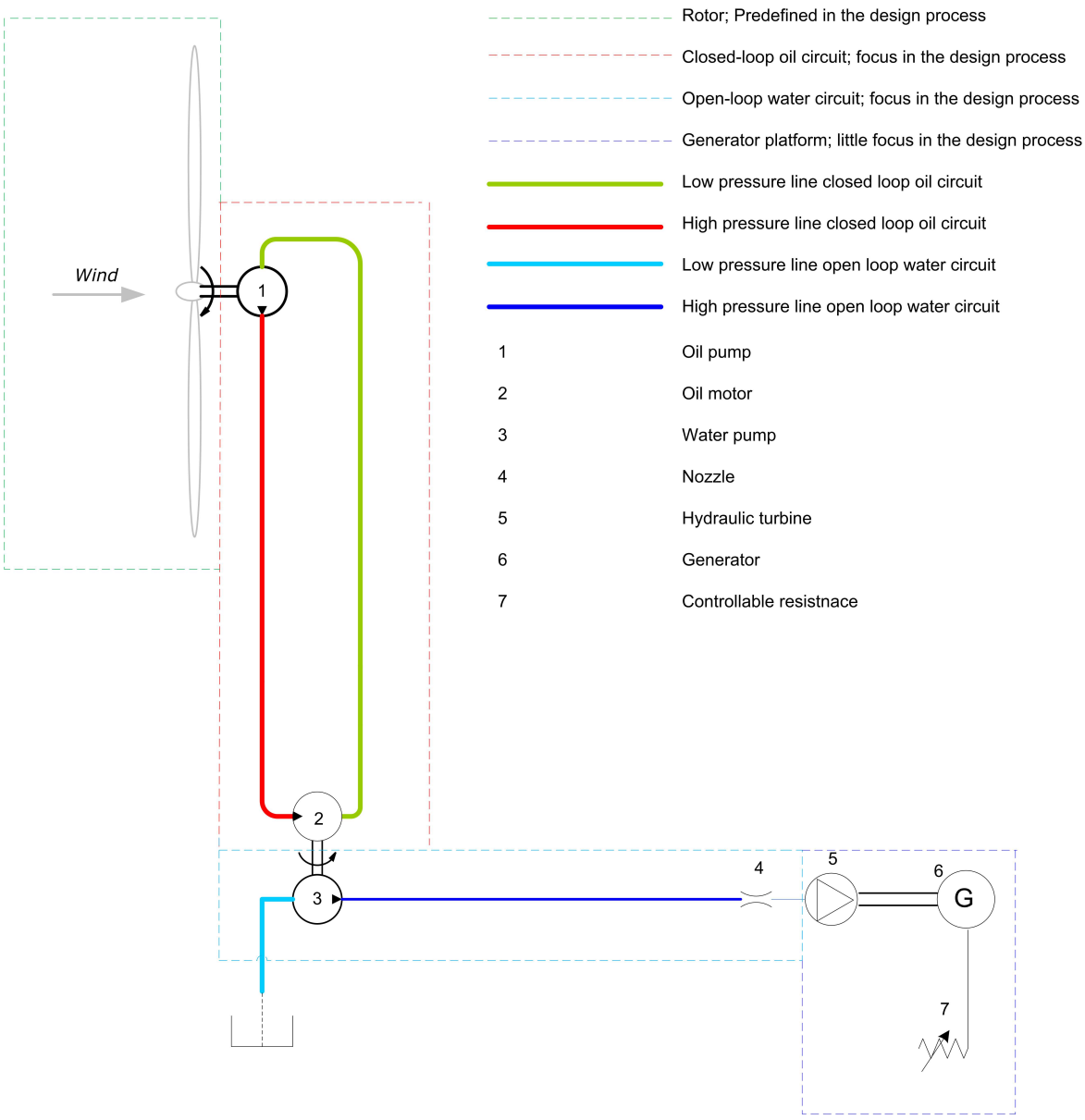


**Figure 2-2:** Diagram of the small scale fluid power transmission

## 2-2 Design Objectives and Requirements

In this section a description and motivation of the design objectives used during the design process are given first. The design requirements are described next. Some of the requirements are caused by the power characteristics required for an optimal functioning rotor and hydraulic turbine at respectively the transmission input and output. The remainder of the design requirements are prescribed by the DOT concept. The final design requirements are summed up at the end of this section.

### 2-2-1 Design Objectives

The design objectives of the transmission were used as a guide line in the design process and for the choices that were made during the process. The design objectives are given in sequential order of importance:

1. Compact transfer of energy in the transmission, also referred to as a high energy density system. This objective was defined in order to achieve small transmission components with less weight. This also results in a transmission with high operating pressures and small flows.
2. A transmission that is easy and simple to operate and control. The designed transmission will be the first constructed transmission of the DOT concept and it is therefore preferred to keep the transmission operation and control as simple as possible. This is also one of the main drivers of the DOT concept.
3. Reasonably efficient energy transfer for a large pressure range in the transmission. The large fluctuations of the wind speed in our environment will cause large power fluctuations at the transmission input. This will cause large pressure fluctuations in the transmission. It is therefore particularly important that the energy is transferred efficiently over a large pressure range.
4. Limited costs. Fulfillment of the design objectives was limited by the costs, these had to stay within the budget.

### 2-2-2 Power Characteristics Required at the Transmission Input

First a brief explanation is given on the working principle of the horizontal axis rotor. The design requirements, caused by the required power characteristics at the transmission input, are a consequence of this working principle and are described next.

The DOT concept prescribes a 2-bladed horizontal axis rotor that directly drives the oil pump, see figure 2-2. An available rotor that meets most of these requirements is an Aircon 3-bladed fixed pitch horizontal axis rotor. At rated conditions with a wind speed of 11m/s the rotor extracts 10 kW of power from the wind. The transmission is designed for this specific rotor. A horizontal axis wind turbine rotor has an optimal efficiency at a certain tip speed ratio $\lambda$. This efficiency is also called the power coefficient or $C_P$ value. It is the ratio of extracted power from the wind divided by the available power in the wind. This is defined as [5]:

$$C_p = \frac{P_{rotor}}{P_{wind}} = \frac{P_{rotor}}{\rho_a A_r {U_a}^3} \tag{2-1}$$

The tip speed ratio is the ratio of the radial velocity at the tip of the blades divided by the wind speed. This is defined as:

$$\lambda = \frac{\omega_r R}{U_a} \tag{2-2}$$

The power coefficient at different tip speed ratios is usually expressed in the so called $C_P - \lambda$ curve [5]. The performance of a specific rotor is then determined from its $C_P - \lambda$ curve. One of the rotor design choices is the tip speed ratio $\lambda$ for which the optimal power coefficient $C_{P,opt}$ is reached. This depends for example on the application for which the rotor is used. For the available rotor the optimal power coefficient and the $C_P - \lambda$ curve are already known. The $C_P - \lambda$ curve is determined from experiments with this rotor at the Energy research centre of The Netherlands (ECN). The measured results have an estimated inaccuracy of approximately 15% for the $C_P$ value, see figure 2-3. When the wind speed and the rotational speed of the rotor are known the rotor power $P_{rotor}$ and torque are determined from this $C_P - \lambda$ curve. Figure 2-3 also shows the torque of the rotor when operated at its optimal tip speed ratio as function of the rotational speed of the rotor. The other rotor properties are shown in table 2-1.

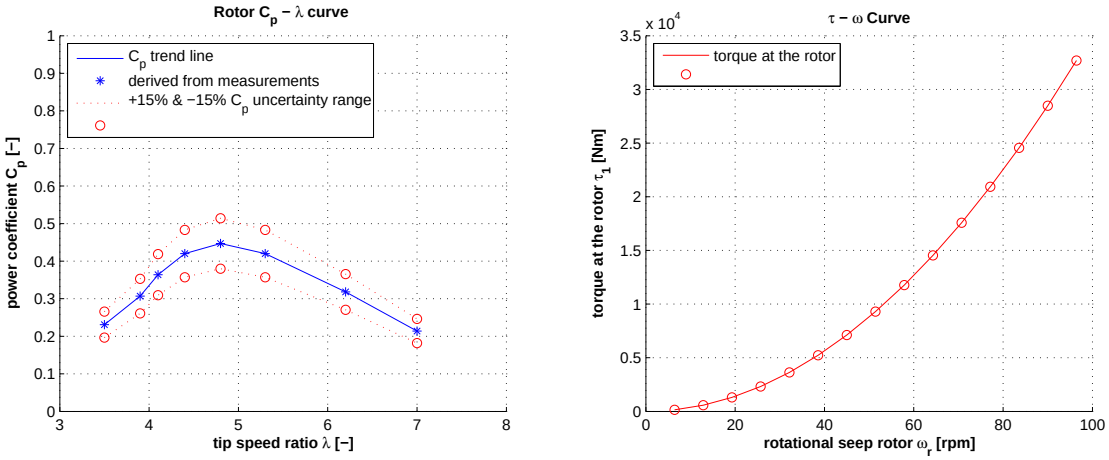


(a) $C_P - \lambda$ curve

(b) $\tau - \omega$ curve

**Figure 2-3:** Estimated performance curves of the 10kW Aircon rotor when operating at its optimal tip speed ratio of 4.8

The rotor converts the wind power into mechanical power at the highest efficiency when the rotor operates close to its optimal tip speed ratio. In order to achieve this, the transmission must control the rotor speed close to this optimal tip speed ratio.

When the rotor is at rest the torque induced by the wind is very little. Therefore the required torque during start-up condition of the rotor must be minimized. The final requirements caused by the required power characteristics at the transmission input are:

| | |
|---|---|
| Rotor diameter $R$ | 7.13m |
| Blade center of gravity (estimated) $c_m$ | 1.53m |
| Rotor swept area $A_r$ | 39.6m$^2$ |
| Blade mass $m_blade$ | 29kg |
| Rotor moment of inertia $J$ | 206.2 kgm$^2$ |
| Rated wind speed $U_{rated}$ | 11 m/s |
| Optimal tip speed ratio $\lambda_{opt}$ | 4.8 |
| Optimal power coefficient $C_{P,opt}$ | 0.44 |
| Hub height | 7.5m |

**Table 2-1:** Properties of the Aircon 10kW rotor, supplied by ECN

- The transmission must control the rotor close to its optimal tip speed ratio.
- The transmission should have an option to minimize the required torque during the start-up process of the rotor.

### 2-2-3 Power Characteristics Required at the Transmission Output

The most suitable hydraulic turbine for the generator platform is the Pelton turbine. A motivation for this choice and a brief explanation of the Pelton turbine working principle are given in this section. The Pelton turbine converts the hydraulic energy into mechanical energy. The efficiency of this conversion depends on the rotational speed of the Pelton turbine. The chosen method to control this rotational speed is also explained briefly in this section. Finally the requirements caused by the required power characteristics at the transmission output are described.

There are different types of hydraulic turbines. The hydraulic turbine that converts the hydraulic energy most efficiently at high operating pressures is the Pelton turbine [3]. The high operating pressure and the efficiency are 2 important design objectives. This makes the Pelton turbine the best choice. The used Pelton turbine in the fluid power transmission is shown on the left in figure 2-4.

The Pelton turbine is an impulse turbine. An impulse turbine converts kinetic energy into mechanical energy. At the generator platform the potential energy in the form of water under high pressure is converted by the nozzle into kinetic energy in the form of a high velocity water jet. The kinetic energy of the high velocity jet is then converted into mechanical energy at the Pelton turbine buckets. On the right of figure 2-4 you can see how the water jet hits the surface of a bucket. For large Pelton turbines the efficiency of the power conversion can be as high as 95% [3]. The pressure range for a reasonable efficient operating Pelton turbine is 5 to 130bar [3]. The pressure at the nozzle must thus be within this range.

The optimal efficiency of Pelton turbines is reached when the jet velocity is approximately twice the radial velocity of the Pelton turbine buckets [6]. This is the optimal working point of the Pelton turbine. The optimal rotational speed of the Pelton turbine as function of the jet velocity is then found by:

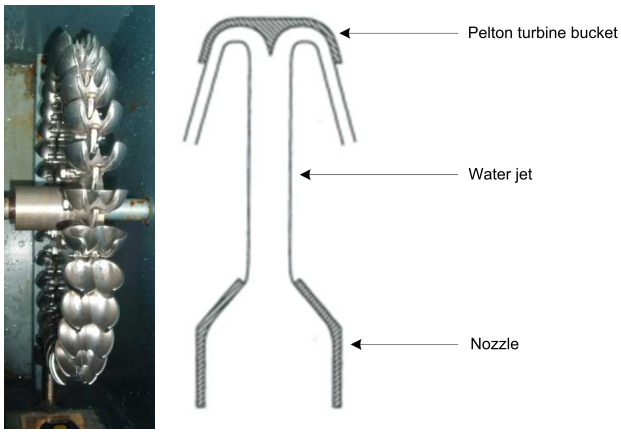


(a) (b)

**Figure 2-4:** Pelton turbine used in the demonstration set-up and the flow profile at the Pelton turbine buckets [6]

$$\omega_p = \frac{2\,U_{jet}}{\pi D_p} \tag{2-3}$$

The Pelton turbine should preferably operate close to this optimal working point. At varying wind speeds the output energy in the water jet and thus the jet velocity will vary. To stay close to this optimal working point of the Pelton turbine, the rotational speed of the Pelton turbine needs to be controlled. The rotational speed control is achieved by a variable load that is connected to the synchronous generator. This variable load is a controllable electrical resistance. By varying this resistance the rotational speeds of the generator and the directly connected Pelton turbine are controlled. The main generator platform properties are mentioned in table 2-2.

| | |
|---|---|
| Pelton turbine diameter Dp | 0.4m |
| Number of buckets | 32 |
| Rated power generator | 10kVA, 8kW |
| Number of poles pares | 2 |
| Generator speed at 50 Hz | 1500 rpm |

**Table 2-2:** Properties of the generator platform used in the demonstration set-up

The only requirement caused by the required power characteristics at the transmission output is that the pressure just before the nozzle must be between 5 to 130 bar. The described control method for the Pelton turbine rotational speed does not require any additional design requirements for the transmission itself.

### 2-2-4 Final Design Requirements

Besides the requirements mentioned in sections 2-2-2 and 2-2-3, the DOT concept prescribes several design requirements. In addition to that several requirements with a practical origin

were also defined. Finally all the design requirements for the transmission are:

- The transmission must consists of a closed-loop oil circuit and an open-loop water circuit, see figure 2-2. The closed-loop oil circuit transfers the energy from the rotor to the base of the turbine. The open-loop water circuit transfers the energy from the hydraulic motor to the generator platform. The main sub systems of the transmission are thus predefined. The type of main components used in the sub systems, e.g. pumps and motor, are however a design choice.
- In the DOT concept the intention is to use sea water in the water circuit. Fresh water is used instead for this demonstration set-up. Reason for this are the extra costs required for stainless steel components and the logistic issues with getting sea water in the laboratory.
- The transmission must contain a hydraulic break that can stop the rotor from turning at any time. This is required for safety reasons and to protect the transmission when the loads become too high.
- The transmission must be as safe as possible.
- The construction and testing of the fluid power transmission takes place in the Water Laboratory at the faculty of Civil Engineering and Geosciences of the TU Delft.
- The transmission must control the rotor speed close to the optimal tip speed ratio.
- The transmission should have an option to minimize the required torque during the start-up process of the rotor.
- The pressure in the water circuit just before the nozzle must be between 5 to 130 bar.

## 2-3 Design Process

The design approach and design process are described in this section. To achieve a good design that meets all the requirements and objectives, a structured design plan is required. The developed design plan for the design process is visualized in the design flowchart which is shown in Figure 2-5.

The design objectives and requirements described in section 2-2 are the input for the flowchart and are also used as the guideline while working through the different flowchart steps. At the end of the flowchart the design is checked whether it meets all the requirements and objectives. If this is the case the design process is finished. The final results for each step in the design flowchart are described in the remainder of this section. The sections in which these results are described are also indicated in Figure 2-5.

### 2-3-1 Selection of Main Component Types

There are four main components in the transmission, these are also indicated in Figure 2-2. The main components are:

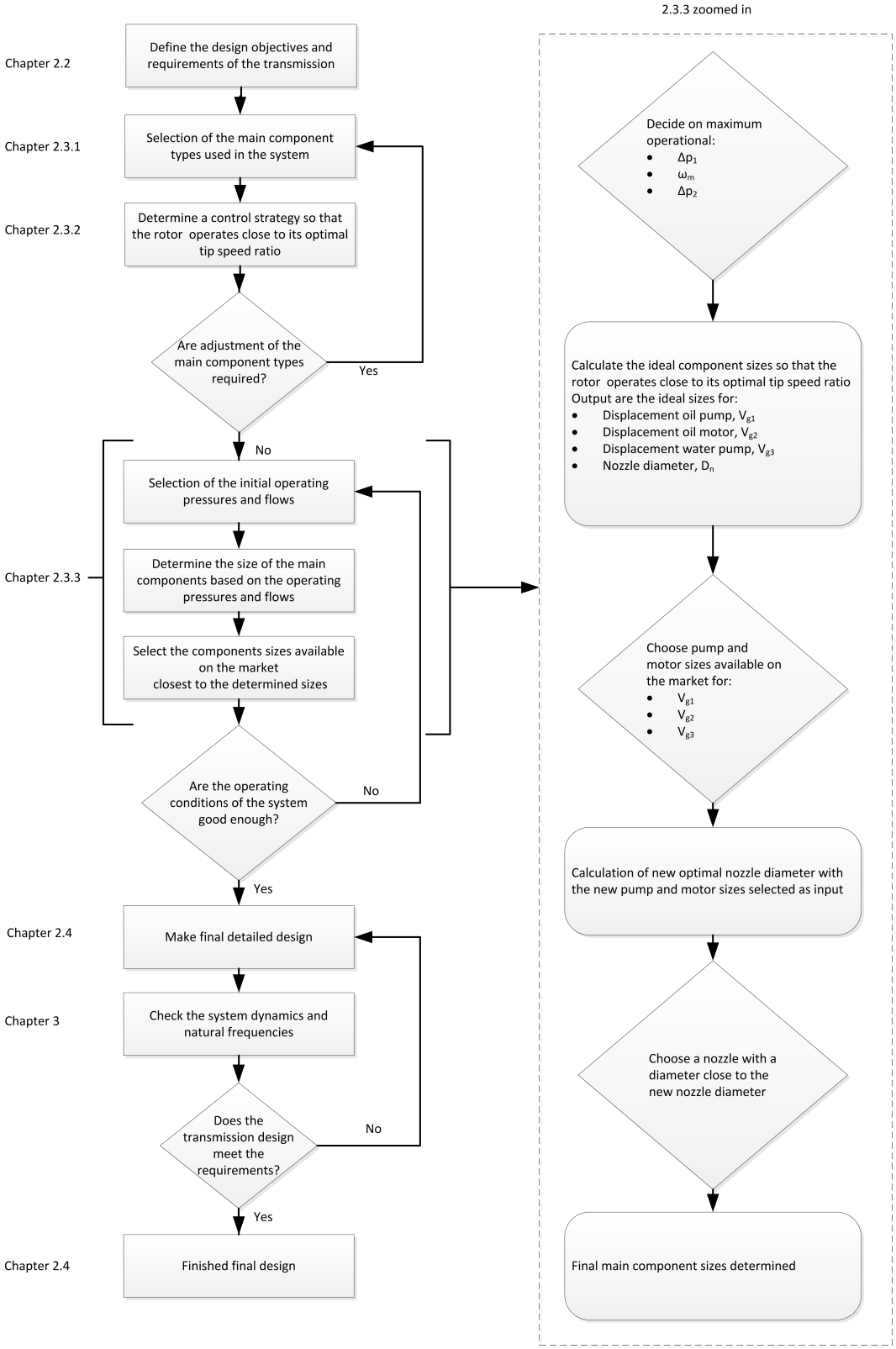


**Figure 2-5:** Design flowchart used for the transmission design [7]

1. Oil pump in the closed-loop oil circuit.
2. Oil motor in the closed-loop oil circuit.
3. Water pump in the open-loop water circuit.
4. Nozzle in the open-loop water circuit.

For each of these main components the best option is chosen. The best option is the option that meets the main design objectives the most.

The so called positive displacement pumps have a displacement that is proportional to the rotational speed of the pump. This is the type of pump that has the highest efficiencies at high operational pressures [8]. Therefore only positive displacement pumps are considered here. The different positive displacement pump options available on the market are shown in table 2-3. In this table the pumps are also compared to each other this is done by indicating how good the pump meets each of the four main design objectives stated in section 2-2-1. The pump option that gets the best total score in this comparison is the constant displacement axial piston pump. This is also the final pump type used for both the oil pump and the water pump.

| Type of pump | Size range [$cm^3$/rev] | $p_{max}$ [bar] | Compact energy transfer | Simplicity | Efficiency for large pressure ranges | Costs |
|---|---|---|---|---|---|---|
| External gear pump | 3-100 | 250 | + + | + + | - | + + + |
| Internal gear pump | 25-50 | 210 | + | + + | - | + + + |
| Vane-type pump | 010-36 | 175 | + | + + | - | + |
| Radial piston pump | 0.4-20 | 700 | + + + | + + | + + | - |
| Axial piston pump | 10-1000 | 400 | + + + | + + | + + | + + |
| Variable vane-type pump | 8-125 | 160 | + | - | - | - |
| Variable axial piston pump | 20-1000 | 315 | + + + | - | + | - |

**Table 2-3:** Comparison of suitable pump options for the transmission, + = reasonable, ++ = good, + + + = very good

The options considered for the oil motor are also only positive displacement motors, for the same reason as the pump. The same selection procedure is used for the motor selection, see table 2-4. The motor option that gets the best total score is also the constant displacement axial piston motor. This is also the final motor type used in the transmission.

The function of the nozzle is to convert the hydraulic potential energy under large pressure into hydraulic kinetic energy. The available nozzle options for the transmission are shown in table 2-5. The same selection procedure is used for the nozzle selection. The option with the highest total score is the constant area nozzle. This is also the nozzle used in the transmission.

| Type of motor | Size range [cm3/rev] | $p_{max}$ [bar] | Compact energy transfer | Simplicity | Efficiency for large pressure ranges | Costs |
|---|---|---|---|---|---|---|
| Gear motor | 06-038 | 250 | + + | + + | - | + + + |
| Radial piston motor | 190-7000 | 420 | + + + | + + | + + | - |
| Axial piston motor | 10-1000 | 400 | + + + | + + | + + | + + |
| Variable radial piston motor | 190-7000 | 420 | + + + | - | + | - |
| Variable axial piston motor | 28-355 | 315 | + + + | - | + | - |

**Table 2-4:** Comparison of suitable motor options for the transmission, + = reasonable, ++ = good, + + + = very good [7]

| Type of nozzle | Compact energy transfer | Simplicity | Efficiency for large pressure range | Costs |
|---|---|---|---|---|
| Constant area nozzle | + + + | + + + | + + | + + + |
| Spear valve (variable area nozzle) | + + + | + | + + | + |

**Table 2-5:** Comparison of suitable nozzle options for the transmission, + = reasonable, ++ = good, + + + = very good

### 2-3-2 Control Strategy

The control strategy section of this report must be kept strictly confidential. The passive control strategy is an idea developed by N.F.B. Diepeveen.

The control strategy developed to control the rotational speed of the rotor is described in this section. One of the design requirements was that the rotor speed needs to be controlled close to its optimal tip speed ratio by the transmission. One of the design objectives was a transmission that is easy and simple to operate and control. Together this resulted in a control strategy for the transmission that is preferable simple and easy to operate. The developed control strategy is a passive control strategy, where no active control of any component in the transmission is required.

Starting point in this analysis is the rotor characteristics described in section 2-2-2. The optimal power coefficient $C_{Popt}$ is reached when the rotor rotates at its optimal tip speed ratio. The rotor power when operating at its optimal power coefficient is then determined as function of the wind speed $U_a$ with:

$$P_{rotor} = C_{popt}\frac{1}{2}\rho_a A_r {U_a}^3 \tag{2-4}$$

Filling equation 2-2 into equation 2-4 then gives the rotor power at its optimal power coefficient as a function of the rotor rotational speed $\omega_r$:

$$P_{rotor} = C_{popt}\frac{1}{2}\rho_a A_r \left(\frac{R}{\lambda_{opt}}\right)^3 \omega_r^3 \tag{2-5}$$

All the terms on RHS are constant terms except for the rotor rotational speed, this equation is then rewritten into:

$$P_{rotor} = \Phi_{rotor}\omega_r^3 \tag{2-6}$$

Where $\Phi_{rotor}$ is the constant term for a rotor operating at its optimal power coefficient.

$$\Phi_{rotor} = C_{popt}\frac{1}{2}\rho_a A_r \left(\frac{R}{\lambda_{opt}}\right)^3 \tag{2-7}$$

The power required at the transmission input is the product of the torque and the rotational speed of the oil pump. The torque required to rotate the oil pump with a certain set rotational speed partly depends on the sizes of the components in the transmission. The equation for the torque at the oil pump is derived next. The derivation of this equation is visualized in the block diagram of figure 2-6. The equations used for the different conversion steps in the block diagram are explained in detail in chapter 3.

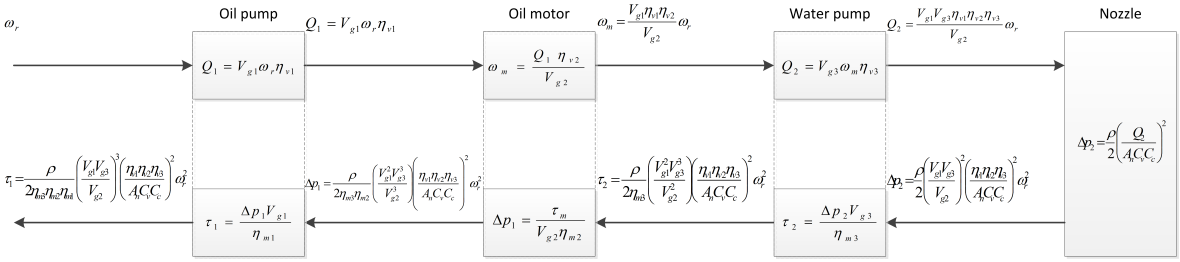


**Figure 2-6:** Derivation of the equation for the required torque at the oil pump using a passive control system

The power into the transmission is then the product of the set rotational speed $\omega_r$ and the required torque at the oil pump $\tau_1$, see figure 2-6:

$$P = \omega_r\tau_1 = \frac{\rho}{2\eta_{m1}\eta_{m2}\eta_{m3}}\left(\frac{\eta_{v1}\eta_{v2}\eta_{v3}}{A_nC_vC_c}\right)^2\left(\frac{V_{g1}V_{g3}}{V_{g2}}^3\omega_r\right)^3 \tag{2-8}$$

If the pump, motor and nozzle efficiencies are assumed constant, all the terms on RHS are constant terms except for the rotor rotational speed. This equation is then rewritten into:

$$P = \Phi_{transmission}\omega_r^3 \tag{2-9}$$

So, like the rotor power, the power required at the transmission input is a function of the rotational speed cubed. Where $\Phi_{transmission}$ is the constant transmission term:

$$\Phi_{transmission} = \frac{\rho}{2\eta_{m1}\eta_{m2}\eta_{m3}}\left(\frac{\eta_{v1}\eta_{v2}\eta_{v3}}{A_nC_vC_c}\right)^2\left(\frac{V_{g1}V_{g3}}{V_{g2}}\right)^3 \tag{2-10}$$

The energy input at the rotor is kinetic energy transported by the fluid air. The energy output at the nozzle in the transmission is also kinetic energy only now transported by the

fluid water. Thus the rotor together with the transmission converts the kinetic energy at the input back into kinetic energy at the output, only the fluid and the fluid velocity are different. This explains the similarity in the power equations for the rotor and the transmission. Both power equations are a function of the rotational speed cubed. So when the transmission is designed such that $\Phi_{transmission}$ is equal to the $\Phi_{rotor}$ the wind turbine rotor will operate close to its optimal power coefficient with passive control only. In order to achieve this, the sizes of the 4 main components in the transmission were chosen such that $\Phi_{transmission}$ is equal to the $\Phi_{rotor}$. The assumptions made in the simplified derivation of $\Phi_{transmission}$ in figure 2-6 are:

- Mechanical and volumetric efficiencies of pumps and motor in the transmission are assumed to be constant.
- Losses in the hydraulic hoses are neglected.
- To determine the pressure at the nozzle the Bernoulli equation is used. The velocity input into the hydraulic hose is neglected in the Bernoulli equation for the nozzle.

Some of the efficiencies will not be constant for the real transmission. The efficiencies of the pumps and motor are a function of the flow and pressures in both circuits. This means that $\Phi_{transmission}$ will vary slightly at varying rotational speeds. This will then result in a turbine that deviates from its optimal tip speed ratio during operation, due to this varying $\Phi_{transmission}$. The magnitude of this variation in the tip speed ratio depends on the variation of the efficiencies.

With this control method no active control of the transmission is required making this control method simple and easy to operate. Therefore the passive control strategy is the method chosen to control the rotor speed. This passive control method is a major simplification and thus improvement, compared to the control methods used in the conventional turbines. Current wind turbine rotors need active control at the generator to operate close to the optimal tip speed ratio of the rotor.

### 2-3-3 Size Selection of the Main Components

The procedure used and the final results of the size selection for the main components are described in this section. The final size selection of the transmission components determines how close the rotor will operate to the optimal tip speed ratio, as explained in section 2-3-2. The strategy used to come to the final sizing of the transmission components is shown in the design flow chart, see Figure 2-5.

Indicated in the flowchart is that the pressures and flows are chosen first. However these vary with varying wind speeds. The main components are limited by a certain maximum operational pressure or flow. The pressures and flows in the transmission are at their maximum at maximum power input. Therefore the situation with maximum power input is chosen as the basis for the size selection process. The power limit of the turbine is at a wind speed of 11m/s, this is the so called rated wind speed. Wind speeds above this value will not result in a larger rotor power because part of the airflow will stall on the blades [5].

The step by step procedure for the components size selection is shown in figure 2-5 on the right side. So first the pressures in the oil and water circuits, $\Delta p_1$ and $\Delta p_2$, together with the rotational speed of the motor $\omega_m$ at maximum power input were selected. An important design objective of the transmission is compact energy transfer, this means high operational pressures in the transmission. As mentioned before the height of the pressures is limited by the maximum operational pressures of the pumps and motor. The final selected operational pressures and rotational speed of the motor were:

- $\Delta p_1 = 200$bar. This was a trade-off between the design objective of compact energy transfer and the costs of the oil pump and motor. The costs of these components increase with increasing maximum operational pressure. In addition to that a safety margin between $\Delta p_1$ and the maximum operational pressures of the components were taken into account.
- $\Delta p_2 = 35$bar. The reason for this relatively low pressure is the low efficiency of the available Pelton turbine at higher pressures. This was found during intermediate experiments with the generator platform. Reason for this low efficiency is that a small water jet diameter has a large negative effect on the efficiency of the Pelton turbine. At constant power a higher pressure in the water circuit will result in less volume flow and thus smaller diameter of the water jet. This selected design pressure in the water circuit was thus a trade-off between the compact energy transfer objective and the reasonable efficiency objective.
- $\omega_m = 1500$rpm. The chosen types of oil motor and water pump are designed to have a maximum efficiency at a rotational speed around 1500rpm.

To achieve a transmission that passively controls the rotor at its optimal tip speed ratio equations that determine the ideal component sizes as a function of $\Delta p_1$, $\Delta p_2$ and $\omega_m$ were derived.

$$\omega_r = \frac{U_{rated}\lambda_{opt}}{R} \tag{2-11}$$

$$\tau_1 = \frac{P_{rotor}}{\omega_r} \tag{2-12}$$

$$V_{g1} = \frac{\tau_1}{\Delta p_1}\eta_{m1} \tag{2-13}$$

$$V_{g2} = \frac{V_{g1}\omega_r}{\omega_m}\eta_{v1}\eta_{v2} \tag{2-14}$$

$$V_{g3} = \frac{V_{g2}\Delta p_1}{\Delta p_2}\eta_{m2}\eta_{m3} \tag{2-15}$$

The equations used to determine the pump and motor sizes are derived from the pump and motor equations explained in section 3.3 and section 3.4. Pumps and motor sizes close to these determined values were found on the market.

- $V_{g1} = 180$ cm$^3$/rev

- $V_{g2} = 16$ cm$^3$/rev
- $V_{g3} = 70.3$ cm$^3$/rev

The final component size that was determined next is the nozzle diameter. With the known pumps and motor sizes the optimal nozzle diameter was determined with:

$$D_n = 2\sqrt{\frac{V_{g1}V_{g3}\omega_r\eta_{v1}\eta_{v2}\eta_{v3}}{V_{g2}C_vC_c\pi}}\sqrt{\frac{\rho}{2\Delta p_2}} \tag{2-16}$$

This resulted in an optimal nozzle diameter $D_n$ of 5.12mm. It must be noted that the specifications of the rotor were not available at the start of the design process. Therefore an optimal tip speed ratio had to be assumed. This assumption was made based on the optimal tip speed ratios of similar rotor sizes. Due to this assumption the transmission was designed to operate the rotor at a tip speed ratio of 5.6 instead of 4.8. This is easily corrected by recalculating the nozzle diameter with equation 2-16.

This then concludes the results of the final size selection of the 4 main component sizes in the transmission. If experiment results indicate that the oil pump does not operate close to the optimal tip speed ratio of the rotor the optimal nozzle diameter will need to be recalculated again. The same equations need to be used only now with the actual determined efficiencies from the experiments.

## 2-4 Final Detailed Design

The final transmission design is described in this section together with an explanation on how some of the design requirements were fulfilled. Before the final design was completed the length and diameters of the hoses in the transmission were determined. In addition to that a suitable boost system was developed for the oil circuit. The hydraulic diagram of the final detailed design is shown in figure 2-7. The legend of all the components in the detailed design is shown in appendix B.

### 2-4-1 Hose Dimensions

The required length of the hoses was determined from the turbine tower height at ECN and the position of the generator platform. The diameter of the hoses will determine the velocity of the oil and water through the hoses. This will determine the pressure drop (energy loss) of the flow through the hoses. The larger the hose diameter, the lower the pressure drop, which is preferred. However larger hose diameters are more costly. The selected diameter of the hose is thus a trade-off between the pressure drop and the costs. In addition to that the pump and motor suppliers also advise typical hose diameters for their pumps and motors. The final selected hose diameters and length are shown in table 2-6.

The fluid velocities shown in table 2-6 are in agreement with the guide lines that were advised by the pumps and motor suppliers [7].

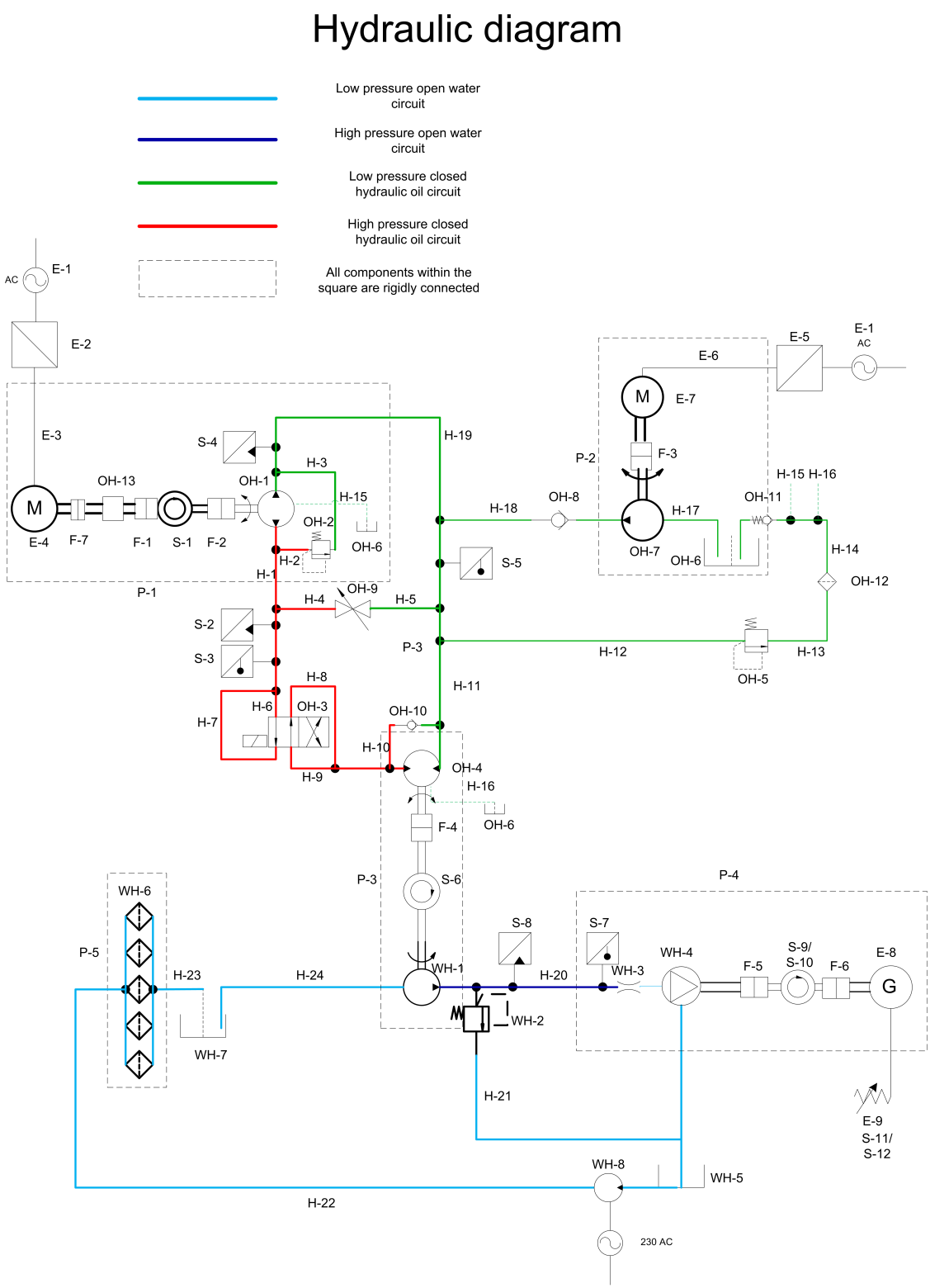


**Figure 2-7:** Hydraulic diagram of the final transmission design. E = electrical component, F = flexible coupling, H = hose, OH = component of the oil circuit, WH = component of the water circuit, S = sensor, P = platform

| Hydraulic hose | Length [m] | Diameter [mm] | Fluid velocity in hose at rated wind speed |
|---|---|---|---|
| High pressure oil circuit | 10 | 19.1 | 1.8m/s |
| Low pressure oil circuit | 10 | 25.4 | 1.0m/s |
| High pressure water circuit | 15 | 25.4 | 3.3m/s |
| Low pressure water circuit | 3 | 38.1 | 1.5m/s |

**Table 2-6:** Specifications of the hydraulic hoses used in the transmission

### 2-4-2 Cooling and Boost Systems

Cooling of the fluid in both the oil and water circuit is also a point of concern. All the energy losses in the transmission are dissipated as heat into the fluids. Cooling can be done by a heat exchanger or by renewing a certain part of the fluid with cold fluid from a reservoir. The water circuit is an open-loop circuit with a large reservoir and the water is thus constantly 100% renewed from this reservoir. Thus for the open-loop water circuit no extra cooling system is required, see also figure 2-7. The closed-loop oil circuit does need an additional system for cooling, because the system is a closed-loop circuit and no fluid is renewed. In addition to that the hydraulic oil circuit needs to be kept above a certain minimum pressure (e.g. 2bar), or else cavitation at the pump could occur. The choice was made to use a boost system because the boost system will take care of both the cooling and the minimum pressure requirements. The boost system is connected to the low pressure side of the oil circuit, see figure 2-7. The flow of the renewed oil is regulated by regulating the rotational speed of the boost pump. The pressure in the low pressure side of the oil circuit is regulated by setting the opening pressure of the pressure relief valve in the boost system, OH-5 in figure 2-7.

### 2-4-3 Hydraulic Break Requirement

One of the design requirements was that the transmission must contain a hydraulic break that can stop the rotor from turning at any time. The choice was made to use an electrical controlled directional valve in the high pressure side of the oil circuit, see OH-3 in figure 2-7 for the exact position. When the valve is excited it is in the open position and the oil can flow to the oil motor. This is the normal operation condition. When the valve is not excited the valve is in closed position, the hydraulic break is then activated. The oil in the high pressure hose is then confined by the closed valve. This will cause the pressure and torque at the oil pump to increase. This will then slow down the rotational speed of the rotor below its optimal tip speed ratio, figure 2-3. This will then reduce the power extracted from the wind. This process shall carry on until the rotor is completely stopped. To ensure safety upon activation of the hydraulic break there is a pressure relief valve installed in the high pressure oil line. This valve will open if the pressure increases above a certain set value, for example when a pressure peak occurs upon activation of the hydraulic break.

The occurrence of a waterhammer must be prevented. This phenomena is accompanied with a considerable noise that is caused by a very large pressure transient. This pressure transient could occur if fluid flow is stopped suddenly by a rapid closing valve like the hydraulic break. A waterhammer can cause considerable damage to the transmission especially when occurring frequently. To prevent a waterhammer the system must be designed such that the fluid

velocity is below 4m/s [8]. The fluid velocity in the high pressure oil line must thus be kept below 4m/s. This requirement is fulfilled, see table 2-6.

### 2-4-4 Minimizing the Required Start-Up Torque

Another significant requirement was that the transmission must have an option to start-up the rotor with a low starting torque. This is accomplished by installing a manual valve (OH-9 in figure 2-7) that shortcuts the high pressure and low pressure side of the oil circuit when in open position. During start-up this valve is in the open position. When sufficient momentum of the rotor is reached, the valve is closed manually and normal operation is achieved.

### 2-4-5 Safety

To ensure safe operation of the transmission the high pressure hoses are all connected to pressure relief valves. These valve will open before maximum operational pressure is reached, see figure 2-7.

This then concludes the final transmission design which fulfills all the design objectives and requirements stated in section 2-2. However before the detailed design was finalized the dynamic response and natural frequencies of the designed transmission were analyzed. A detailed description of the developed dynamic model for this analysis and the results of this analysis are explained in detail in chapter 4.

# Chapter 3

# Modeling of the Transmission Sub Systems

## 3-1 Introduction

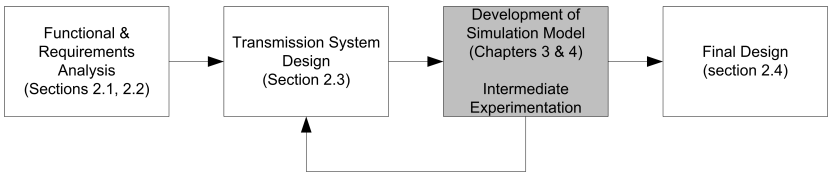


**Figure 3-1:** Chapter 3 highlighted in project approach flow chart

The development of models for each sub system in the transmission is described in this chapter. The development of the final dynamic transmission model and simulations results of this model are described in chapter 4, see figure 3-1.

A model is a mathematical representation of a physical system. What elements of the physical system are included or neglected in the model, depends on the analysis objective and the understanding of the physical system by the model author. It is thus possible to make several models for the same physical system. A simplified diagram of the physical transmission for which a model was developed is shown in figure 3-2.

The transmission contains sub systems in the mechanical rotational and hydraulic domain. A model for each of these sub systems was developed by using the three fundamental laws for fixed control volume analysis explained in appendix A. A model for the rotor inertia is also developed. This was done because of the large influence of the rotor inertia on the dynamic behavior of the complete system. The development of the final model and the simulation results from this model are explained in chapter 4.

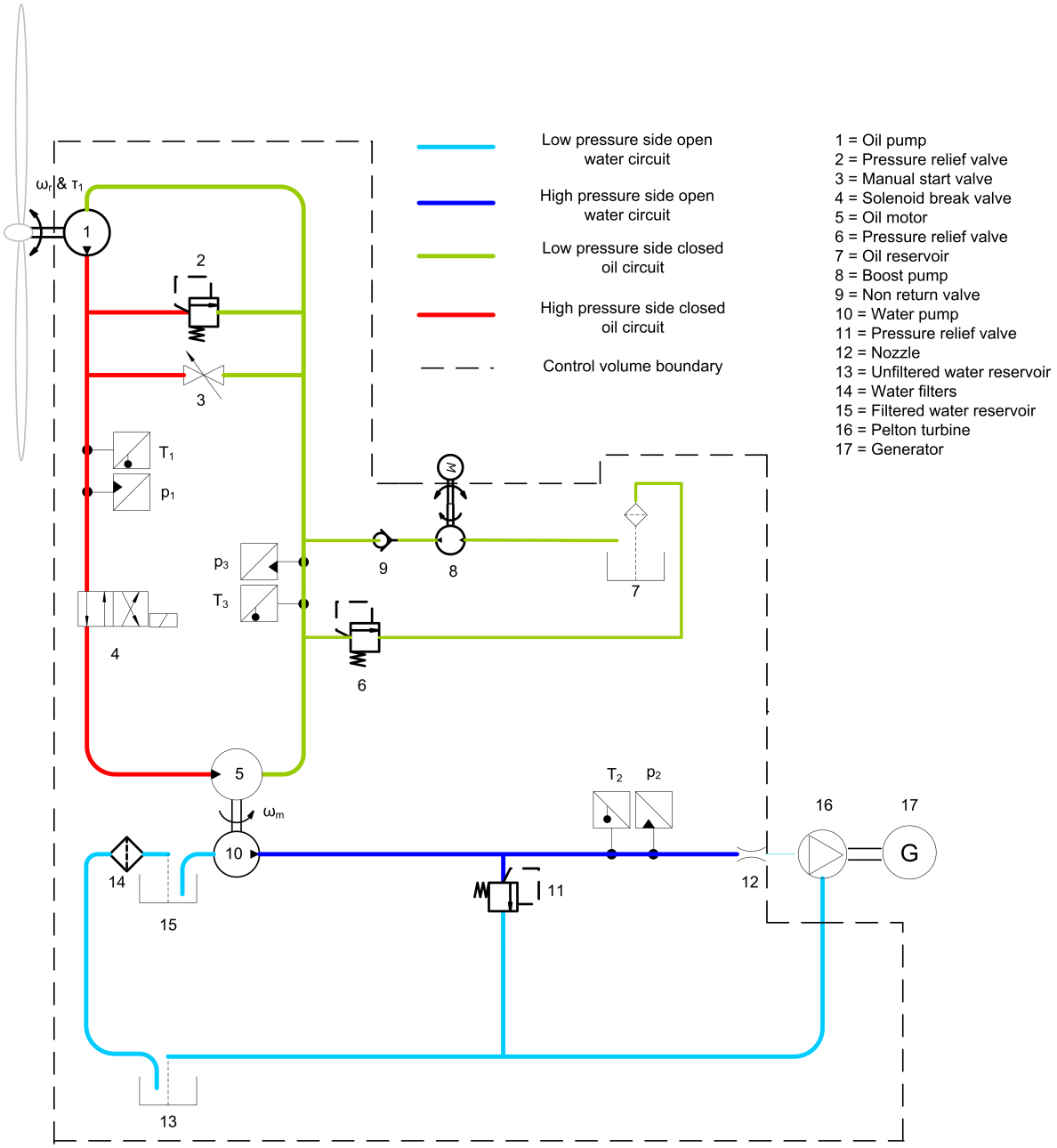


**Figure 3-2:** Simplified diagram of the designed transmission including rotor

## 3-2 Lumped Fluid Flow Model

Flow through a hydraulic hose is modeled by the so called lumped fluid flow model. With this approach a good estimate of the dynamic response of the fluid flow system is reached [9]. Any physical system can be modeled by using only three types of elements; capacitance, inertia and resistance [9]. The units of the elements differ depending on the domain in which the physical system operates. Fluid flow systems are also modeled with these elements. These elements are derived from the three fundamental laws for fixed control volume analysis, see appendix A.

First some general assumptions and simplifications are required for the lumped fluid flow model [10]:

- The control volume is fixed in space with constant area inputs and outputs. This is also visualized in figure 3-3.
- The lumped fluid flow model is a model with a one-dimensional input and output where the velocity and pressure are assumed to be uniform within the control volume. In reality they are non-uniform due to the no-slip condition at the hose walls caused by viscous effects of the fluid. The assumed uniform velocity and pressure in the model are based on the average velocity and pressure of the fluid.
- The density is also assumed to be uniform throughout the control volume.
- The velocity, pressure and density are allowed to vary over time in the model.

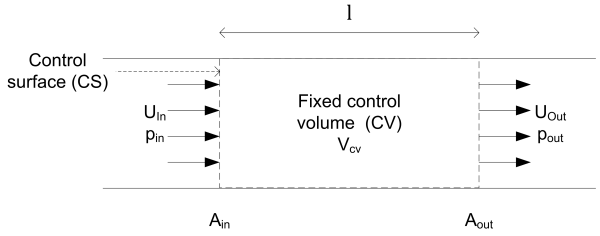


**Figure 3-3:** Lumped fluid model for fluid flow through a hydraulic hose

### 3-2-1 Fluid Inertia

Fluid inertia is also referred to as the fluid inductance and represents the inertial effects of the fluid lump [9]. The inertia element of fluid is derived from the linear momentum law. The inflow and outflow are one dimensional and normal to the control surface, see figure 3-3. Together with the assumptions of uniform velocity, pressure and density throughout the control volume the linear momentum law reduces to, see equation A-8 in appendix A:

$$\sum F = \frac{d}{dt}\left(U \rho V_{cv}\right) + \sum U^2 \rho A_{out} - \sum U^2 \rho A_{in} \tag{3-1}$$

With the above made assumptions the inflow and outflow terms cancel each other out. The assumption of small density change with time is also made, meaning that the density change with time is neglected. This reduces the equation to:

$$\sum F = \rho V_{cv} \frac{dU}{dt} \tag{3-2}$$

As stated in the general assumptions, only one dimensional flow is considered here. The only forces acting in the direction of the fluid flow are normal to the control surface of the fluid lump. In reality there is also a small wall resistance, caused by viscous effects. This resistance needs to be overcome by the fluid and is neglected in this derivation of fluid inertia. [10].

$$A\left(p_{in} - p_{out}\right) = \rho A l \frac{dU}{dt} \tag{3-3}$$

$$A\left(p_{in} - p_{out}\right) = \rho l \frac{dQ}{dt} \tag{3-4}$$

$$\Delta p = \frac{\rho l}{A} \frac{dQ}{dt} \tag{3-5}$$

Where dQ/dt is the accelerated fluid flow through the control volume at that particular pressure difference. The fluid inertia is then defined as:

$$I_f = \frac{\rho l}{A} \tag{3-6}$$

A small correction on the fluid inertia is required due to the assumption of a uniform fluid velocity [11]. This correction is derived next. In reality the velocity profile of a fluid is non-uniform and either has a laminar or a turbulent profile, see figure 3-4.

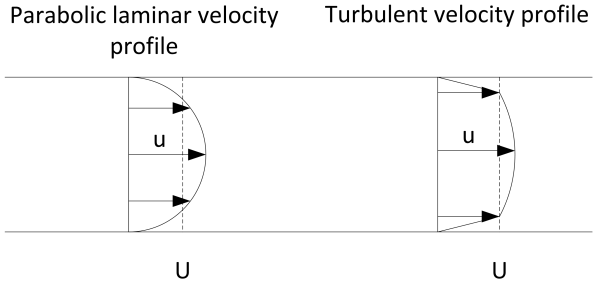


**Figure 3-4:** Laminar and turbulent flow profiles

The assumption of uniform one dimensional flow gives a momentum flux of:

$$\int_{CS} U\rho\left(U_n\right) dA_{out} = U^2 \rho A \tag{3-7}$$

The laminar velocity profile of a fully developed Poiseuille flow in a round pipe is described with the following equation, see figure 3-4 [11].

$$u = U\left(1 - \frac{r_h^2}{R_h^2}\right) \tag{3-8}$$

The velocity profile equation for laminar flows is filled into the LHS of equation 3-7. This then gives the following result for a laminar velocity profile:

$$\rho \int u^2 dA = \varepsilon \rho A U^2 \tag{3-9}$$

$$\varepsilon = \frac{1}{A} \int \left(\frac{u}{U}\right)^2 dA = \frac{4}{3} \tag{3-10}$$

The corrected fluid inertia element for laminar flow then becomes [11] [10]:

$$I_{fc} = \frac{4}{3} I_f = \frac{4\rho l}{3A} \tag{3-11}$$

Turbulent flow profiles have a more uniform shape and therefore the correction factor is much smaller and is usually neglected (equal to unity), see figure 3-4 [11]. In this model the correction factor for turbulent flow profiles is also neglected.

The inertia of the fluid element is analogue to the mass in a mechanical system. From equation 3-6 it is concluded that the inertia of a fluid element is reduced when the density and length decrease or when the area increases.

### 3-2-2 Fluid Capacitance

Real fluids are to some extend compressible although incompressibility is often assumed in simple steady state fluid flow analysis. However, the working pressure in the transmission will go up to 200bar. At these pressures compressibility needs to be taken into account [9]. It can also be seen as mass storage or release element and is analogue to the capacitance element in an electrical circuit. The capacitance of the hydraulic system is derived from the conservation of mass law. By assuming a one dimensional uniform flow, as for the fluid inertia element, the conservation of mass equation reduces to, see equation A-7 in appendix A:

$$\left(\frac{d\left(\rho V_{cv}\right)}{dt}\right)_{cv} + \sum \left(\rho A U\right)_{out} - \sum \left(\rho A U\right)_{in} = 0 \tag{3-12}$$

Again the assumption of small density change around an operating point is used, this then results into:

$$\left(\left(AU\right)_{out} - \left(AU\right)_{in}\right) \rho dt = -\rho dV_{cv} \tag{3-13}$$

The bulk modulus of the fluid relates the change of volume $dV_{cv}$ with respect to the starting volume $V_{cv_0}$ as a function of the pressure change $dp$. A more detailed explanation of the bulk modulus and the effective bulk modulus is given in appendix A. Here the bulk modulus is assumed to be a constant and defined as:

$$E_{fl} = -V_{cv0} \frac{dp}{dV_{cv}} \tag{3-14}$$

Filling this into the equation 3-13 gives:

$$\left(Q_{out} - Qin\right) dt = \frac{V_{cv0} dp}{E_{fl}} \tag{3-15}$$

Because the control volume and the bulk modulus remain constant with time both sides can be integrated to get:

$$\frac{V_{cv0}}{E_{fl}} \int dp = \int (Q_{out} - Qin)\, dt \tag{3-16}$$

This is then simplified to:

$$p = \frac{E_{fl}}{V_{cv0}} \int (Q_{out} - Qin)\, dt \tag{3-17}$$

Here the term $Q_{out} - Q_{in}$ represent the amount of flow that is stored or released at pressure $p$. The hydraulic capacitance is then defined as:

$$C_h = \frac{V_{cv0}}{E_e} = \frac{Al}{E_e} \tag{3-18}$$

Here $E_e$ is the effective bulk modulus. It takes into account the air entrained in the fluid and the stiffness of the hydraulic hoses. The effective bulk modulus is determined with equation A-22 in appendix A. The capacitance of the hydraulic system is analogue to a spring in a mechanical system. The stiffness in a mechanical system is related to its capacitance by:

$$C = \frac{1}{k} \tag{3-19}$$

A system with a very large stiffness and thus small capacitance can be viewed as a system that approaches the behavior of a rigid body system. From equation 3-18 it is seen that the fluid capacitance element becomes smaller with increasing bulk modulus and decreasing volume.

### 3-2-3 Fluid Resistance

The viscous effects of a fluid flow will cause a certain energy loss. This is related to the fluid resistance. This can be caused by frictional losses at the wall or by other geometry changes or obstructions in the flow. The frictional losses will result in a pressure drop in the fluid flow. The fluid resistance is derived from the conservation of energy law [10]. To derive this resistance the flow is assumed to be incompressible, in steady state and one dimensional. In addition to that no work is done by the control volume and the heat exchange is neglected. With these assumptions the conservation of energy law reduces to, see equation A-14 in appendix A.

$$\rho U A \left( \hat{u} + \frac{p}{\rho} + \frac{U^2}{2} + gz \right)_{out} - \rho U A \left( \hat{u} + \frac{p}{\rho} + \frac{U^2}{2} + gz \right)_{in} = 0 \tag{3-20}$$

In the transmission the height differences are neglected and constant area hoses are used. The fluid velocity is then equal at in and outlet so that the velocity terms cancel each other out. In addition to that the small density change is assumed. The equation then reduces to:

$$\Delta p_{ft} = \rho \Delta \hat{u} \tag{3-21}$$

The term on the LHS is also referred to as the total pressure loss. This term accounts for the losses caused by friction at the walls, geometry changes or other obstructions in the flow. There is only one case where the pressure loss in a pipe flow system can be determined analytically. This is for a fully developed laminar flow without geometry changes or obstructions. A general equation for the pressure loss caused by frictional losses at the wall in a pipe flow system is [11]:

$$\Delta p_f = f\frac{\rho l U^2}{2D} \tag{3-22}$$

Where f stands for the Darcy friction factor. For laminar flows the Darcy friction factor is a function of the Reynolds number Re. For turbulent flows it is a function of the Reynolds number and the dimensionless surface roughness $\frac{\varepsilon}{D}$ on the inside wall.

$$f = func\left(Re_d, \frac{\varepsilon}{D}\right) \tag{3-23}$$

$$Re_d = \frac{\rho U D}{\mu} \tag{3-24}$$

The Reynolds number is a dimensionless number indicating the effects of viscous forces on the fluid. The larger the Reynolds number the smaller the effect of the viscous forces on the fluid. For pipe flow systems the flow becomes turbulent at Reynolds numbers larger than 2100. For laminar flows the friction factor can be derived analytically. The result is the following equation [11].

$$f = \frac{64}{Re_d} \tag{3-25}$$

An equation approximating the friction factor for a turbulent flows with smooth walls and Reynolds number up to $10^5$ was developed by Blasius [11].

$$f = 0.316 Re_d^{-0.25} \tag{3-26}$$

The Reynolds numbers of the flows in the transmission do not exceed $10^4$. So this equation is sufficient to model the resistance of the fluid flows in the transmission.

Besides the frictional losses at the wall there are other sources of minor losses in the flow system. Sources of these losses are geometry changes or other obstructions, such as valves and T-pieces. These must be reduced to a minimum in the system. The losses caused by these obstructions were measured experimentally and correlated with pipe flow systems in the following way [11]:

$$\Delta p_{ft} = \frac{\rho U^2}{2}\left(\frac{fl}{D} + \sum K\right) \tag{3-27}$$

Where K is the factor that takes the losses due to obstructions and geometry changes into account. This theory is very weak but the best available approximation to take the losses of these obstructions into account [11]. In table 3-1 the K values of several different obstructions in fluid flow systems are given as an example.

| Diameter [mm] | 12.5 | 25 | 50 |
|---|---|---|---|
| Valve globe | 14 | 8.2 | 6.9 |
| Valve gate | 0.3 | 0.24 | 0.16 |
| Valve check | 5.1 | 2.9 | 2.1 |
| Elbow 90° | 2 | 1.5 | 0.95 |
| T-piece line flow | 0.9 | 0.9 | 0.9 |

**Table 3-1:** K-values for different obstructions in fluid flow systems [11]

Rewriting equation 3-27 and using $Q = UA$ gives:

$$\Delta p = \frac{\rho U}{2A}\left(\frac{fl}{D} + \sum K\right) Q \tag{3-28}$$

The resistance element of the fluid is then:

$$R_{fh} = \frac{\rho U}{2A}\left(\frac{fl}{D} + \sum K\right) \tag{3-29}$$

The resistance element is not a constant term, both the velocity U and the friction factor $f$ depend on the flow rate. This makes the fluid resistance element a non-linear model. The resistance should thus be determined separately for every time step in the simulation.

## 3-3 Axial Piston Pump Model

The axial piston pump is a so called fixed positive displacement pump. The pump is the component that transforms the rotational mechanical power into fluid power. The pump control volume has rotational mechanical power and fluid power under a low pressure as input. The output of the control volume is fluid power under a high pressure, see figure 3-5. There are three main equations relating the input and output of a pump to each other [8].

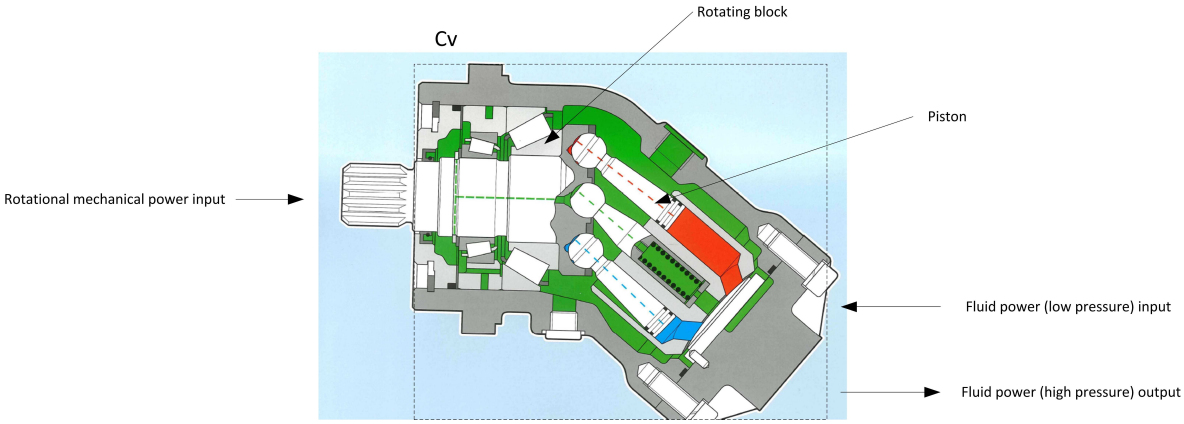


**Figure 3-5:** Control volume axial piston pump [7]

$$Q = V_g \omega \eta_v \tag{3-30}$$

$$\tau = \frac{\Delta p V_g}{\eta_m} \tag{3-31}$$

$$P_{in} = \tau \omega \tag{3-32}$$

The total losses of the energy conversion from mechanical to hydraulic energy consist of two types of losses, the friction losses and the leakage flow losses [8]. The friction losses consist of two parts. One of the losses is caused by the viscous effects of the fluid which cause losses when the fluid is sheared into the cylinders of the pump. These losses are dimensionally sized using the damping coefficient $C_d$. The second part is the friction between the moving mechanical components in the pump. These losses are dimensionally sized using the friction coefficient $C_f$. A measure for the total friction losses is given by the mechanical efficiency. The equation used to determine the mechanical efficiency is [8]:

$$\eta_m = \frac{1}{1 + C_d \frac{\mu\omega}{\Delta p} + C_f} \tag{3-33}$$

The dimensionless coefficients $C_d$ and $C_f$ are derived from efficiency test data supplied by the manufacturer, see confidential supplement.

The leakage flow losses are caused by internal and external leakage flows. The internal leakage flow is caused by small clearances through which fluid can flow internally back from the outlet (high pressure) to the inlet (low pressure) of the pump. External leakage is a small leakage flow from the high pressure side to the pump housing. The volumetric efficiency gives a measure of how large these leakage losses are. The equation used to determine the volumetric efficiency is [8]:

$$\eta_v = 1 - C_s \frac{\Delta p}{\mu\omega} \tag{3-34}$$

The dimensionless coefficient of slip Cs is also derived from efficiency test data supplied by the manufacturer, see confidential supplement. The total efficiency is the product of the mechanical and volumetric efficiency:

$$\eta_t = \frac{1 - C_s \frac{\Delta p}{\mu\omega}}{1 + C_d \frac{\mu\omega}{\Delta p} + C_f} \tag{3-35}$$

The oil pump efficiencies used in the model are given in figure 3-6 as a function of the pressure difference and the rotational speed. These efficiency curves are based on tests carried out by the manufacturer. The graphs in figure 3-6 show the following trends:

- The volumetric efficiency decreases with increasing pressure as is also expected from equation 3-34.
- The volumetric efficiency increases with increasing rotational speed as is also expected from equation 3-34.
- The mechanical efficiency increases with increasing pressure as is also expected from equation 3-33.

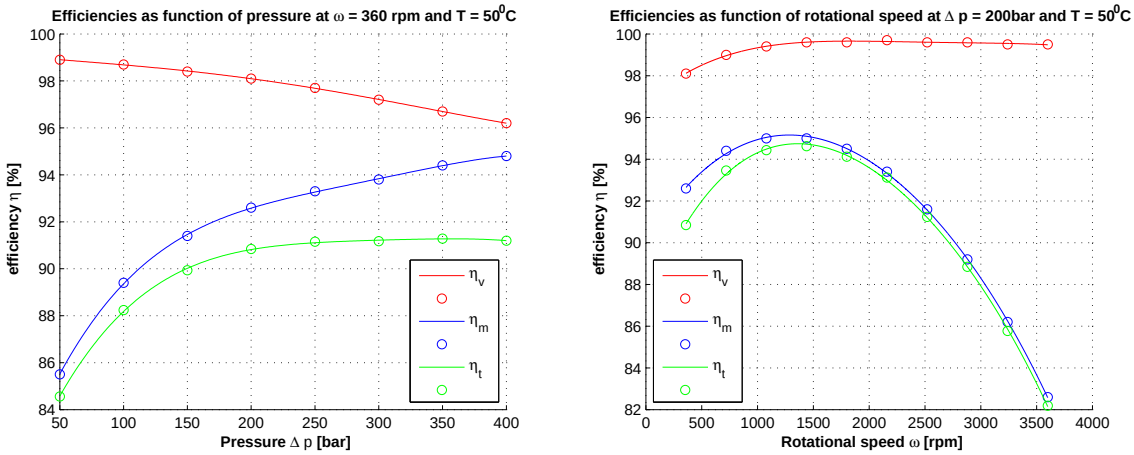


(a) as function of $\Delta p$ at $\omega = 360$rpm and $T = 50^{\circ}$C (b) as function of $\omega$ at $\Delta p = 200$bar and $T = 50^{\circ}$C

**Figure 3-6:** Pump efficiencies used for modeling

- The mechanical efficiency has an optimal value first it increases with rotational speed then it decreases. The damping and friction coefficients are not constant coefficients this causes the trend of the mechanical efficiency.

The energy losses due to the leakage flow and friction are dissipated in the form of heat into the fluid. This will result in a temperature increase of the fluids, until a certain equilibrium is reached. At this equilibrium point the heat dissipated into the fluid is equal to the dissipated heat into the environment. In the model the temperature of the fluid is assumed to be at this equilibrium point, and is thus constant.

### 3-3-1 Pump Inertia

The fluid inertia derived in section 3-2 can also be expressed as:

$$I_f = \frac{\Delta p}{\frac{dQ}{dt}} \tag{3-36}$$

The equations for volume flow $Q$ and pressure difference $\Delta p$ for the ideal pump are assumed here. The losses are taken into account later in the resistance element of the pump [8].

$$Q_{ideal} = V_g \omega \tag{3-37}$$

$$\tau_{ideal} = \Delta p V_g \tag{3-38}$$

The torque of the pump is also determined by the linear rotational momentum equation:

$$\tau = J_p \frac{d\omega}{dt} \tag{3-39}$$

The volume flow acceleration is determined from the volume flow equation giving:

$$\frac{dQ}{dt} = \frac{V_g d\omega}{dt} \tag{3-40}$$

Combining the equations for the torque 3-38 and 3-39 gives:

$$\Delta p V_g = J_p \frac{d\omega}{dt} \tag{3-41}$$

Now with equation 3-40 it is rewritten into [2]:

$$\frac{\Delta p}{\frac{dQ}{dt}} = \frac{J_p}{V_g^2} \tag{3-42}$$

The fluid inertia for the pump system is:

$$I_{hp} = \frac{J_p}{V_g^2} \tag{3-43}$$

### 3-3-2 Pump Capacitance

The pump capacitance is determined in a similar way as the hydraulic hose capacitance by equation 3-18. Only now hose volume is replaced with the sum of the starting volumes (before compression) of the pump cylinders. This results in the pump capacitance of:

$$C_{hp} = \frac{V_{g0}}{E_e} \tag{3-44}$$

The mechanical part of the pump is assumed as a rigid body, this is done because the pumps mechanical shaft stiffness is much larger than the fluid stiffness [2]. The walls of the pump are also assumed as rigid. Thus only the fluid bulk modulus and the entrapped air bulk modulus are taken into account to determine the effective bulk modulus, see equation A-22 in appendix A.

### 3-3-3 Pump Resistance

The pump losses are derived from the conservation of energy law. In order to derive these losses, the flow is assumed to be incompressible, in steady state and one dimensional. Work is done on the control volume by the pump. The heat exchange is neglected. There are no height differences and the small density change is assumed. Finally the cross section area of in and outlet is equal. With these assumptions the conservation of energy law reduces to, see equation A-14 in appendix A:

$$\frac{dW_s}{dt} = \rho U A \left(\hat{u} + \frac{p}{\rho}\right)_{out} - \rho U A \left(\hat{u} + \frac{p}{\rho}\right)_{in} \tag{3-45}$$

$$\frac{dW_s}{dt} = U A \left(p_{out} - p_{in}\right) - \rho U A \left(\hat{u}_{in} - \hat{u}_{out}\right) \tag{3-46}$$

Both pump losses mechanical and volumetric are taken into account in the second term in the reduction of internal energy:

$$\frac{dW_{pumplosses}}{dt} = \rho U A \left(\hat{u}_{in} - \hat{u}_{out}\right) \tag{3-47}$$

The pump losses are divided in mechanical and volumetric losses. The resistance that cause these losses are determined separately. The volumetric los is the volume flow lost due to leakage and is determined by:

$$Q_{lost} = Q_{ideal} - Q \tag{3-48}$$

Filling in equations 3-30, 3-34 and 3-37 into equation 3-48 gives:

$$Q_{lost} = V_g\omega - V_g\omega\left(1 - C_s\frac{\Delta p}{\mu\omega}\right) \tag{3-49}$$

$$Q_{lost} = \frac{V_g C_s}{\mu}\Delta p \tag{3-50}$$

The volumetric pump resistance is then:

$$R_{pv} = \frac{V_g C_s}{\mu} \tag{3-51}$$

The mechanical loss is the torque lost due the viscous effects and mechanical frictional losses and is determined by:

$$\tau_{lost} = \tau - \tau_{ideal} \tag{3-52}$$

Filling in equations 3-31, 3-33 and 3-38 into equation 3-52 gives:

$$\tau_{lost} = \Delta p V_g\left(1 + C_d\frac{\mu\omega}{\Delta p} + C_f\right) - \Delta p V_g \tag{3-53}$$

$$\tau_{lost} = C_d V_g \mu\omega + C_f V_g \Delta p \tag{3-54}$$

The lost torque consists of a term that is a function of the rotational speed and a term that is a function of the pressure. The pump mechanical resistances are then:

$$R_{pm1} = C_d V_g \mu \tag{3-55}$$

$$R_{pm2} = C_f V_g \tag{3-56}$$

## 3-4 Axial Piston Motor Model

The axial piston motor is very similar to the axial piston pump. The main difference is that the motor transforms the fluid power into mechanical rotational power at the output. An axial piston motor is a so called fixed displacement motor, like the pump. The control volume of the motor has fluid power under high pressure as input. Rotational mechanical power and fluid power under low pressure are the outputs of the control volume, see figure 3-7.

There are 3 main equations relating the input and output of a motor to each other [8].

$$Q = \frac{V_g\omega}{\eta_v} \tag{3-57}$$

$$\tau = \Delta p V_g \eta_m \tag{3-58}$$

$$P_{in} = \Delta p Q \tag{3-59}$$

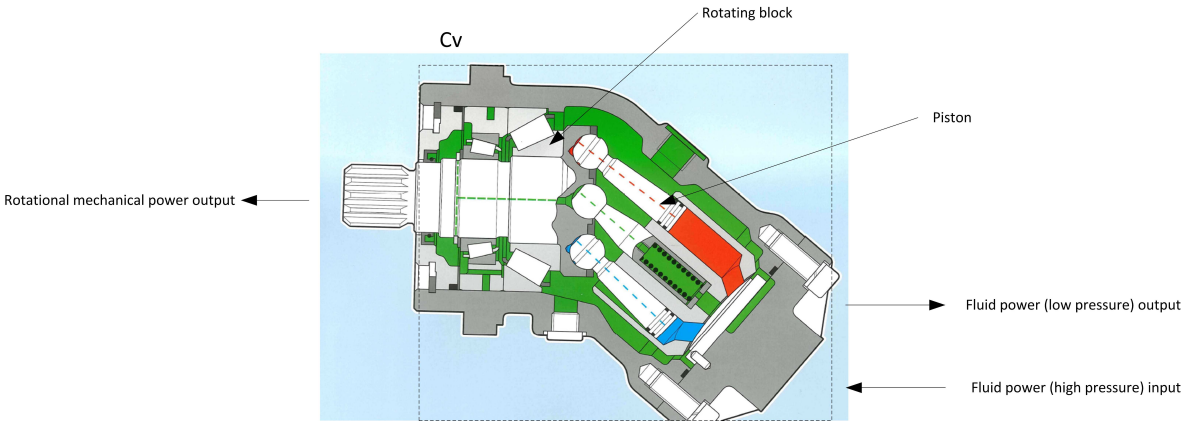


**Figure 3-7:** Control volume axial piston motor [7]

The total losses of the energy conversion from hydraulic to mechanical energy is built up in the same way as for a pump, see section 3-3 [8]. There are some small differences in the efficiency equations. The equation used to determine the mechanical efficiency is [8]:

$$\eta_m = 1 - C_d \frac{\mu\omega}{\Delta p} - C_f \tag{3-60}$$

Like the pump the 2 dimensionless coefficients are derived from efficiency test data supplied by the manufacturer, see confidential supplement

The equation used to determine the volumetric efficiency is [8]:

$$\eta_v = \frac{1}{1 + C_s \frac{\Delta p}{\mu\omega}} \tag{3-61}$$

The dimensionless coefficient of slip Cs is also derived from efficiency test data supplied by the manufacturer, see confidential supplement. The total efficiency is the product of the mechanical and volumetric efficiency:

$$\eta_t = \frac{1 - C_d \frac{\mu\omega}{\Delta p} - C_f}{1 + C_s \frac{\Delta p}{\mu\omega}} \tag{3-62}$$

The energy losses due to the leakage flow and friction are dissipated in the form of heat into the fluid. This will result in a temperature increase of the fluids, until a certain equilibrium is reached. At this equilibrium point the heat dissipated into the fluid is equal to the dissipated heat into the environment. In the model the temperature of the fluid is assumed to be at this equilibrium point and is thus constant.

### 3-4-1 Motor Inertia and Capacitance

The equations used for the pump inertia and capacitance are also valid for the motor inertia and capacitance [2]. These equations are thus also used for the motor model, see section 3-3.

### 3-4-2 Motor Resistance

The motor losses are derived from the conservation of energy law. In order to derive these losses, the flow is assumed to be incompressible, in steady state and one dimensional. Work is done by the control volume on the motor. The heat exchange is neglected. There are no height differences and the small density change is assumed. Finally the cross section area of in and outlet is equal. With these assumptions the conservation of energy law reduces to, see equation A-14 in appendix A:

$$-\frac{dW_s}{dt} = \rho U A \left(\hat{u} + \frac{p}{\rho}\right)_{out} - \rho U A \left(\hat{u} + \frac{p}{\rho}\right)_{in} \tag{3-63}$$

$$\frac{dW_s}{dt} = U A \left(p_{in} - p_{out}\right) + \rho U A \left(\hat{u}_{in} - \hat{u}_{out}\right) \tag{3-64}$$

Like for the pump the losses for the motor are taken into account in the second term in the reduction of internal energy:

$$\frac{dW_{motorlosses}}{dt} = \rho U A \left(\hat{u}_{in} - \hat{u}_{out}\right) \tag{3-65}$$

The motor losses are again divided in mechanical and volumetric losses. The resistance that cause these losses are determined separately. The volumetric los is the volume flow lost due to leakage and is determined by:

$$Q_{lost} = Q - Q_{ideal} \tag{3-66}$$

Filling in equations 3-37, 3-57 and 3-61 into equation 3-66 gives:

$$Q_{lost} = V_g \omega \left(1 + C_s \frac{\Delta p}{\mu \omega}\right) - V_g \omega \tag{3-67}$$

$$Q_{lost} = \frac{V_g C_s}{\mu} \Delta p \tag{3-68}$$

The equation for the volumetric motor resistance is then the same as for the volumetric pump resistance.

$$R_{mv} = \frac{V_g C_s}{\mu} \tag{3-69}$$

The mechanical loss is again the torque lost due the viscous effects and mechanical frictional losses and is determined by:

$$\tau_{lost} = \tau_{ideal} - \tau \tag{3-70}$$

Filling in equations 3-38, 3-58 and 3-60 into equation 3-70 gives:

$$\tau_{lost} = \Delta p V_g - \Delta p V_g \left(1 - C_d \frac{\mu \omega}{\Delta p} - C_f\right) \tag{3-71}$$

$$\tau_{lost} = C_d V_g \mu \omega + C_f V_g \Delta p \tag{3-72}$$

This gives the same result as for the pump. The lost torque again consists of a term that is a function of the rotational speed and a term that is a function of the pressure. The motor mechanical resistances are then:

$$R_{mm1} = C_d V_g \mu \tag{3-73}$$
$$R_{mm2} = C_f V_g \tag{3-74}$$

## 3-5 Nozzle Model

At the nozzle the hydraulic potential energy is transformed into hydraulic kinetic energy. A typical nozzle is seen in figure 3-8. The control volume of the nozzle is much smaller than the control volume of the hydraulic hose sub system. Therefore the inertia and capacitance of the nozzle are much smaller, and are neglected.

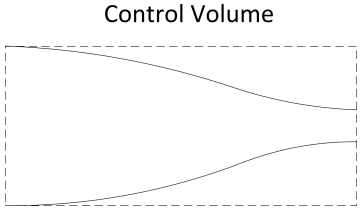


**Figure 3-8:** Typical nozzle geometry

This means that only the resistance of the nozzle is taken into account. The starting point to determine the resistance is the conservation of energy law as given in appendix A. Like for the hydraulic hose the flow is assumed to be in steady state, incompressible with one dimensional in and outflow ports. In addition to that no work is done and the heat exchange is neglected. When the flow is also assumed to be frictionless (no viscous effects) the conservation of energy law is reduced to the Bernoulli equation [11].

$$\left(\frac{p}{\rho} + \frac{1}{2}U^2 + gz\right)_{in} = \left(\frac{p}{\rho} + \frac{1}{2}U^2 + gz\right)_{out} \tag{3-75}$$

This is for an ideal nozzle with no losses. If the height difference is neglected, the following equation is derived for the velocity at the nozzle exit:

$$\sqrt{\frac{2\Delta p_{inid}}{\rho} + U_{in}^2} = U_{jetid} \tag{3-76}$$

In reality the viscous effects cannot be neglected. The nozzle losses, that are caused by viscous effects of the fluid, are described by the velocity coefficient [11]. For well-designed nozzles the velocity coefficient ranges from 0.92 to 0.98 [11]. This then gives the following equation for the jet velocity.

$$C_v \sqrt{\frac{2\Delta p_{in}}{\rho} + U_{in}^2} = U_{jet} \tag{3-77}$$

The water jet coming out of a nozzle will in reality keep converging. This carries on till a certain minimum jet diameter is reached the so called vena contracta. The effect of this on the jet velocity is that it keeps on increasing until the minimum diameter is reached. The vena contracta phenomena does not influence the nozzle efficiency. The real jet velocity is now determined by [12]:

$$U_{jet} = \frac{Q}{C_c A_n} \tag{3-78}$$

Where Cc takes into account the effect of the vena contracta on the jet velocity. Filling this into equation 3-77 gives:

$$C_v \sqrt{\frac{2\Delta p_{in}}{\rho} + U_{in}^2} = \frac{Q}{C_c A_n} \tag{3-79}$$

The pressure difference with the ideal pressure is determined by combining equation 3-76 and 3-79.

$$\Delta p_{ndiff} = \Delta p_{in} - \Delta p_{inid} \tag{3-80}$$

$$\Delta p_{ndiff} = \frac{\rho}{2} \left( \frac{Q}{A_{out}} \right)^2 \frac{1 - C_c^2 C_v^2}{C_c^2 C_v^2} \tag{3-81}$$

Both the velocity and contraction coefficient depend on the geometrical shape of the nozzle. From equation 3-81 it is seen that both coefficients have an influence on the jet velocity. However, only the velocity coefficient has an influence on the nozzle efficiency [12]. The nozzle efficiency is determined by:

$$\Delta p_{nloss} = \frac{\rho}{2} \left( \frac{Q}{A_{out}} \right)^2 \frac{1 - C_v^2}{C_v^2} \tag{3-82}$$

$$\eta_n = 1 - \frac{\Delta p_{nloss}}{\Delta p_{in}} \tag{3-83}$$

Nozzles with a larger resistance result in larger losses at the nozzle and an increase in actual pressure, see equation 3-82. The pressure loss at the nozzle is a non-linear function of the volume flow. This makes the nozzle resistance element a non-linear model. This resistance should thus be determined separately for every time step in the simulation.

## 3-6 Rotor Model

A model for the rotor inertia is also developed. This was done because of the large influence of the rotor inertia on the dynamic behaviour of the complete system. The inertia of the total rotor is determined with:

$$J = B_b m_{blade} C_m^2 + J_{shaft} \tag{3-84}$$

Filling in the rotor values from table 2-1 and the inertia of the shaft 3.6 kgm2 gives an inertia of 206.2 kgm2. The losses at the rotor are taken into account when the transmission model is coupled to the rotor model, this is explained in section 7-1.

# Chapter 4

# Modeling of Full Transmission Model

## 4-1 Introduction

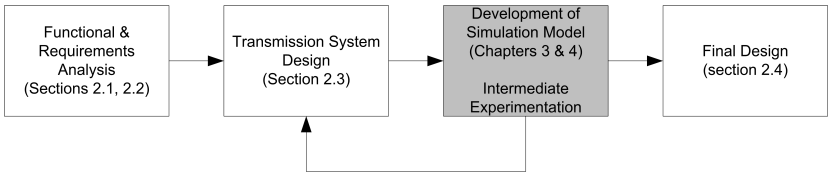


**Figure 4-1:** Chapter 4 highlighted in project approach flow chart

The goal was to develop a model that represents the physical transmission as simple as possible but not simpler. This goal was inspired by Einstein; "make everything as simple as possible, but not simpler". This resulted in a model that contains all the elements that have a significant influence on the losses and the dynamic behavior of the transmission. Elements that have a minor influence on the complete system losses and dynamic behavior were neglected.

In order to achieve this goal, five transmission models were developed from the sub system models of chapter 3. The developed transmission models have an increasing level of complexity. The step function response and the Bode plots of the models were then compared. This was done in order to find the model that gives the best representation of the transmission with as little elements as possible. During the design process the transmission model was also used to analyze the dynamic behavior and estimate the natural frequencies of the transmission system with rotor.

## 4-2 Modeling using the Bond Graph Language

This section gives a brief description of the modeling language used to develop the different transmission models. The different developed models are then described next. The sub systems within the black dotted line of figure 3-2 together with the rotor inertia represent

the system for which the different models are developed. The inputs are the power from the rotor and the power from the electric motor that drives the boost pump. The output is the power from the nozzle.

The Bond Graph language is a suitable modeling language in which models can be developed and compared with little effort. The bond graph method is based on the fact that physical systems interact with each other by transmitting power to one another [13]. The bond graph language is a language were physical systems are described by ideal physical elements. These ideal physical elements are interconnected to each other by a network of bonds, that represent the energy flow between the elements. Different physical domains are modeled with the same elements. It is therefore relatively simple to model a system that contains sub systems with different energy domains, like the transmission. The advantages of using the bond graph language for modeling physical systems such as the transmission are [13]:

- The same symbols and elements are used to represent the power interaction in a large selection of physical systems.
- A complex system with several energy domains is converted into a graphical diagram that shows the energetic structure of the system.
- The method is applicable for both linear and non-linear systems.
- From the bond graph it is directly visible for each element which variables are output (dependent) and input (independent) variables.
- The bond graph method uses an algorithmic procedure that combines the mathematical equations of each element into mathematical equations that describe the complete system. This can either be done manually or it can be done by a software program suitable for bond graph modeling such as 20-sim.

A further explanation of the Bond Graph language is given in appendix C. A detailed explanation on the Bond Graph language is given in "Modeling, Simulation and Analysis of Dynamic Systems" by E. Pedersen [13].

Five models were developed with increasing complexity. The block diagram of the four simplest developed models are shown in figure 4-2. Each of the blocks represents one of the sub systems for which a model was developed in chapter 3. The elements modeled in each sub systems are indicated in table 4-1. Model five is the most complex model in which several other subsystems like the boost systems are also modeled, see figure 4-3. The modeled elements in each sub systems of model 5 are also indicated in table 4-1.

## 4-3 Analysis of Transmission Model

The analysis of the five models is based on step function and Bode plot results. This was done to select the model that gives the best representation of the transmission with as little elements as possible. The step function results were verified with steady state calculations. The Bode plot results were verified with a simplified equation that determines the natural frequency of a hydrostatic transmission.

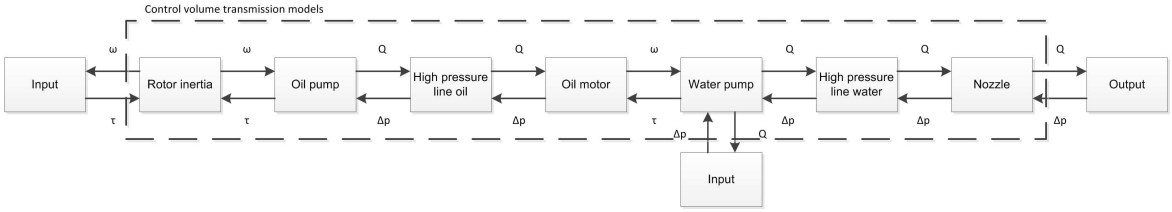


**Figure 4-2:** Block diagram of transmission models 1, 2, 3 and 4. Table 4-1 shows the modeled elements for each model

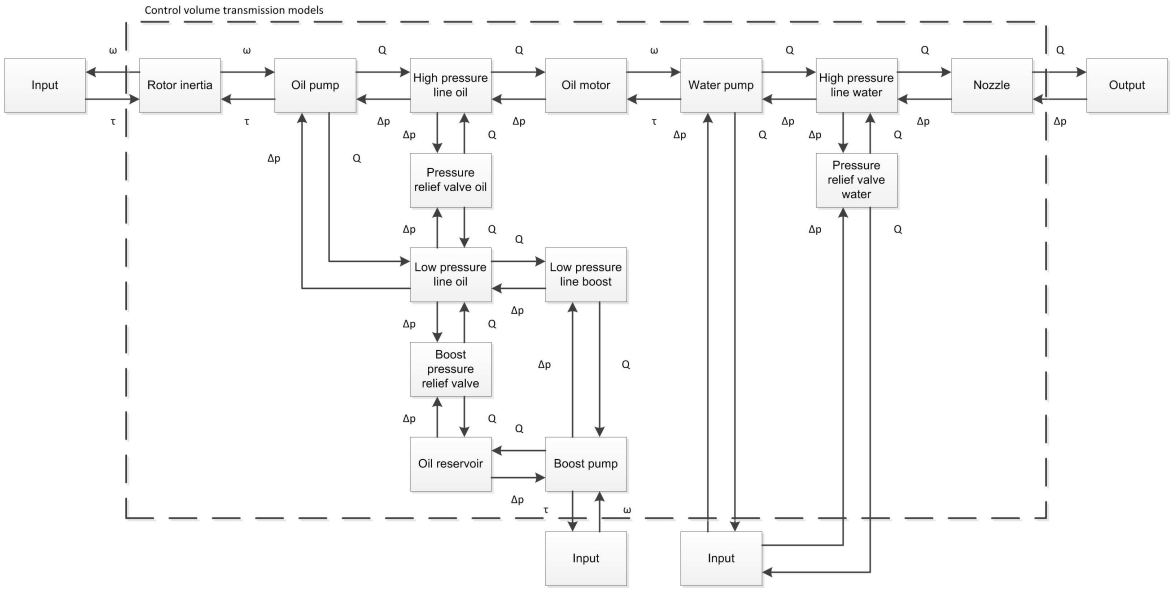


**Figure 4-3:** Block diagram of transmission models 5. Table 4-1 shows the modeled elements for model 5

| | Model 1 | Model 2 | Model 3 | Model 4 | Model 5 |
|---|---|---|---|---|---|
| Rotor | $I$ | $I$ | $I$ | $I$ | $I$ |
| Oil pump | $R_v$, $R_m$ | $R_v$, $R_m$ | $R_v$, $R_m$ | $R_v$, $R_m$ | $I$, $C$, $R_v$, $R_m$ |
| High pressure line oil | $C$ | $C$, $R$ | $I$, $C$, $R$ | 8 lumps: $I$, $C$, $R$ | $I$, $C$, $R$ |
| Oil motor | $R_v$, $R_m$ | $R_v$, $R_m$ | $R_v$, $R_m$ | $R_v$, $R_m$ | $I$, $C$, $R_v$, $R_m$ |
| Water pump | $R_v$, $R_m$ | $R_v$, $R_m$ | $R_v$, $R_m$ | $R_v$, $R_m$ | $I$, $C$, $R_v$, $R_m$ |
| High pressure line water | $C$ | $C$, $R$ | $I$, $C$, $R$ | 8 lumps: $I$, $C$, $R$ | $I$, $C$, $R$ |
| Nozzle | $R$ | $R$ | $R$ | $R$ | $R$ |
| Pressure relief valve oil | - | - | - | - | Pos valve |
| Low pressure line oil | - | - | - | - | $I$, $C$, $R$ |
| Boost pressure relief valve | - | - | - | - | Pos valve |
| Low pressure line boost | - | - | - | - | $I$, $C$, $R$ |
| Oil reservoir | - | - | - | - | $C$ |
| Boost pump | - | - | - | - | $I$, $C$, $R_v$, $R_m$ |
| Pressure relief valve water | - | - | - | - | Pos valve |

**Table 4-1:** Modeled elements in each sub system. $I$ = Inertia, $C$ = Capacitance, $R_m$ = Mechanical resistance, $R_v$ = Volumetric resistance, Pos valve = Position valve

The step function applied to the models was a step from 0Nm to 600Nm at the input of the rotor, see figure 4-2 and 4-3. Some of the simulation results of this comparison are shown in figure 4-4 and 4-5. The numbers in the legend of the graphs refer to the model numbers as indicated in table 4-1. Figure 4-4 shows the power response at the rotor and the pressure response at the nozzle after subtracting the nozzle losses. Figure 4-5 shows the response of the rotational speed of the rotor.

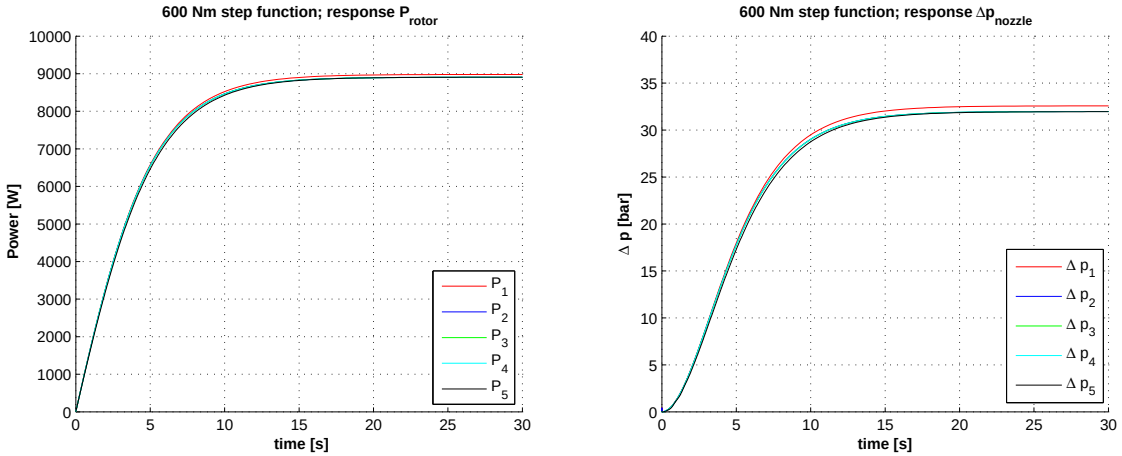


(a) (b)

**Figure 4-4:** Response to a 600Nm step function of the power input at the rotor and of the pressure at the nozzle taking into account the nozzle losses

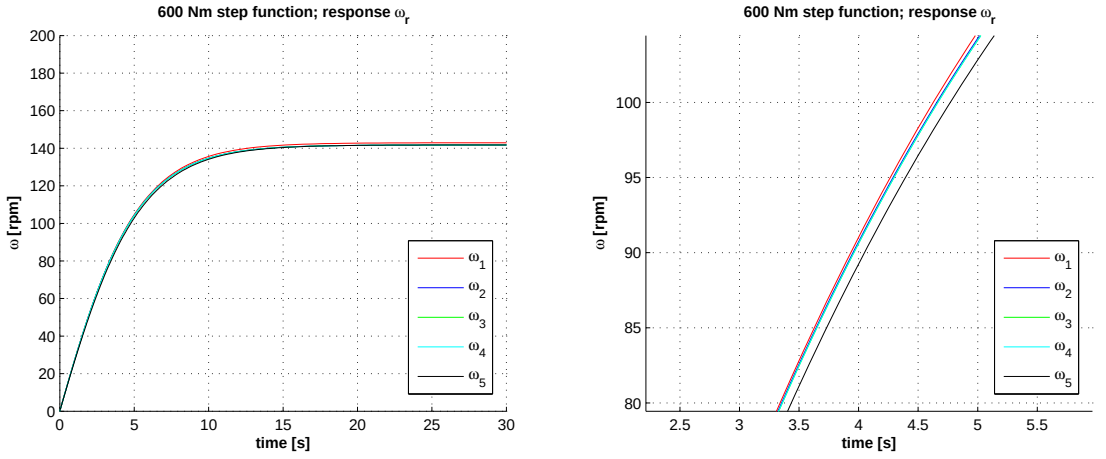


(a) (b)

**Figure 4-5:** Response to a 600Nm step function of the rotor rotational speed and a zoomed in graph of the rotor rotational speed

The step function response of the models are in good agreement with each other. From the graphs the following findings were made:

- Neglecting the losses in the hydraulic hose of the fluids as in model 1 results in a slightly larger pressure at the nozzle compared to the other models, see figure 4-4.

- The steady state values of models 2, 3, 4 and 5 are approximately the same and are reached around 18-22 seconds.
- The step function response of models 2, 3 and 4 are the same.
- A minor difference in the step function response of the advanced model is visible in the right zoomed in graph of figure 4-5. The added sub systems and elements when compared to the other models cause the minor difference in the results of the dynamic response. From this graph it is concluded that all the extra sub systems and elements have a minor influence on the step function response.

Figure 4-6 shows the results of the step function response for model 3. In the figure the power at different points in the transmission is shown. This gives a good impression of the step function response throughout the transmission. The losses at steady state operation are also determined from this figure.

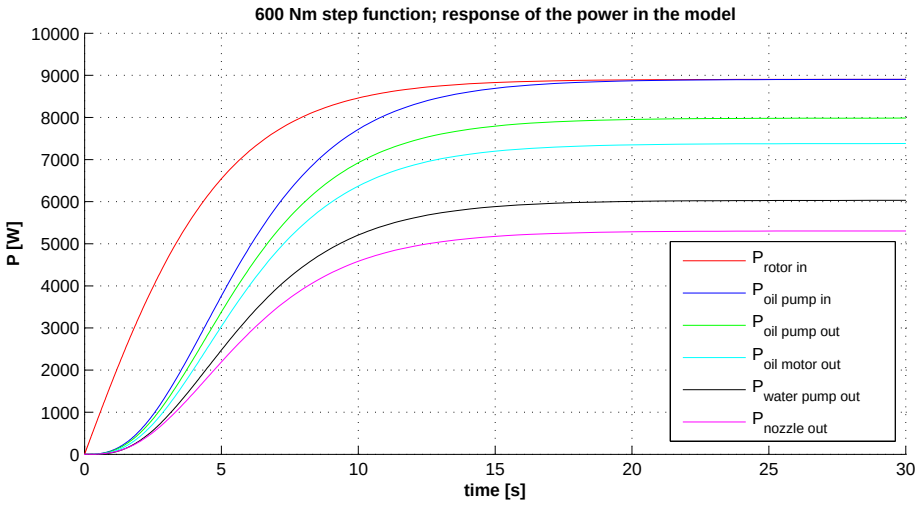


**Figure 4-6:** Power response of model 3 to a 600Nm step function at different points throughout the transmission

From figure 4-6 the following finding were made:

- The difference in response between the power input at the rotor and the power input at the oil pump clearly indicates the influence of the rotor inertia on the step function response.
- The complete system steady state efficiency is 60%. These losses occur for the largest part in the oil pump and water pump. The losses in the oil motor and the nozzle also make a significant contribution to the total losses.

The steady results of the step function are reached after 18 to 22 seconds. The steady state results from model 3 were verified with steady state calculations, see table 4-2.

The minor differences between the results are probably caused by the fact that the pressure losses in all the hoses have not been taken into account in the steady state calculations. This also shows that the pressure losses in the hoses are insignificant compared to the total losses.

| Power [kW] | Steady state calculations | Steady state results model 3 |
|---|---|---|
| $P_{rotor}$ | 8.92 | 8.90 |
| $P_{oilpumpout}$ | 8.00 | 7.98 |
| $P_{oilmotorout}$ | 7.40 | 7.38 |
| $P_{waterpumpout}$ | 6.05 | 6.03 |
| $P_{nozzleout}$ | 5.34 | 5.31 |

**Table 4-2:** Verification of the steady state simulation results of model 3 with steady state calculations

The Bode diagrams of the models were compared next. The models are non-linear due to the losses at the nozzle as was shown in section 3-5. This means that Bode plots differ at different input values (operational points). In order to compare the Bode plots of the 4 models, the models were linearized at one operational point of 600Nm torque at the input. This is shown in figure 4-7. Model 5 could not be linearized because of the valves in the model which make the model discrete. The model numbers in the legend again refer to the numbers in table 4-1.

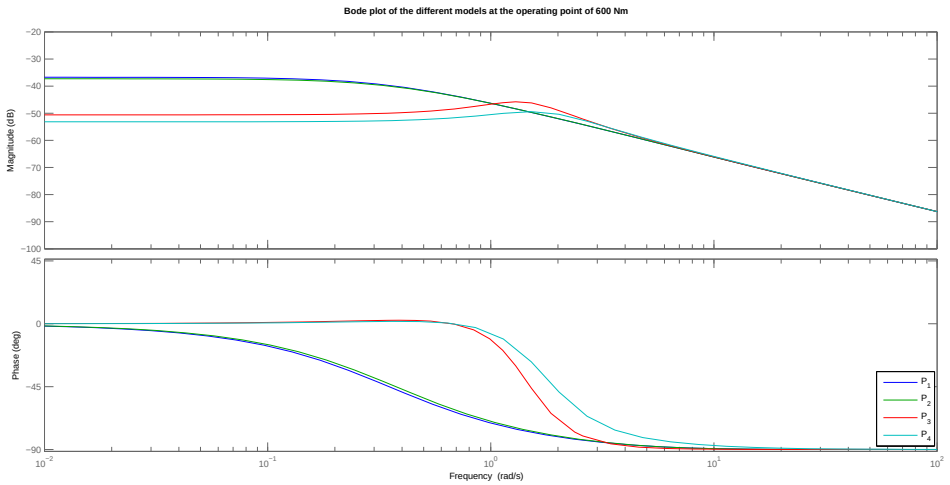


**Figure 4-7:** Bode plots of the different models at operational point of 600Nm torque at the input

The following findings were made from this Bode plot comparison:

- The Bode plots show that all models are strongly damped and stable.
- The Bode plots of models 1 and 2 are approximately the same. The difference between the Bode plots of models 1 and 2 compared to model 3 and 4 is caused by the fluid inertia that is taken into account in models 3 and 4 and not in models 1 and 2.
- The Bode plots of models 3 and 4 are in good agreement with each other. The small difference between the Bode plots of model 3 and 4 is caused by the fluid flow through the hydraulic hoses that are divided in 8 lumps in model 4 and in 1 lump in model 3.
- The lowest natural frequencies of models 1 and 2 are 0.35 and 0.38 rad/s respectively. The lowest natural frequencies of models 3 and 4 are 1.28 and 1.36 rad/s respectively.

The difference between the lowest natural frequency of models 1 and 2 compared to model 3 and 4 is caused by the fluid inertia that is taken into account in models 3 and 4 and not in models 1 and 2.

- The second natural frequency of model 3 and 4 is less damped then in models 1 and 2.

In order to verify the Bode plots of the models a simplified equation that determines the lowest natural frequency of a hydrostatic transmission was used [2, 14].

$$\omega_n = \sqrt{\frac{V_{g1}^2 E_e}{J V_0}} \tag{4-1}$$

This simplified equation is only valid for the natural frequency of the closed-loop oil circuit together with the rotor. It is not valid for the open loop water circuit. Therefore it was only possible to verify the natural frequency of the closed-loop oil circuit connected to the rotor. The natural frequency of the hydrostatic transmission is then determined by the inertia of the rotor $J$, the displacement of the hydraulic oil pump $V_{g1}$, the effective bulk modulus $E_e$ and the fluid volume in the hydraulic oil hose $V_0$. For the operational point of 600Nm this results in a natural frequency $\omega_n$ of 1.47rad/s.

In order to make a valid comparison, the influence of the water circuit on the lowest natural frequency of the models was minimized by making the length of the water hoses very short so that the water circuit acted as a rigid body. The lowest natural frequency of the model increased slightly due to the minimized influence of the water circuit. However, the natural frequencies from the models remained slightly lower.

The model that gives the best representation of the transmission with as little elements as possible is model 3. In models 1 and 2 some elements are neglected that do affect the total system losses and the dynamic behavior of the system. In models 4 and 5 some elements are modeled that only contribute to the complexity of the model while the total system losses and dynamic behavior of these models are almost exactly the same as in model 3.

From this model analysis it was also concluded that the main elements that determine the dynamic behavior of the transmission with rotor are:

- Rotor inertia, see section 3-6.
- Effective compressibility of the oil and water in the hoses, see section 3-2.
- Damping caused by the nozzle, see section 3-5. The open connection with the atmosphere at the nozzle output causes this strongly damped response of the model. For example a small pressure increase in the water circuit will directly cause the jet velocity to increase, and thus the flow in the water circuit. This damps the pressure fluctuation immediately.

The main elements that determine the transmission losses are:

- The oil pump, water pump and oil motor resistances which are modeled as mechanical and volumetric resistances, see sections 3-3 and 3-4.

- The nozzle resistance, see section 3-5.

The pressure losses in the hose and the fluid inertia are also modeled in model 3. The influence of these elements on the dynamic behavior and the transmission losses is far less than the above mentioned elements.

# Chapter 5

# The Demonstration Setup

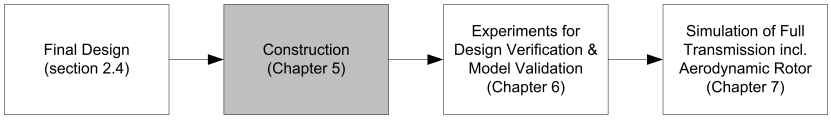


**Figure 5-1:** Chapter 5 highlighted in project approach flow chart

The transmission demonstration set-up was built in the water laboratory at the Civil Engineering and Geosciences faculty at TU Delft. The construction occurred in several phases with intermediate experiments. Due to these intermediate experiments, the majority of the practical challenges were identified and resolved before the final construction phase started. The construction of the demonstration set-up was a process that involved many challenges with a practical origin. The most time consuming challenge was to reduce the measured noise on the output signal of the sensors. Initially the noise on the signals was so dominant that the sensor signals were useless. This noise was caused by two frequency converters used in the transmission set-up. The noise was finally minimized to acceptable values (approximately 1% of the maximum sensor output signal) by connecting al the sensors to an earthed wire and by shielding the frequency converters and their output cables from the transmission.

In figure 5-2 an overview picture of the demonstration set-up in the laboratory is shown together with the hydraulic diagram of the transmission. The main transmission components are numbered in the hydraulic diagram and the position of these components in the demonstration set-up are shown by arrows. The position of the main transmission components in the final test turbine are also indicated in figure 5-2. The specifications, limitations and control method of the main transmission components are given in table 5-1.

The rotor is simulated by an electrical asynchronous motor in the demonstration set-up. The rotational speed of the motor can be regulated between 0-200rpm, by setting the frequency of the output current from the converter that feeds motor. This can either be done manually or automatically with the measurement and control computer. During normal operation of the transmission this is the only varied property. The other controllable properties are kept at a constant setting during normal operation. The other controllable properties are:

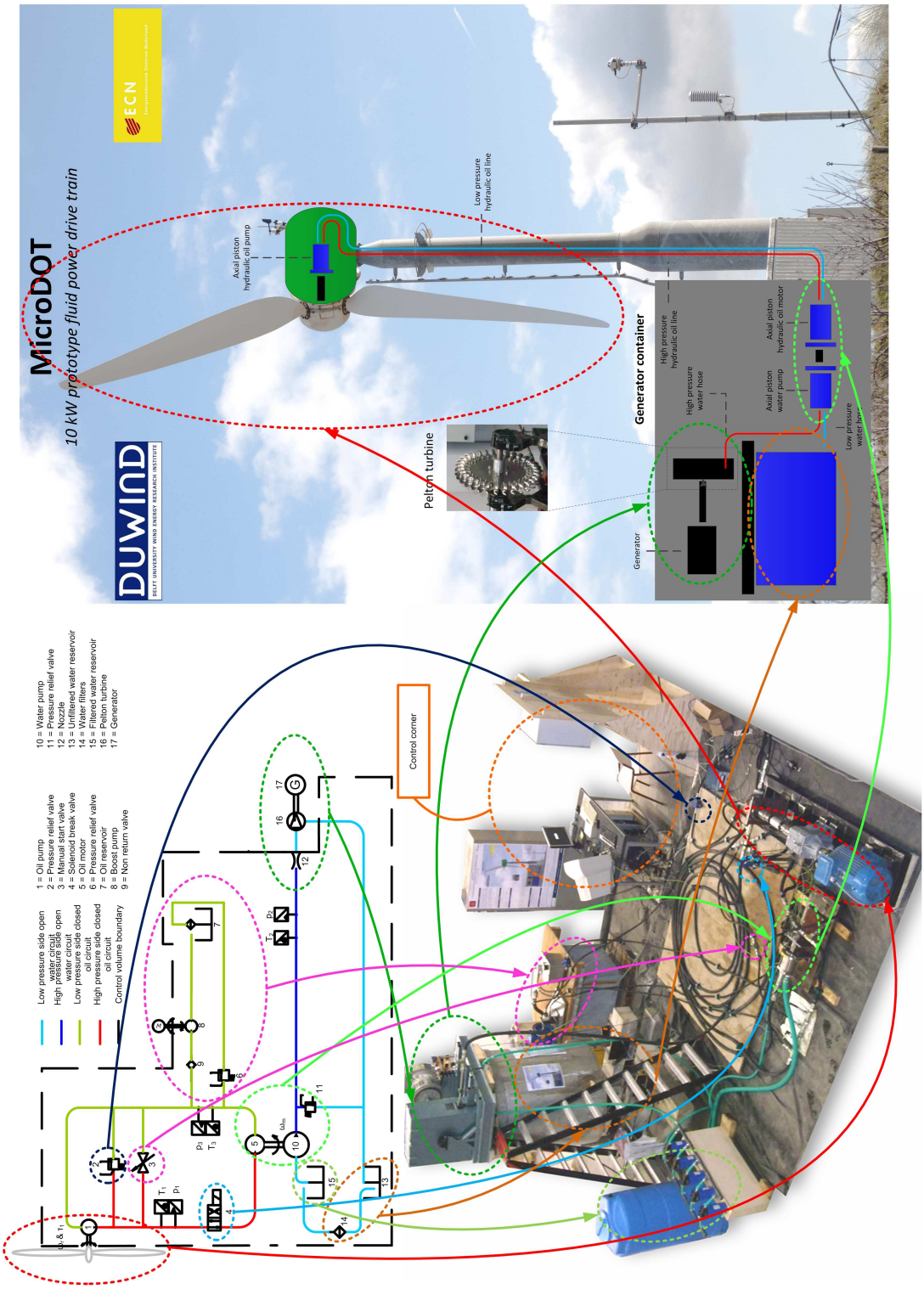


**Figure 5-2:** Hydraulic diagram, overview picture of the demonstration set-up and test turbine at ECN

| Component | Specifications | Control | Limitations |
|---|---|---|---|
| 1.Oil pump | Fixed displacement 180cc/rev | Manual & automatic control of rpm | 350bar & 3600rpm |
| 2.Pressure relief valve | Direct operated | Manual control of opening pressure | 315bar & 120l/min |
| 3.Start-up bypass valve | Manual ball valve | Manual control of position | 300bar |
| 4.Solenoid break valve | Directional valve 4/2 way | Manual & automatic setting of position | 210bar & 120l/min |
| 5.Oil motor | Fixed displacement 16cc/rev | No control | 350bar & 8000rpm |
| 6.Pressure relief valve | Direct operated | Manual control of opening pressure | 315bar & 120l/min |
| 7.Oil reservoir and filter | 20 liters capacity | No control | 20 liters |
| 8.Boost pump | Gear pump 14cc/rev | Manual & automatic control of rpm | 250bar & 3000rpm |
| 9.Non return valve | Pretension 0.5bar | No control | 400bar |
| 10.Water pump | Fixed displacement 70.3cc/rev | No control | 160bar & 1800rpm |
| 11.Pressure relief valve | Direct operated | Manual control of opening pressure | 200bar & 100l/min |
| 12.Nozzle | Fixed diameter nozzle | No control | - |
| 13.Unfiltered $H_2O$ reservoir | Volume $2m^3$ | No control | $2m^3$ |
| 14.Water filters | 5 x 10 micron filter elements | No control | 5.5bar & 60l/min |
| 15.Filtered water reservoir | Volume $0.5m^3$ | No control | 0.5m3 |
| 16.Pelton turbine | Pitch circle diameter 0.4m | Manual & automatic control of rpm | - |
| 17.Generator | Synchronous 8kW generator | Manual & automatic control of rpm | 10kVA & 2000rpm |

**Table 5-1:** Specifications, limitations and control method of the main transmission components

- The opening pressure of the pressure relief valve in the high pressure line of the oil circuit is set manually between 1-315bar. It regulates the maximum possible pressure in the high pressure oil line. Under normal operation conditions the opening pressure is set at 210bar.

- The position of the start-up bypass valve is set manually in open or closed position. When the valve is in open position, an open connection exists between the high and low pressure lines of the oil circuit. This open connection is required during start-up of the transmission with the rotor, see section 2-2-2. The closed position is the normal operation condition.

- The position of the solenoid break valve is set manually or automatically in the open or closed position. When the solenoid is excited, the valve is in open position and the oil flows freely to the oil motor. This is the normal operation condition. When the valve is not excited, the valve is in close position, obstructing the oil flow to the oil motor. This will keep the rotor stopped or stop it from rotating, see section 2-4.

- The opening pressure of the pressure relief valve in the low pressure line of the oil circuit is set manually between 1-25bar. It keeps the pressure in the low pressure oil line at a constant set value, see section 2-4. Under normal operation conditions this pressure is set at 10bar.

- The rotational speed of the boost pump is controlled manually or automatically. This regulates the oil flow which is required for cooling, see section 2-4. Before start-up all the hoses of the oil circuit are filled with oil by the pump. Under normal condition operation it is set at a constant value of 1000 rpm.

- The opening pressure of the pressure relief valve in the high pressure line of the water circuit is set manually between 1-200bar. It regulates the maximum possible pressure in the high pressure water line. Under normal operation conditions the opening pressure is set at 50bar.
- The resistance of the electrical load connected to the generator can also be regulated manually or automatically. This controls the rotational speed of the generator and the Pelton turbine, which influences the conversion efficiency at the Pelton turbine, see section 2-2-3. However this was not researched during the experiments for this thesis.

The sensors and their position in the transmission are also indicated in the hydraulic diagram of figure 5-2. The sensor signals are processed and logged by the measurement and control computer. There are two type of sensors used; analogue and pulse sensors. The analogue sensors give a continuous DC voltage signal that is linearly related to the measured property. The pulse sensors give a pulse when a metal object comes close to the magnetic field of the pulse sensor. The pulse sensor were only used for measuring rotational speeds in steady state conditions. Appendix E gives an explanation why this sensor is only suitable for steady state conditions. The measured properties, the type, the limitation and accuracy of each sensor are given in table 5-2.

| Measured property | Type | Measuring range | Accuracy (without noise) |
|---|---|---|---|
| Pressure $p1$ | Analogue sensor | 0-250bar | $<$ 2.5 bar |
| Pressure $p3$ | Analogue sensor | 0-25bar | $<$ 0.25 bar |
| Pressure $p2$ | Analogue sensor | 0-250bar | $<$ 2.5 bar |
| Temperature $T1$ | Analogue sensor | 0-100°C | $<$ 1 oC |
| Temperature $T2$ | Analogue sensor | 0-100°C | $<$ 1 oC |
| Temperature $T3$ | Analogue sensor | 0-100°C | $<$ 1 oC |
| Torque at oil pump $t1$ | Analogue sensor | -1000-1000Nm | $<$ 10 Nm |
| Rotational speed $?r$ | Pulse sensor | 0-3000rpm | - |
| Rotational speed $?m$ | Pulse sensor | 0-3000rpm | - |
| Electrical frequency $?e$ | Analogue sensor | 0-50Hz | $<$ 0.5 Hz |

**Table 5-2:** Measured property, sensor type, measuring range and accuracy of each sensor in the demonstration set-up

# Chapter 6

# Experimental Results and Validation of the Model

## 6-1 Introduction

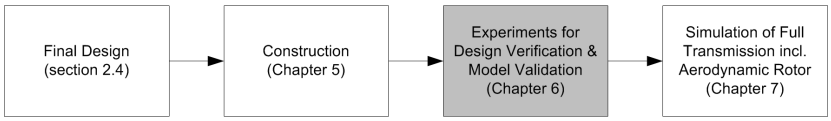


**Figure 6-1:** Chapter 6 highlighted in project approach flow chart

After the construction of the demonstration set-up in the laboratory was completed several experiments were executed with the transmission. Main purposes of these experiments were:

- Validation of simulation model with steady state experiments.
- Validation of the passive control strategy as described in section 2-3-2.
- Validation of the simulation model described in chapter 3 with dynamic experiments.
- Validation of the practical transmission requirements defined in section 2-2-4. This especially concerns the start-up system that needs to reduce the start-up torque for the rotor.

In table 6-1 an overview of the different experiments and the purpose of these experiments is given, together with the indication in which section the experiments are discussed.

## 6-2 Validation of the Model in Steady State Conditions

First the modifications made to the original model are described briefly in section 6-2-1 and in detail in appendix D. The steady state experiment results are then compared to the modified

| Experiments | Main purpose | Explained in section |
|---|---|---|
| Steady state | Prove passive control strategy | 6-2 |
| Sinusoidal | Validate dynamic model | 6-3 |
| Step function | Validate dynamic model | 6-3 |
| Random input | Validate dynamic model | 6-3 |
| Break | Validate practical transmission requirements | 6-4-1 |
| Start-up | Validate practical transmission requirements | 6-4-2 |

**Table 6-1:** Overview of the experiments and the purpose of the experiments

model, see section 6-2-2. This comparison validates the transmission model under steady state conditions. The experiment results and the validated model are then used to prove the passive control strategy under steady state conditions, see section 6-2-3.

### 6-2-1 Modifications in the Original Model

First a validation between steady state experiments and the original model was executed. Based on this comparison some modifications were made to the model. A brief explanation of these modifications is given here. In this validation the predicted pressures, torque and rotational speeds of the model were compared to the measured values of the steady state experiments. In general the trend of the measured values was in agreement with the predicted values of the original model. However, some significant differences between the predicted efficiencies and the measured efficiencies were found at several points in the transmission. As a consequence of these differences modifications were made to the efficiency equations in the model. The efficiency equations in the modified model are based on polynomial fittings of the measured values in the steady state experiments. This means that the model gives accurate results for the input range $\omega_r$ used in the experiments. Outside of this range the results predicted by the modified model are not validated with measurements and are thus less reliable. In the final modified model all the efficiencies are calculated as a function of the input (rotational speed of the oil pump) $\omega_r$ and the nozzle diameter $D_n$. The inertia and capacitance elements of the model described in chapter 4 are not adjusted in the modified model. All the results shown in this chapter are results of the modified model. A detailed explanation of these modifications and results of the original model are given in appendix D.

### 6-2-2 Steady State Experiments

The procedure during the steady state experiments was:

- The controllable input of the transmission $\omega_r$ was set at 20rpm and increased with steps of 10rpm until the maximum allowable pressure in the oil circuit of 210bar was reached.
- At each of these input settings the steady state measurements were logged.

The steady state experiments were carried out for three different nozzle diameters. The three different nozzle diameters are:

- 4.24mm
- 5.14mm
- 5.96mm

The measurements were carried out three times for each nozzle so that false measurements could be filtered out later if necessary. This resulted in experiment results with the full possible input range of $\omega_r$ for each nozzle.

The available sensors logging the data during the experiments were:

- Rotational speed sensor of the oil pump $\omega_r$, this measures the actual input
- Rotational speed sensor of the oil motor $\omega_m$
- Pressure in the high pressure oil line $p_1$
- Pressure in the low pressure oil line $p_3$
- Pressure in the high pressure water line $p_2$
- Torque at the oil pump $\tau_1$

See figure 5-2 for the sensor locations.

The measured values and the predicted values by the model are plotted as function of the input setting $\omega_r$ for each nozzle. Figure 6-2 shows the rotational speed of the oil motor $\omega_m$ and the pressure in the water circuit $\Delta p_2$. Figure 6-3 shows the pressure in the oil circuit $\Delta p_1$ and the torque at the oil pump $\tau_1$.

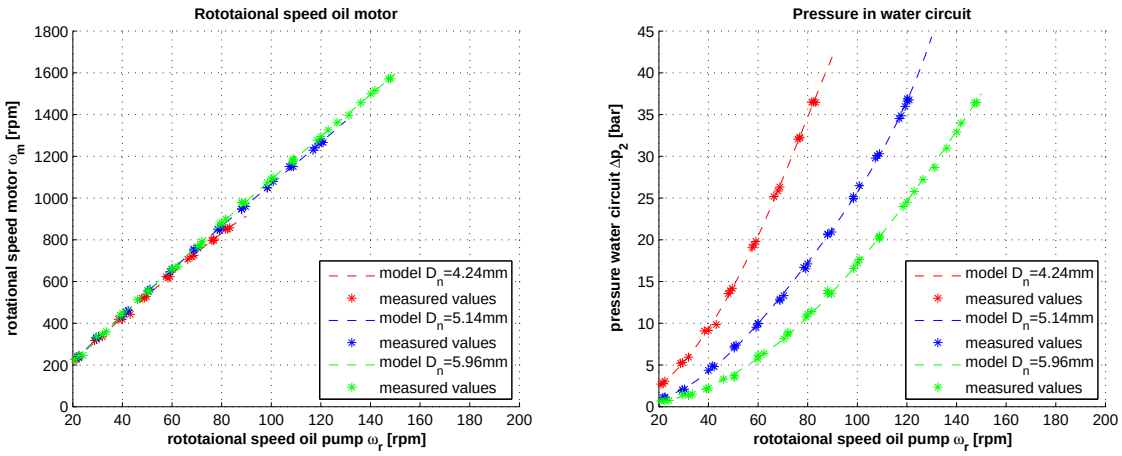


(a) (b)

**Figure 6-2:** Comparison between the predicted and measured values for the rotational speed of the oil motor and the pressure in the water circuit

From these experiments and simulation results the following findings are made:

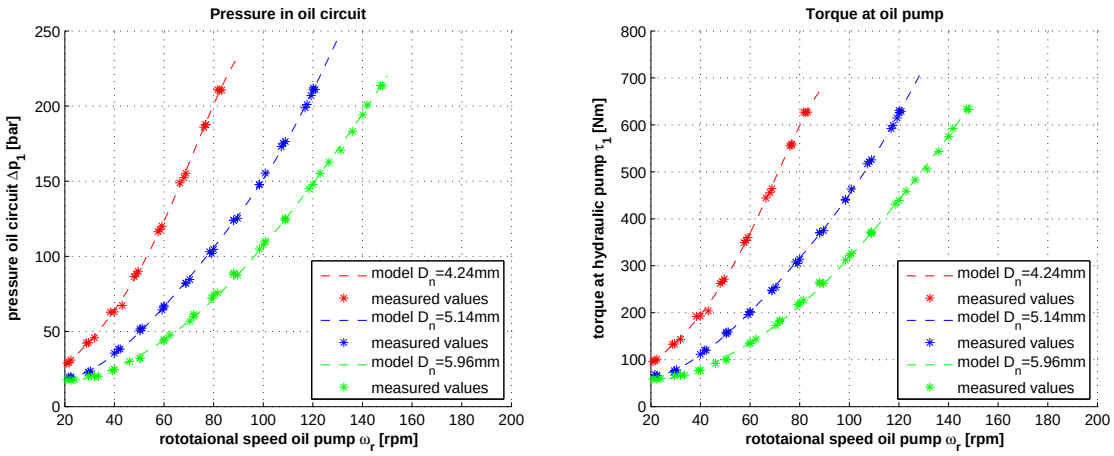


(a) (b)

**Figure 6-3:** Comparison between the predicted and measured values for the pressure in the oil circuit and the torque at the oil pump

- The data points in figures 6-2 and 6-3 show that for any specific input condition the output result differs by less than 2%. This shows that the sensors measurements are consistent.
- The values predicted by the model are in good agreement with the measured values. There is not more than 3% difference between the two. This also proves that the modifications carried out on the original model were successful, see appendix D.
- Figure 6-2 shows a linear increasing $\omega_m$ as function of the input $\omega_r$. This is in agreement with the equations from figure 2-6. This also indicates small volumetric losses of the oil pump and motor.
- Figures 6-2 and 6-3 show quadratic increasing pressures and torque at the oil pump as function of the input $\omega_r$. This is also in agreement with the equations from figure 2-6.
- Figures 6-2 and 6-3 show that the steepness of the pressures and torque graph increases with decreasing nozzle diameter. This is also in agreement with the equations from figure 2-6. This proves the large influence of a small change in the nozzle diameter on the tip speed ratio at which the transmission operates.

The efficiency of the consecutive energy conversion steps predicted by the model are shown in figure 6-4, at steady state conditions, with the 5.14mm nozzle. The procedure used to determine the different efficiencies is explained in appendix D. The graphs of the two other nozzle diameters show similar results for the different efficiencies.

From these simulation results with the validated model the following findings are made:

- The total efficiency of the oil pump is approximately constant above 40rpm between 90 and 93%.
- The total efficiency of the oil motor keeps increasing slightly with increasing input $\omega_r$ from 73 to 94%.

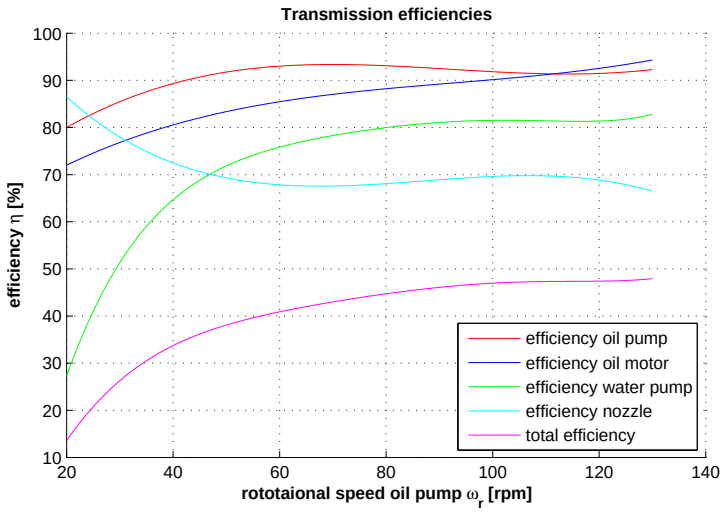


**Figure 6-4:** Efficiency of the energy conversion steps in the transmission with a nozzle diameter of 5.14mm

- The efficiency of the water pump is poor at low input speeds of $\omega_r$. This is mainly caused by the low pressures at low input speeds. This low pressure has a negative effect on the mechanical efficiency of the pump as is also indicated by equation 3-33. Above 70rpm a constant efficiency around 80% is achieved.

- The derived efficiency at the nozzle is approximately constant above an input of 50rpm. The efficiency of the nozzle is fairly poor with a value just below 70%. This is probably caused by the poor design of the nozzle that has a fairly sharp edge. This nozzle efficiency is also based on a conservative assumption which is explained next. To determine the efficiency at the nozzle equation 3-83 must be used. The pressure loss at the nozzle $\Delta p_{nloss}$ must be known to determine the nozzle efficiency. However, the pressure difference at the nozzle $\Delta p_{ndiff}$ between the measured and the ideal pressure was the only property that could be determined from the measurements, see equation 3-81. Therefore this pressure difference $\Delta p_{ndiff}$ was used instead in equation 3-83 to determine the nozzle efficiency. It was thus assumed that the pressure difference $\Delta p_{ndiff}$ is completely caused by the velocity coefficient, and that this pressure difference is thus a pressure loss. However, nozzles with similar shape are estimated to have a contraction coefficient that lies between 0.83-0.95 [6]. The consequence of this assumption is that the derived efficiency shown in figure 6-4 is probably lower than the actual nozzle efficiency.

- The total efficiency of the transmission is fairly poor at low input speeds. This is mainly caused by the poor efficiency of the water pump at low input speeds. Above an input speed of 70 rpm the total system efficiency is approximately constant between 43 and 48%.

To have an optimal working passive control strategy it is important that the total system efficiency is approximately constant for the complete operational profile of the transmission, see section 2-3-2 for an explanation. This is only the case above 70 rpm input speed. In section 6-2-3 a further explanation is given on the implications of these results found here.

### 6-2-3 Proof of the Passive Control Strategy for Steady State Conditions

One of the main objectives of the experiments was to prove that the passive control strategy, explained in section 2-3-2, is a suitable control method to control the rotational speed of the rotor. The proof of this passive control method under steady state conditions is given in this section.

In steady state condition the power output from the rotor, see equation 2-5, is equal to the power input of the transmission, see equation 2-8.

$$P_{rotor} = P_{transmission} \tag{6-1}$$

$$C_P \frac{1}{2} \rho_a A_r \left(\frac{R}{\lambda}\right)^3 \omega_r^3 = \frac{\rho}{2\eta_{m1}\eta_{m2}\eta_{m3}} \left(\frac{\eta_{v1}\eta_{v2}\eta_{v3}}{A_n C_v C_c}\right)^2 \left(\frac{V_{g1}V_{g3}}{V_{g2}}\right)^3 \omega_r^3 \tag{6-2}$$

Equation 6-2 has two important implications for the ability of the fluid power transmission to control the rotational speed of the rotor:

- The losses in the transmission influences the tip speed ratio $\lambda$ and thus the power coefficient $C_P$ at which the rotor operates.
- A change in the nozzle diameter also results in a change in the tip speed ratio and power coefficient at which the rotor operates.

The $C_P - \lambda$ curve in figure 6-5 is the curve of the rotor for which the transmission is designed. Indicating an optimal tip speed ratio $\lambda_{opt}$ of 4.8 and an optimal power coefficient $C_{P,opt}$ of 0.44. The experiment results of section 6-2-2 indicate that the total efficiency of the transmission varies in the operational profile of the rotor. This will cause a varying tip speed ratio in the operational profile of the rotor. The section of the $C_P - \lambda$ curve to the right of the optimal tip speed ratio has a smaller gradient. The negative effect of the varying tip speed ratio on the power coefficient is thus smaller on the right side of the curve. It is therefore preferred to choose the nozzle diameter such that the turbine will operate with a slightly larger $\lambda$ than $\lambda_{opt}$. This also results in slightly higher efficiencies of the pumps and motor in the transmission.

The rotor $C_P - \lambda$ curve was not available during the design process so an optimal tip speed ratio of 5.6 for similar size rotors was assumed. The power coefficient of the rotor at a $\lambda$ of 5.6 is 90% of $C_{P,max}$, which is also acceptable. Therefore an operating range for the rotor was defined between a $\lambda$ of 4.8 and 5.6. The measured $\tau_1$-$\omega_r$ curve for the transmission with the different nozzles is shown together with the $\tau_1$-$\omega_r$ curve for the rotor operating at a $\lambda$ of 4.8 and 5.6 in figure 6-5. These measured $\tau_1$-$\omega_r$ curves should preferably lie within the two $\tau_1$-$\omega_r$ curves of the rotor.

Based on the experiments results and the rotor curves the following findings are made:

- The measured $\tau_1$-$\omega_r$ curve for the 5.96mm nozzle is within the two boundaries for almost the complete operational profile of the rotor. This is therefore the most suitable nozzle choice out of these three.
- The tip speed ratio of the transmission with 5.96mm nozzle is smaller than 4.8 below rotational speeds of 40rpm. This is caused by the poor total efficiency at these low

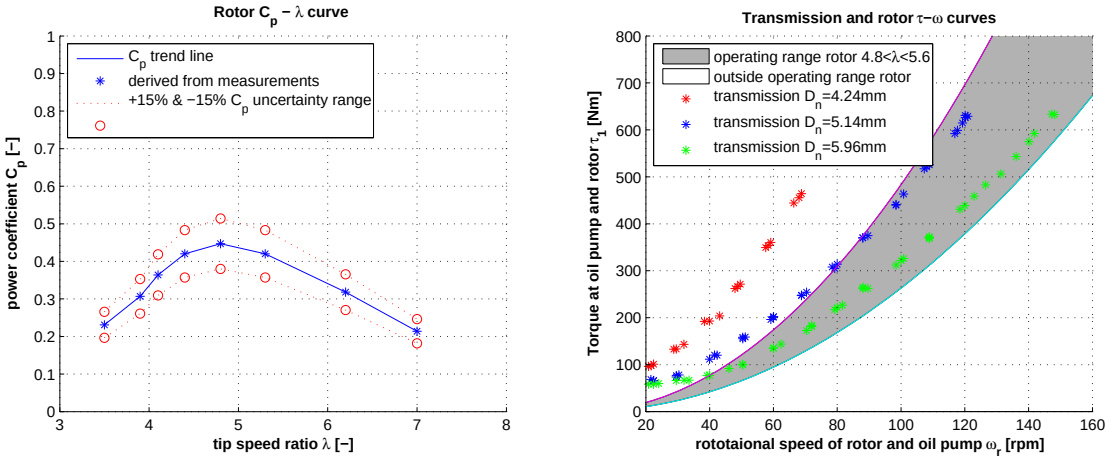


(a) (b)

**Figure 6-5:** $C_P - \lambda$ curve rotor and $\tau$-$\omega$ curve of rotor and transmission

rotational speeds. The passive control method is not capable of controlling the rotor within the defined tip speed ratio range at rotational speeds below 40 rpm, thus at low wind speeds.

This proves the functionality of the passive control method for the rotor in steady state conditions. An attempt to completely prove the functionality of this control method for the rotor operating in dynamic conditions is made in chapter 7.

## 6-3 Validation of the Dynamic Model

The final dynamic model developed for this thesis is described in chapter 4. In this section it was also concluded that the main elements that determine the dynamic behaviour of the transmission with rotor are:

- Rotor inertia
- Effective compressibility of the oil and water in the hoses
- Damping caused by the nozzle

The demonstration set-up in the laboratory did not include a rotor. Thus the experiments executed in the laboratory were without rotor inertia. This results in transmission with a significant higher natural frequency and a faster dynamic response to fluctuations. Therefore a version of the dynamic model without the rotor inertia was used to validate the dynamic model with the demonstration set-up, see figure 6-6.

A block diagram of the demonstration set-up in the laboratory is shown including the asynchronous electric motor that drives the oil pump of the demonstration set-up. The rotational speed of the electric motor is controlled by regulating the frequency of the current that drives

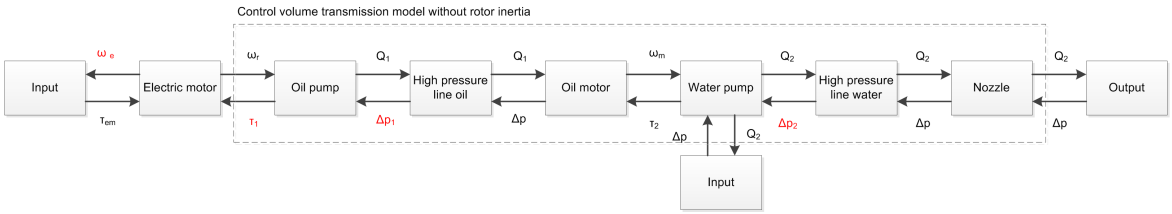


**Figure 6-6:** Fluid power transmission model without rotor inertia. Measured properties during the experiments are indicated in red

the electric motor. The measured properties in the demonstration set-up are indicated with red letters in the block diagram. The control volume of the model without the rotor inertia is also indicated in the block diagram. The asynchronous electric motor is thus not included in the model, because its only function is to drive the oil pump during the experiments in the laboratory instead of the rotor. It was therefore out of the scope of this thesis to create a model for this motor and include it in the dynamic model.

The two pulse sensors that record the rotational speed of the oil pump $\omega_r$ and motor $\omega_m$ only give correct results when the transmission operates in a steady state situation. So during the dynamic experiments these pulse sensors were not used. An alternative sensor from which the rotational speed of the oil pump was derived, is the analogue electric frequency sensor. This sensor measures the frequency of the electric current $\omega_e$ in the electric motor. From this sensor the real time rotational speed of the oil pump $\omega_r$ is determined fairly accurately. However, at maximum torque and pressures, up to 4% difference between the measurements of $\omega_r$ and $\omega_e$ was measured. This is caused by slip in the asynchronous motor, see appendix E for an explanation. The only sensors used during the dynamic experiments were analogue sensors, measuring:

- The frequency of the electric input current driving the transmission $\omega_e$
- Pressure in the high pressure oil line $p_1$
- Pressure in the low pressure oil line $p_3$
- Pressure in the high pressure water line $p_2$
- Torque at the oil pump $t_1$

The following experiments were used to validate the dynamic model without rotor inertia:

- Step function experiments, see figure 6-7. In these experiments the electrical frequency at the start of the experiment was set at 20 rpm and increased to the maximum value as fast as possible. This experiment was repeated 4 times with similar results.
- Sinusoidal experiments, see figure 6-8. In these experiments the electrical frequency driving the transmission had a sinusoidal shape. A range of experiments with increasing frequency and constant amplitude was carried out.
- Random input experiments, see figure 6-9. In these experiments the input of the transmission was randomly varied up and down. This was done to simulate the turbulent character of the wind speed.

The frequency of the electrical current $\omega_e$ was logged for all experiments. A simulation for each of the experiments was run with the logged $\omega_e$ from the experiment as input into the dynamic model. To validate the dynamic model, the response of the demonstration set-up was then compared to the response of the dynamic model. For each of the above described experiments one comparison is shown.

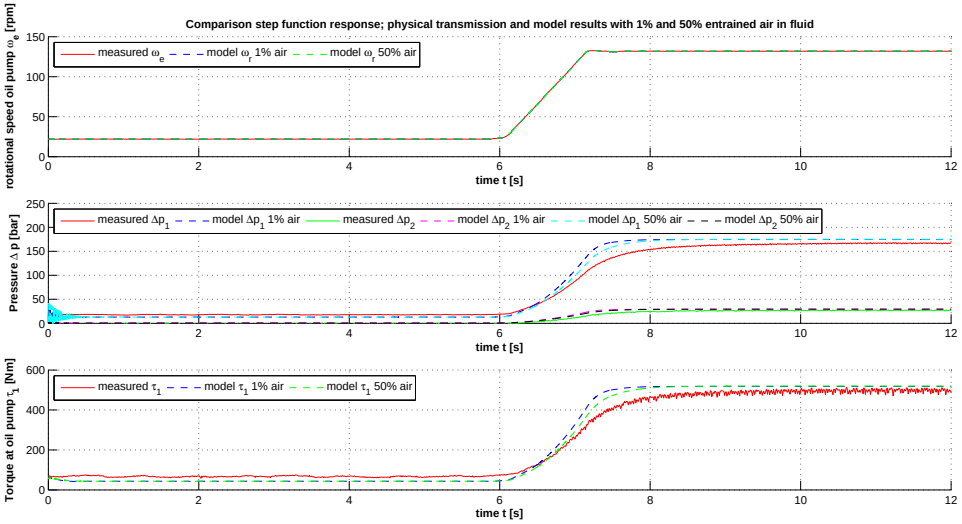


**Figure 6-7:** Step function; comparison of the demonstration set-up and the dynamic model with 1% and 50% entrained air in the fluid

From these experiments and simulation results the following findings are made:

- As predicted by the model, all experiment results show that the response to fluctuations at the input are strongly damped without any overshoot.
- When more air is entrained in the transmission fluids, the dynamic response is slower. Entrained air in the fluid increases the effective compressibility of the fluid, which reduces the stiffness of the transmission. However the influence on this response is relatively small, see figure 6-7.
- The step function response of the demonstration set-up is approximately 1 second slower than the response of the dynamic model. This is most probably caused by the dynamic effects of the electric motor in the demonstration set-up that are not modeled. This also explains the slightly slower response of the demonstration set-up in the sinusoidal and random input experiments.
- The energy storage capacity of the rotor inertia in the electric motor causes a smaller amplitude of the demonstration set-up response than is predicted by the dynamic model, see figure 6-8.
- There is a slight difference between the measured and the predicted values at steady state, this is best seen in figure 6-7. The frequency of the electric current that drives the transmission $\omega_e$ is used as the input for the dynamic model. The explained 4% difference

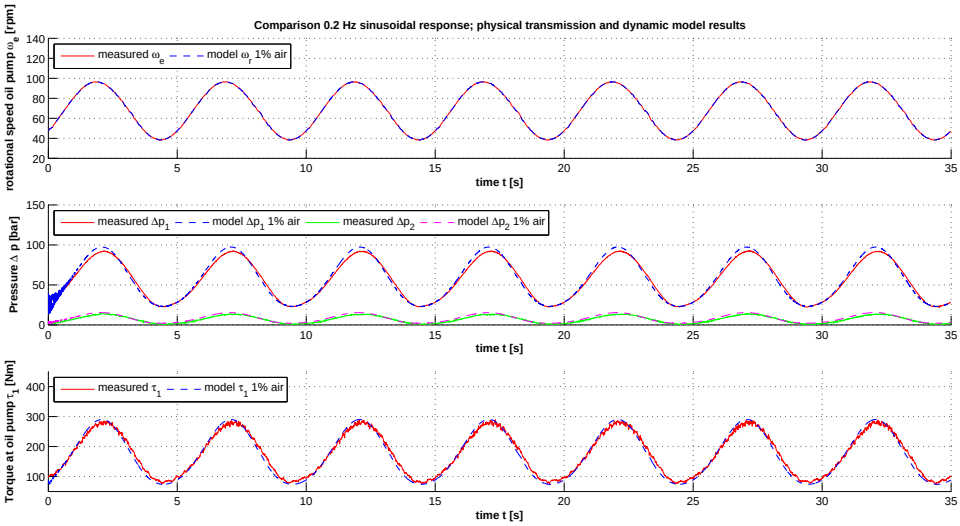


**Figure 6-8:** Sinusoidal input 0.2 Hz; comparison of the demonstration set-up and the dynamic model with 1% entrained air in the fluid

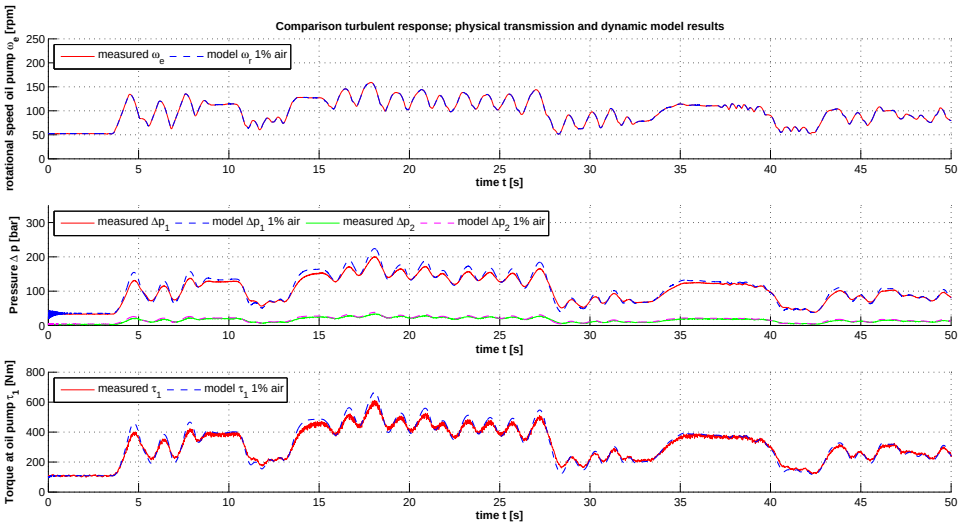


**Figure 6-9:** Random input; comparison of the demonstration set-up and dynamic model with 1% entrained air in the fluid

between the $\omega_r$ and $\omega_e$ probably causes the slight difference between the measured and the predicted values at steady state

It is found that the dynamic model gives a reasonable prediction of the demonstration set-up response to a fluctuating input. However, the predicted response is slightly faster than the measured response due to the dynamic effects of the electric motor that are not modeled.

## 6-4 Validation of the Practical Transmission Requirements

In the design requirements several important requirements of a more practical origin were defined. These requirements are:

- The operation of the fluid power transmission must be as safe as possible.
- The boost system should provide sufficient cooling and pressure in the low pressure line of the oil circuit. See section 2-4 for a more detailed explanation of the boost system.
- The hydraulic break should be able to stop the rotor from rotating.
- The rotor must be able to spin up at minimum torque.

The safety of the transmission is ensured by pressure relief valves in the high pressure oil and water line. These were tested several times and opened immediately above their set pressure. Thus, high pressure peaks are prevented. During the hydraulic break experiments the pressure relief valve in the high pressure oil line also opened, see section 6-4-1.

During all the experiments the oil temperature in the low pressure line did not rise above 30°C. This is far below the maximum allowable temperature. The pressure in the low pressure line of the oil circuit was also maintained at 10 bar during all experiments. Thus the boost system functions according to expectation.

Several experiments were carried out to verify that the hydraulic break and start-up requirements are fulfilled. The results and findings of these experiments are discussed in the remainder of this section.

### 6-4-1 Hydraulic Break Experiment

A detailed explanation of the working principle of the hydraulic break is given in section 2-4. In the demonstration set-up the controllable input of the transmission is the frequency of the electric current to the electric motor $\omega_e$. This is a set value and the electric motor will keep driving the oil pump at this set rotational speed. So whether the hydraulic break can really stop the rotor, cannot be demonstrated with the demonstration set-up. However, during several experiments the hydraulic break was activated to verify the working principle of the hydraulic break and the safety upon activation of the break. In figure 6-10 the pressures and torque response of an experiment, in which the hydraulic break was activated at 5.9 seconds, are shown.

From these experiment results the following findings are made:

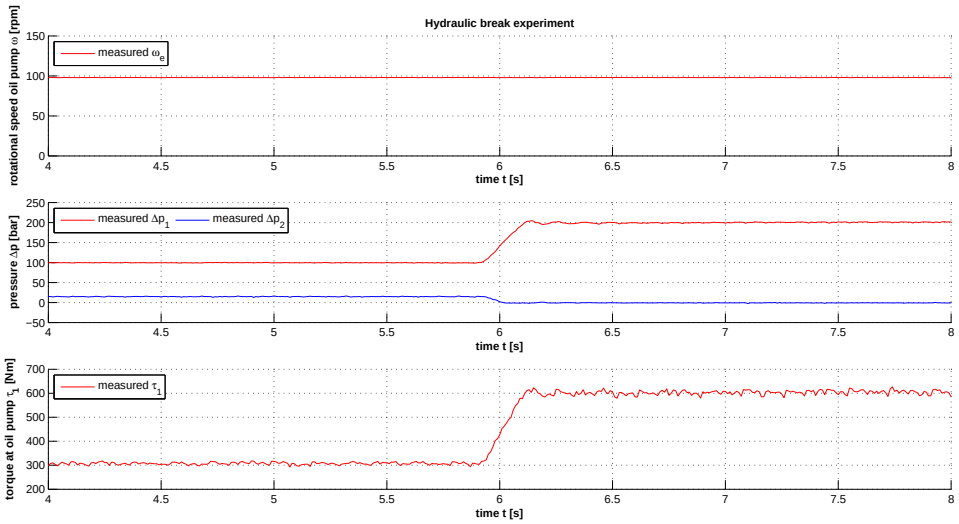


**Figure 6-10:** Measured response of an experiment where the hydraulic break was activated at 5.9 seconds

- The input $\omega_e$ remains constant at the set value during the experiment.

- When the hydraulic break is activated, this causes a jump in the torque at the oil pump from 200 to 600 Nm. If instead a rotor would be driving the oil pump, this would reduce the tip speed ratio of the rotor far below its optimal. This reduces the extracted power from the wind. This process reinforces itself until the rotor is stopped. However, to fully prove the working principle of the break, an experiment with a rotor connected to the transmission is required.

- During this experiment the opening pressure of the pressure relief valve in the high pressure oil line was set at 200 bar. A small overshoot of this pressure is measured after activation of the break, see the second graph. This overshoot is caused by the almost instantly closing break valve. Closing time is 60ms. However the pressure is still strongly damped. This also shows that the safety upon activation of the hydraulic break is indeed ensured by the pressure relief valve.

- No waterhammer was observed during any of the hydraulic break experiments. This shows that the velocity in the high pressure oil line is below the limit at which a waterhammer occurs. See section 2-4 for a more detailed explanation of the waterhammer phenomena.

These experiments prove the working principle of the hydraulic break. These experiments also show that the safety upon activation of the break is ensured. In order to prove that the hydraulic break can completely stop the rotor, an experiment with the rotor connected to the transmission is required.

### 6-4-2 Start-up Experiment

The working principle of the low torque start-up system for the rotor is explained in section 2-4. The main objectives of this experiment was to find out the start-up torque of the transmission with an open and closed start-up valve. With these values an estimation of the minimum required wind speed to drive the transmission was made. This is also referred to as the cut-in wind speed. figure 6-11 and 6-12 show the results of a start-up experiment with an open and closed start-up valve respectively.

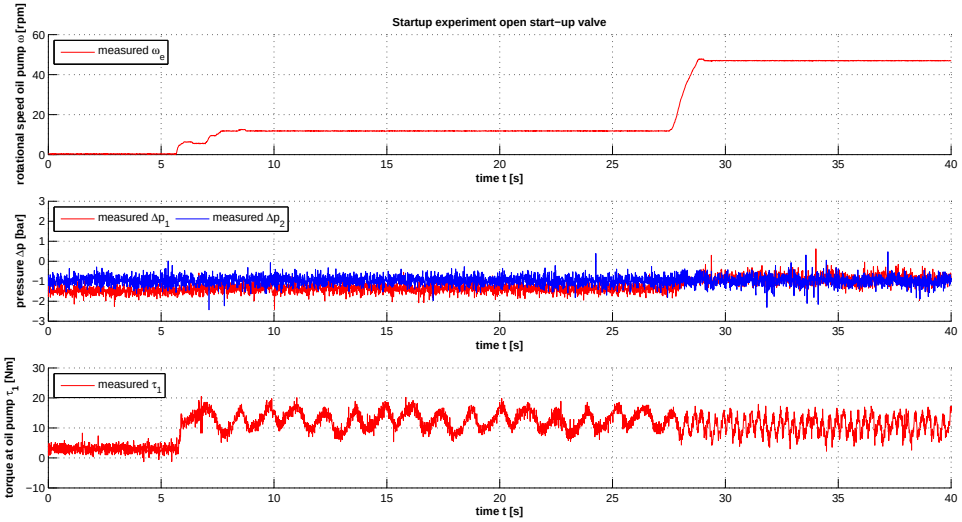


**Figure 6-11:** Measurements recorded during a start-up experiment with open start-up valve

The minimum torque required to run the transmission with open start-up valve is approximately 20 Nm, see the third graph of figure 6-11. This torque stays constant with increasing rotational speed of the oil pump. This shows that the rotor can spin up easily with a minimum torque until the rotor has reached sufficient momentum.

Another finding from this experiment is the sinusoidal shaped torque that is clearly visible at this low rotational speed of the oil pump. The frequency of the measured torque fluctuation is 4 times higher than the rotational frequency of the oil pump. The frequency of the measured torque fluctuation also increases linearly with the rotational frequency of the oil pump. The movement of the pistons in the axial piston pump can cause small fluctuations in the torque required to drive the oil pump [2]. However, the number of pistons in the used pump is 7 and not 4. This indicates a different cause for the measured fluctuation. It could also be caused by a small noise in the measured signal. Further research is required to find the cause of this fluctuation in the measured signal. For the purpose of this experiment this measured fluctuation is of no importance.

During the start-up experiments with closed start-up valve interesting results were found. The minimum required start-up torque to run the transmission with closed valve is 220Nm, see the third graph of figure 6-12. This high torque is caused by the required start-up torque of the water pump. After start-up a minimum torque of only 80 Nm is required at the oil pump, to keep the water pump rotating. To determine the required wind speed in order to

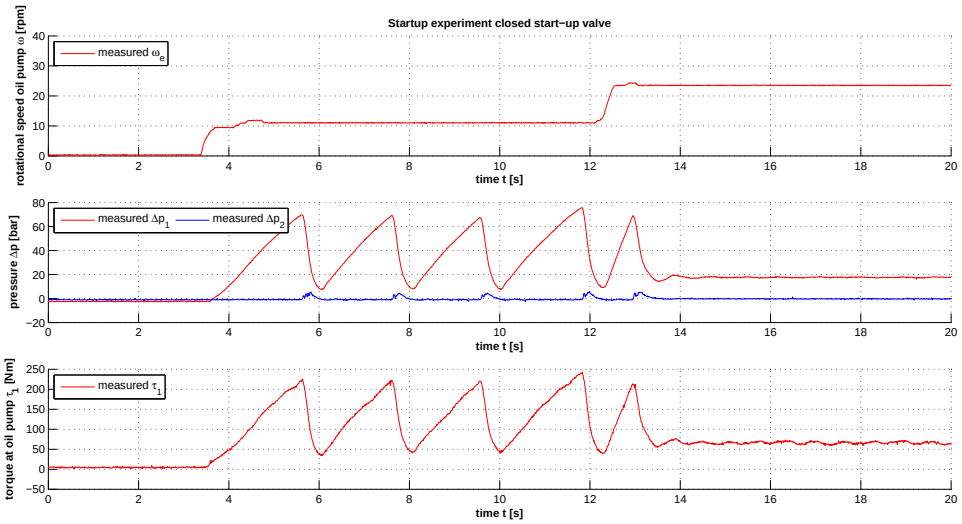


**Figure 6-12:** Measurements recorded a during start-up experiment with closed start-up valve

reach a certain torque at the oil pump, equation 2-5 and 2-2 are combined into:

$$U_a = \sqrt{\frac{2\tau_1 \lambda}{C_p \rho_a A_r R}} \tag{6-3}$$

A tip speed ratio $\lambda$ of 5.6 that relates to 90% of the maximum power coefficient $C_{P,max}$ is used in this estimation. To reach 220Nm torque at the oil pump, a wind speed of 6.1m/s is required. To reach 80 Nm torque at the oil pump, a wind speed of 3.7m/s is required. If sufficient momentum is built up by the rotor inertia, the water pump can also be started at wind speeds between 3.7 and 6.1m/s. The 220Nm torque that needs to be reached at start-up, is then supplied by the momentum stored in the rotor inertia. The minimum required wind speed of 3.7 m/s will probably turn out to be slightly higher as the resistance of the rotor bearings are neglected in this calculation. Similar sizes wind turbines have cut-in wind speeds between 3 to 4m/s. The final cut-in wind speed of this transmission with rotor is expected to be comparable.

# Chapter 7

# Complete Model Analysis with a Simplified Rotor Model and the Validated Transmission Model

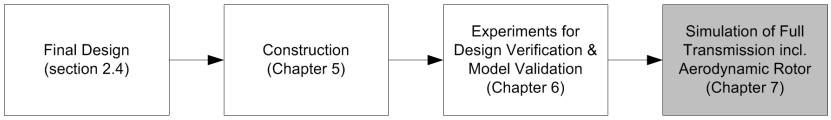


**Figure 7-1:** Chapter 7 highlighted in project approach flow chart

In this chapter the functionality of the transmission for a 10kW rotor is proven. This is done with simulations of the validated transmission model together with a simple rotor model. The results of these simulations can also be used to prepare for the planned future experiments with the transmission and 10kW rotor.

The extracted power from the wind is modeled with the $C_P - \lambda$ curve of the available rotor shown in figure 2-3. The inertia of the rotor is included in the model. Aerodynamic effects and other phenomena at the rotor are not modeled. For the purpose of this analysis, this simplified rotor model is a sufficient representation of the actual rotor. A block diagram of the complete model is shown in figure 7-2, where the wind velocity is now the input of the model.

To further analyze and prove the passive control strategy, several simulations were run with constant input wind speeds and with turbulent wind speeds, see section 7-1. The turbulent wind speeds used in the simulations are comparable to the wind speeds in the outside environment. Finally the dynamics of the complete model were analyzed. This was done by linearizing the non-linear complete model at different operational points. From these linearizations a Campbell diagram was constructed, see figure 7-6.

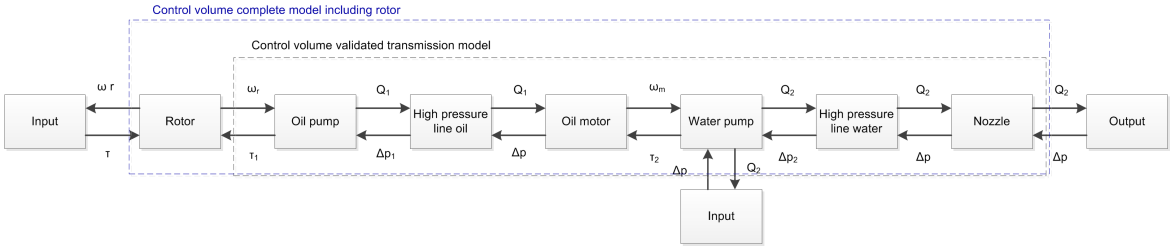


**Figure 7-2:** Block diagram of complete model including rotor

## 7-1 Passive Control Analysis with Complete Model

The validated passive control strategy (see section 6-2-3) was analyzed further with simulations of the complete model including rotor. First several simulations were run with increasing constant wind speeds. From these simulation results the power $P$, the power coefficient $C_P$ and the tip speed ratio $\lambda$ are determined as a function of the wind speed. These are steady state values. The results of these experiments are shown in figure 7-3(a).

From these simulation results the following findings are made:

- At wind speeds above 4.7m/s the rotor is passively controlled by the transmission at an almost constant tip speed ratio, see figure 7-3.
- At wind speeds below 4.7m/s the tip speed ratio is lower. This is caused by the poor efficiency of the water pump in this area, see section 6-2-2. The consequence of this poor efficiency at low wind speeds is limited, as the estimated cut-in wind speed is between 4- 6 m/s, see section 6-4-2.
- The graphs of figure 7-3(a) stop at 11m/s, because the transmission model is not validated for wind speeds above 11 m/s. The results of simulations with wind speeds above 11m/s are thus less reliable.

In the outside environment the wind speed has a turbulent character. Several simulations were run with a turbulent wind speed to analyze the passively controlled rotor in turbulent wind speeds. The results for one simulation with a turbulent wind speed are shown in figure 7-4.

From these simulation results the following findings are made:

- The strongly damped response of the transmission is clearly indicated by the fast fluctuating rotor power and the smooth output power from the nozzle.
- In these turbulent wind speed conditions the tip speed ratio varies between 5 and 7. The variation in tip speed ratio is much larger than for constant input wind speeds as shown in figure 7-3. However, the transmission still passively controls the rotor within an acceptable power coefficient range between 75% and 90% of the maximum power coefficient $C_{P,max}$. These simulation results indicate the suitability of the transmission for turbulent wind speed conditions.

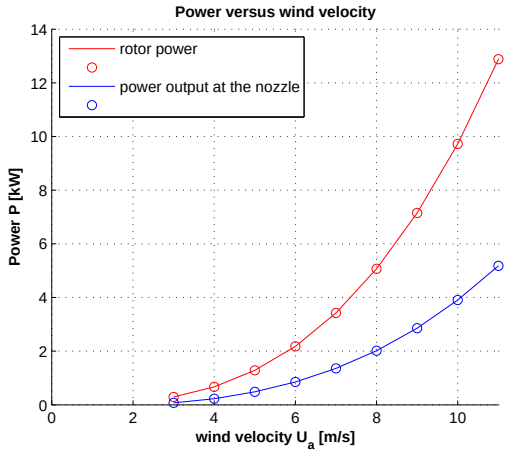


(a) Rotor power and output power from the nozzle

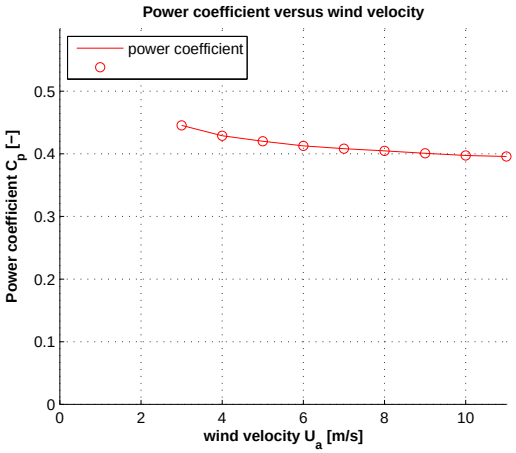


(b) Power coefficient

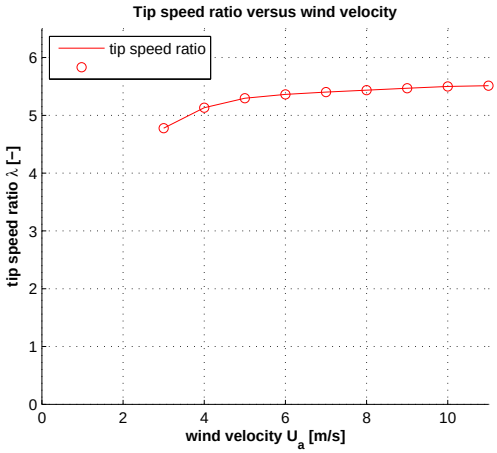


(c) Tip speed ratio

**Figure 7-3:** Rotor power and output power from the nozzle, power coefficient and tip speed ratio as function of the wind speed in steady state condition, $D_n = 5.96$mm

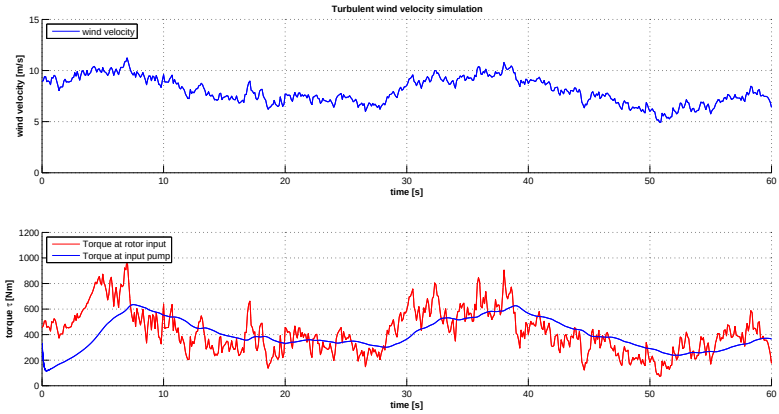


(a)

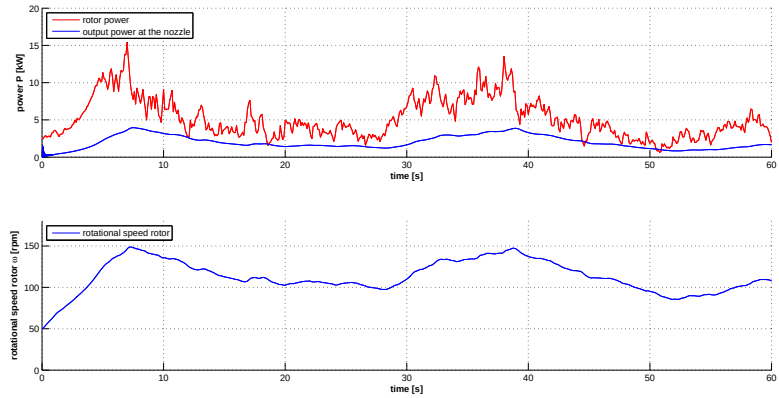


(b)

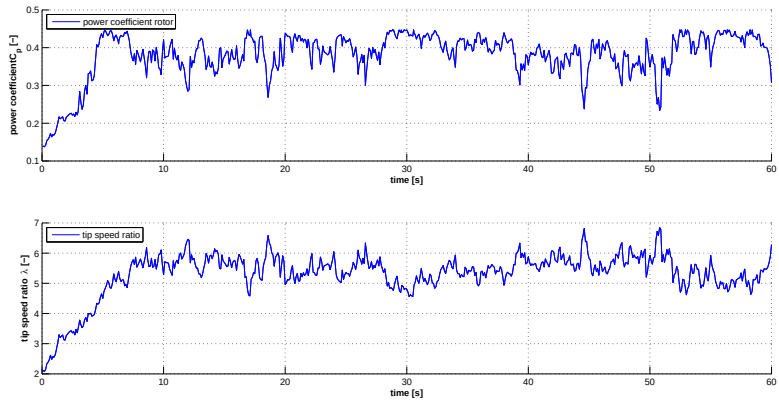


(c)

**Figure 7-4:** Results of a simulation with a turbulent wind speed

If fluid power transmissions are applied to large scale turbines in a wind farm, the seawater pipes will be in the order of several 100 meters or even kilometers. The suitability of the passive control strategy for this large scale application requires a further in-depth research. From the analysis carried out here it is expected that long seawater pipes will increase the response time of the transmission to fluctuations in wind speed.

## 7-2 Analysis of the Complete Model Dynamics

The validated transmission model with the simplified rotor model was linearized at a range of wind speeds from 4m/s to 11m/s. The Bode plots for each of these linearizations are shown in figure 7-5.

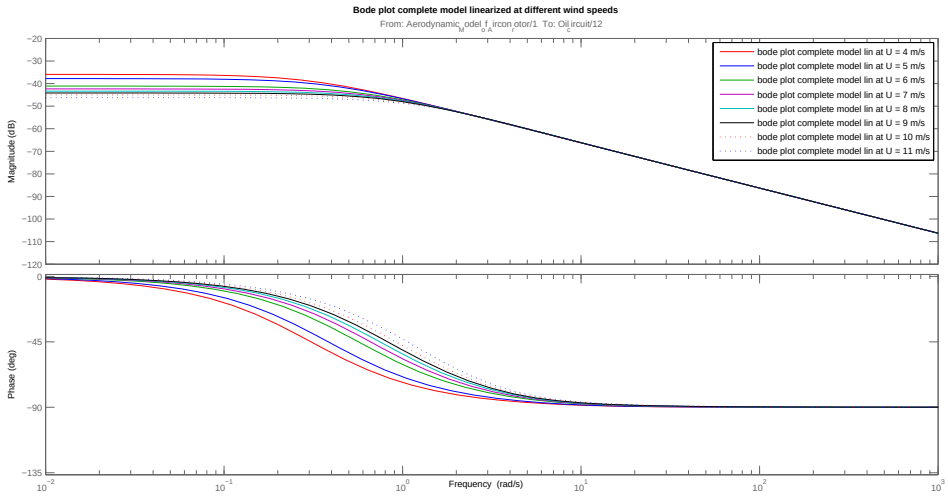


**Figure 7-5:** Bode plots of the validated transmission model with simple rotor model linearized at different wind speeds

Based on these Bode plots the following findings are made:

- All the Bode plots are completely damped. So if the transmission is excited at its natural frequency, its response will be completely damped.
- The Bode plots are the same for all the wind speeds at frequencies above 2rad/s.
- At lower frequencies than 2 rad/s the Bode plot magnitude decreases and the phase angle increase with increasing wind speed. These differences are caused by the non-linearity in the nozzle model and the resistance elements of the pumps and motor, see section 3-3.

A small difference in the damping ratio is noticed between these Bode plots and the Bode plot of model 3 in figure 4-7. The Bode plot of model 3 in figure 4-7 is a Bode plot of the original model without modified efficiency equations, but with the same inertia and capacitance elements. It was first thought that these differences were caused by the modified efficiency

equations in the model of figure 7-5. However, as shown in appendix F, this difference also exists between the original model linearized in Simulink and the same original model linearized in 20-Sim. For this case the exact same Bode plots were expected. The difference between model 3 of figure 4-7 and the model of figure 7-5 might also be caused by the different linearization methods used in the two software programs. Above a frequency of 5 rad/s the Bode plots of the two models give the same result. See appendix F for a comparison between the Bode plot of the original model linearized in 20-sim and the Bode plot of the model linearized in Simulink.

A Campbell diagram is often used to analyze the dynamics of wind turbines. It provides a useful graphical indication of the possible overlap between the natural frequency of the turbine and the excitation frequencies. From the made linearizations at the different wind speeds a Campbell diagram of the complete model is constructed. The Campbell diagram with the two lowest natural frequencies of the validated transmission model with simplified rotor model is shown in figure 7-6.

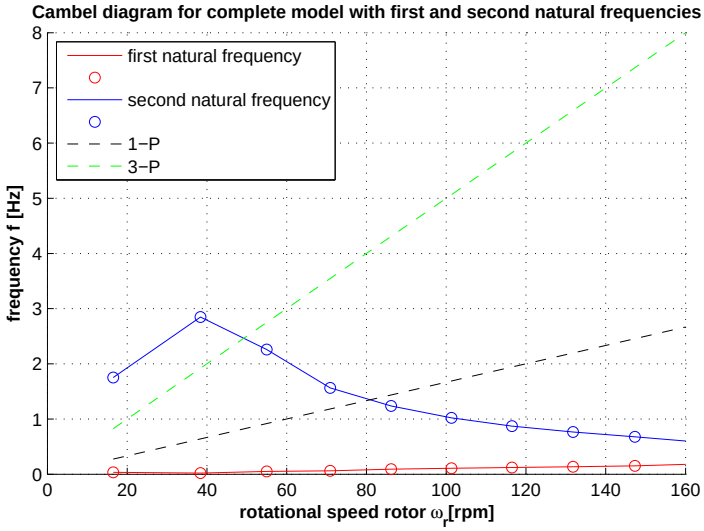


**Figure 7-6:** Campbell diagram with the 2 lowest natural frequencies of the complete fluid power transmission model

The two most important excitation frequencies are the frequency of the rotor (1-P) and the blade passing frequency (3-P). Resonance is expected during normal operation, when a natural frequency crosses one of the excitation frequencies or is close to one of these frequencies.

From the Campbell diagram it is seen that:

- The lowest natural frequency increases from 0.22 to 1.15rad/s with increasing rotational speed of the rotor. This frequency does not cross any of the excitation frequencies.
- The second natural frequency decreases from 17.9 to 3.7rad/s with a peak at a rotational speed of 40rpm. The Campbell diagram shows that the second natural frequency crosses the excitations frequencies at rotor speeds of 50 and 80rpm. However, as indicated by the Bode plots, all the natural frequencies are very well damped. Therefore resonance is not expected, even when the turbine is excited with one of its natural frequencies.

# Chapter 8

# Conclusions and Recommendations

## 8-1 Conclusions

For this thesis project a transmission based on the DOT concept is designed for the 10kW rotor. This designed transmission was successfully constructed and tested in the water laboratory at the faculty of Civil Engineering of the TU Delft. The developed dynamic model of the transmission was validated with experiments that were carried out with the demonstration set-up. The functionality of the transmission for the 10kW rotor was proven by a computer simulation with the validated transmission model and a simplified rotor model.

The results and conclusions for each of the phases in the thesis project are described next.

1. *Design a transmission suitable for a 10 kW rotor using the DOT concept*
   The transmission was successfully designed for the available 10 kW rotor. The transmission design consisted of a design for the closed-loop oil circuit and the open-loop water circuit as prescribed in the DOT concept. The design objectives are:

   - Compact transfer of energy
   - Simple and easy controlled rotor speed
   - Reasonably efficient energy transfer for a large pressure range in the transmission
   - Limited costs

   To assist in the design process a dynamic model and intermediate experiments were used.

   The final selected types and sizes of the main components are:

   - Axial piston oil pump of 180 cc/rev
   - Axial piston oil motor of 16 cc/rev
   - Axial piston water pump of 70.3 cc/rev
   - Fixed area nozzle with a diameter 5.12mm.

In order to easily control the rotor speed with the transmission, a passive control strategy is implemented. This method does not require any active control to regulate the rotor around its optimal tip speed ratio. The tip speed ratio of the rotor is easily adjusted by changing the nozzle diameter.

2. *Develop a dynamic model of the transmission*
The goal was to develop a model that represents the physical transmission with as little elements as possible. This resulted in model that contains all the elements that have a significant influence on the losses and the dynamic behavior of the transmission, these are:

   - Rotor inertia
   - Effective compressibility of the oil and water in the hoses
   - Damping caused by the nozzle
   - Resistance of the oil pump, water pump and oil motor
   - Nozzle resistance

   The pressure losses in the hose and the fluid inertia are also modeled. However, the influence of these elements is far less than the above mentioned elements.

3. *Construction of the transmission demonstration set-up in the laboratory*
The demonstration set-up of the transmission was constructed successfully in the laboratory. In the demonstration set-up the rotor is simulated by an electric motor that drives the oil pump. The rotational speed of the motor can be controlled manually or automatically to simulate different wind speeds.

4. *Run experiments with the demonstration set-up and validate the model with these experiments*
First, a comparison between steady state experiments and the original model was carried out. Some significant differences between the predicted efficiencies and the measured efficiencies were found at several points in the transmission. Due to these differences modifications were made in the efficiency equations of the model.

   This modified model was validated with several experiments. The conclusions from this validation are the following:

   - The found consistency of the sensors during measurements was more than 98%.
   - In steady state condition the predicted values by the modified model differ with less than 3% from the experiment results. Thus, the modified model is a good representation of the demonstration set-up.
   - The total transmission efficiency derived from the measurements is fairly constant above a rotor speed of 70 rpm (equivalent to a wind speed of 4.7m/s) between 43 and 48%. This includes the efficiency at the nozzle that, could not be derived exactly with the available demonstration set-up. A conservative assumption was made to derive the efficiency at the nozzle.
   - The total transmission efficiency reduces rapidly below 70rpm. This is caused by the poor efficiency of the water pump under these partial load conditions

- The experiment results show that the dynamic behavior of the transmission is strongly damped under all input conditions.
- The dynamic response of the demonstration set-up is slower than the response of the dynamic model. This is probably caused by the dynamic effects of the electric motor in the demonstration set-up that are not included in the model.

These experiments also demonstrated that all design requirements are complied with. The minimum required wind speed to operate the transmission with rotor is estimated between 4 and 6m/s.

5. *Prove the functionality of the transmission for a 10kW rotor*
   The functionality of the transmission was proven by simulations of the validated transmission model combined with a simplified rotor model. The conclusions from these simulations are the following:

   - For constant wind speed conditions above 4.7m/s the transmission with 5.96mm nozzle diameter passively controls the rotor at a constant tip speed ratio of 5.6. At this tip speed ratio the rotor operates at 90% of the maximum power coefficient.
   - For constant wind speeds below 4.7m/s the rotor operates far from its optimal tip speed ratio which has a negative effect on the extracted energy from the wind. This is caused by the poor total efficiency of the transmission at these partial load conditions.
   - In turbulent wind speed conditions the tip speed ratio variation is much larger than for constant wind speed conditions. However, in turbulent wind speed conditions the transmission still passively controls the rotor speed between 75 and 90% of the maximum power coefficient. The relatively slow response to fluctuations in the transmission cause the larger variations in tip speed ratio for turbulent wind speed conditions. The simulated turbulent wind speed conditions are comparable to the wind speed conditions in the environment.
   - The model is not validated for wind speeds above 11m/s. The results of simulations with wind speeds above 11m/s are thus less reliable.
   - The completes system of rotor and transmission is strongly damped. Therefore no problems are expected when the system is excited at one of its natural frequencies.

## 8-2 Recommendations

In the near future experiments with the transmission and a 10kW rotor are planned. Two recommendations are made to further improve the performance of the transmission for these planned experiments.

1. The total efficiency of the transmission can be increased from 45% to 60% with a custom made well-designed nozzle. A very efficient nozzle is a tapered nozzle with an angle of approximately 14° and a very smooth inner surface [6]. Replacing the nozzle is the cheapest improvement to increase the efficiency. When determining the final nozzle design and diameter, it is very important to keep in mind that both the nozzle diameter

and the geometrical shape will influence the tip speed ratio at which the rotor operates. The nozzle should be designed such that the rotor is controlled at its optimal tip speed ratio.

2. To improve the transmission efficiency and the power coefficient of the rotor at wind speeds below 4.7m/s, a hydraulic water pump with a more constant efficiency in partial load conditions is required.

It is recommended to analyze how the current generator platform can be redesigned or adjusted to completely match the operational profile of the constructed transmission. With this improved generator platform the working principle and performance of the generator platform, and in particularly the Pelton turbine, within the DOT concept can be further researched.

The simplicity of the passive control strategy is a great advantage of this control method. An in-depth research of the suitability of this method for large single turbines or wind farms is recommended. Based on the analysis in this thesis, the main concern for large scale application is the slow response of the transmission to fluctuations in the wind speed. The response time will increase due to the reduced stiffness caused by longer pipelines with larger diameters.

# Bibliography


[1] "Europe's onshore and offshore wind energy potential," tech. rep., European Environmental Agency; Copenhagen Office for Official Publications of the European Communities, 2009.

[2] H. Murrenhoff, *Grundlagen der Fluidtechniek*. Shaker, 2001.

[3] A. J. Laguna, "Steady state performance of the delft offshore turbine," Master's thesis, 2010.

[4] N. Diepeveen, "Seawater-based hydraulics for offshore wind turbines," tech. rep., 2009.

[5] J. Manwell, J. McGowan, and A. Rogers, *Wind Energy Explained*. John Wiley & Sons, LTD, 2002.

[6] J. Thake, *The Micro-Hydro Pelton Turbine Manual*. Itdg Publishing, 2000.

[7] P. Drexler, H. Faatz, F. Feicht, H. Geis, J. Morlok, E. Wiesman, A. Krielen, N. Achten, and M. Reik, *The Hydraulic Trainer Volume 3: Planning and design of Hydraulic Power Systems*. 2003.

[8] H. Merritt, *Hydraulic control systems*. John Wiley & Sons, Inc, 1966.

[9] E. Doebelin, *System Modeling and Response, Theoretical and Experimental Approaches*. John Wiley & Sons, Inc, 1980.

[10] K. M. Nassar, "Development and analysis of the lumped parameter model of a piezo hydraulic actuator," Master's thesis, 2000.

[11] F. White, *Fluid Mechanics sixth edition*. Mc Graw-Hill International, 2008.

[12] M. Annoni, L. Cristaldi, M. Norgia, and C. Svelto, "Efficiency measurement of water jet orifices by a novel electro-optical technique," *IEEE Transactions on instrumentation and measurement*, vol. 57, no. 1, pp. 48–54, 2008.

[13] E. Pedersen and H. Engja, "Modelling, simulation and analysis of dynamic systems," tech. rep., 2008.

[14] K. Rydberg, *Dynamic analyses and control of hydrostatic transmission.* 2009.

[15] M. Moran and H. Shapiro, *Fundamentals of Engineering Thermodynamics.* John Wiley & sons, Inc, fifth ed., 2006.

[16] "`www.engineeringtoolbox.com`," December 2011.

[17] A. Bahadori and H. Vuthaluru, "Prediction of bulk modulus and volumetric expansion coefficient of water for leak tightness test pipelines," *International Journal of Pressure Vessels and Piping*, vol. 86, pp. 550–554, 2009.

[18] R. Fine and F. Millero, "Compressibility of water as function of temperature and pressure.,"

# Appendix A

# Modeling Theory of Fluid Power Systems

The modeling theory required to develop a dynamic model for the transmission is described in this appendix. The modeling approach used is the integral relations for control volume analysis. The three fundamental laws of mechanics are first recapitulated briefly. These three laws were then converted into laws applicable for the control volume analysis. Finally the state equations required to determine the fluid properties in the dynamic model are explained.

## A-1 Modeling Approach of Fluid Power Systems

There are two options to analyze fluid flow systems [11]:

1. Integral relations for a control volume, or large scale, analysis.
2. Differential relations for fluid flow, or small scale, analysis.

The control volume analysis method is based on average property values (such as mass flow, induced force, energy exchange) at the boundaries of the control volume. This method is specifically useful for one dimensional fluid flow systems. It gives good engineering estimates of the systems properties.

The differential analysis method is used when a detailed flow pattern, at every point defined, in the system is required. However, with this method there are only a few cases where analytical solutions can be reached. Numerical modeling of the differential equations in a computational fluid dynamics Computational Fluid Dynamics (CFD) software program gives good estimates of the flow pattern for the cases were no analytical solutions can be found.

The final model must give a good representation of the overall power transmission behavior, including the dynamic behavior of the system. The main purpose of the model is to accurately describe the one-dimensional energy transfer in the power transmission. Therefore the most

suitable method used to develop the transmission model was the control volume analysis. The differential analysis method would have resulted in an overly detailed and complex model, therefore this method was not used [11].

For both methods there are three fundamental laws of mechanics that need to be satisfied. These are:

1. Conservation of mass (continuity)
2. Conservation of linear momentum equation (Newtons second law)
3. Conservation of energy (first law of thermodynamics)

Besides these three laws, thermodynamic state equations are required to determine the properties of the fluids used in the transmission [11].

## A-2 Three Fundamental Laws of Mechanics

In a mechanical system, the system is defined as a fixed quantity of mass. Everything outside the system boundaries is called the surroundings. The laws of mechanics describe the interaction with the system and its surroundings [11]. The first law is the conservation of mass. The system is defined as a fixed quantity of mass, resulting in the following law:

$$\frac{dm}{dt} = 0 \tag{A-1}$$

NewtonŠs second law states that the system will accelerate when a force from the surroundings is exerted on the system mass .

$$F = m\frac{dU}{dt} \tag{A-2}$$

The first law of thermodynamics states that the systems energy will change when work is done by the system or heat is exchanged with the surroundings.

$$\frac{dQ_h}{dt} - \frac{dW}{dt} = \frac{dE}{dt} \tag{A-3}$$

## A-3 Conversion of the Laws to Fixed Control Volume Analysis

The conversion of the three fundamental laws of mechanics into applicable laws for the fixed control volume analysis is described in this section. For this conversion the so called Reynolds transport theorem was used [11]. The Reynolds transport theorem for an arbitrary control volume is:

$$\frac{d}{dt}\left(B_{syst}\right) = \frac{d}{dt}\left(\int_{CV} \beta\rho dV\right) + \int_{CS} \beta\rho U_n dA_{out} - \int_{CS} \beta\rho U_n dA_{in} \tag{A-4}$$

$B_{syst}$ can be any property of the fluid flow being mass, momentum, angular momentum or energy. Where $\beta$ is the amount of $B$ per unit mass.

$$\beta = \frac{dB}{dm} \tag{A-5}$$

The terms of the Reynolds transport theorem in equation A-4 represent the following:

1. The instantaneous change of $B_{syst}$ in the system: $\frac{d}{dt}\left(B_{syst}\right)$
2. A change of $\beta$ within the control volume: $\frac{d}{dt}\left(\int_{CV} \beta\rho dV\right)$
3. Outflow of $\beta$ from the control volume: $\int_{CS} \beta\rho U_n dA_{out}$
4. Inflow of $\beta$ to the control volume: $\int_{CS} \beta\rho U_n dA_{in}$

Thus the change of $B_{syst}$ in the system is the sum of the change within the control volume, plus the outflow and minus the inflow. This is visualized for a one dimensional inflow and outflow situation in figure A-1. Where $U_n$ represent the flow normal to the control surface.

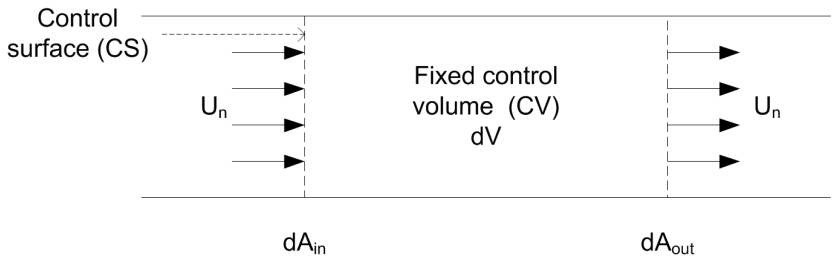


**Figure A-1:** Fixed control volume system with one dimensional in and out flow

For a fixed control volume the volume does not vary. This simplifies the Reynolds transport theorem to:

$$\frac{d}{dt}\left(B_{syst}\right) = \frac{d}{dt}\int_{CV} \frac{\partial}{\partial t}\left(\beta\rho\right) dV + \int_{CS} \beta\rho U_n dA_{out} - \int_{CS} \beta\rho U_n dA_{in} \tag{A-6}$$

In the remainder of this appendix this simplified Reynolds transport theorem for a fixed control volume is used to convert the three fundamental laws of mechanics into applicable laws for a fixed control volume analysis.

For the conservation of mass $B = m$ and $\beta = dm/dm = 1$. Filling this into Reynolds transport theorem gives the conservation of mass for a fixed control volume analysis:

$$\left(\frac{dm}{dt}\right)_{syst} = 0 = \int_{CV} \frac{\partial\rho}{\partial t} dV + \int_{CS} \rho U_n dA_{out} - \int_{CS} \rho U_n dA_{in} \tag{A-7}$$

For the linear momentum equation $\mathbf{B} = \mathbf{m}\,\mathbf{U}$ and $\beta = dm/dm\,\mathbf{U} = 1$, where the bold letters indicate vectors. Filling this into Reynolds transport theorem gives the linear momentum equation for fixed control volume analysis:

$$\frac{d}{dt}\left(m\mathbf{U}\right)_{syst} = \sum \mathbf{F} = \int_{CV} \frac{\partial U\rho}{\partial t} dV + \int_{CS} \mathbf{U}\rho\left(U_n\right) dA_{out} - \int_{CS} \mathbf{U}\rho\left(U_n\right) dA_{in} \tag{A-8}$$

For the conservation of energy equation $B = E$ and $\beta = dE/dm = \hat{e}$. Filling this into Reynolds transport theorem gives the conservation of energy equation for fixed control volume analysis:

$$\frac{dQ_h}{dt} - \frac{dW}{dt} = \frac{dE}{dt} = \int_{CV} \frac{\partial \hat{e}\rho}{\partial t} dV + \int_{CS} \hat{e}\rho \left(U_n\right) dA_{out} - \int_{CS} \hat{e}\rho \left(U_n\right) dA_{in} \tag{A-9}$$

The system energy per unit mass $\hat{e}$ is the sum of internal, kinetic and potential energy.

$$\hat{e} = \hat{e}_{internal} + \hat{e}_{kinetic} + \hat{e}_{potential} \tag{A-10}$$

which is also written as:

$$\hat{e} = \hat{u} + \frac{1}{2}U^2 + gz \tag{A-11}$$

The term $\frac{dQ_h}{dt}$ takes the heat transfer into the control volume into account, where positive $Q$ stands for heat input into the system. The term $\frac{dW}{dt}$ takes the work transfer into the control volume, where positive $W$ stands for work done by the control volume. Work transfer in fluid flow systems is subdivided into to three parts, giving:

$$\frac{dW}{dt} = \frac{dW_s}{dt} + \frac{dW_p}{dt} + \frac{dW_v}{dt} \tag{A-12}$$

The shaft work $W_s$ term is the work that is done by an external machine such as a pump for example. The pressure work term $W_p$ is the total pressure work integral over the control surface and can also be written as:

$$\frac{dW_p}{dt} = \int_{CS} pU_n dA \tag{A-13}$$

The work due to viscous stresses $W_v$ is the work done by the system on the control surface. When the control surface is a solid surface the work done to the surface is zero due to the no slip condition at the surface of fluid flow systems. Viscous stresses at an inlet or outlet are extremely small for the usual fluid flow systems and are usually neglected [11]

Inserting the equations for energy and work into the conservation of energy law gives the general form for the energy equation for a fixed control volume:

$$\begin{aligned}\frac{dQ_h}{dt} - \frac{dW_s}{dt} - \frac{dW_v}{dt} = &\int_{CV} \frac{\partial \left(\left(\hat{u} + \frac{1}{2}U^2 + gz\right)\rho\right)}{\partial t} dV \\ &+ \int_{CS} \left(\hat{h} + \frac{1}{2}U^2 + gz\right) \rho U_n dA_{out} - \int_{CS} \left(\hat{h} + \frac{1}{2}U^2 + gz\right) \rho U_n dA_{in}\end{aligned} \tag{A-14}$$

Here enthalpy is defined as:

$$\hat{h} = \hat{u} + \frac{p}{\rho} \tag{A-15}$$

These three laws that need to be satisfied for a fixed control volume analysis were the basis of all the developed models for each of the transmission sub systems.

## A-4 Fluid Property State Equations

The state equations used to determine the fluid properties in the transmission are described next. Thermodynamic state equations are required to set the properties of the fluid [11]. The so-called simple compressible systems are pure single-phase substances such as water, hydraulic oil or a mixture of non-reacting gases (like air). For these single-phase substances at least two independent thermodynamic properties must be known to determine the other thermodynamic properties [15]. So for example the density and viscosity can both be determined when the pressure and temperature are known. The pressure and temperature are properties that are measured easily.

$$\rho = f(T, p) \tag{A-16}$$

$$\mu = f(T, p) \tag{A-17}$$

The state equation used here to determine the density of a fluid is [2, 16].

$$\rho = \frac{\rho_0}{(1 - \beta_e \Delta p)(1 + \gamma \Delta T)} \tag{A-18}$$

$$E_{fl} = \frac{1}{\beta_{fl}} = -V_{fl,0} \left( \frac{\partial p}{\partial V_{fl}} \right)_T \tag{A-19}$$

$$\gamma = \frac{1}{V_0} \left( \frac{\partial V}{\partial T} \right)_P \tag{A-20}$$

$E_{fl}$ is the isothermal fluid bulk modulus. It describes the change in pressure divided by the change in volume at constant temperature. The term $\left(\frac{\partial p}{\partial V_{fl}}\right)_T$ of equation A-19 is always a negative value as an increase in pressure will always lead to a decrease in volume and a decrease in pressure results in an increase in volume. A larger bulk modulus indicates that more effort is required to compress the fluid. The inverse of the bulk modulus is the compressibility modulus $\beta_{fl}$. The bulk modulus is a function of the pressure and temperature. Figure A-2 shows the bulk modulus as function of temperature and pressure for both the used oil and water.

The plots show that the bulk modulus of oil decreases with increasing temperature. Thus the compressibility increases with increasing temperature. The compressibility of water decreases with increasing temperature from 0 to 45°C, where it reaches its minimum and increases again above 45°C.

The $\gamma$ is the cubical expansion coefficient. It describes the change in volume due to a change in temperature with constant pressure. The pressure dependence of $\gamma$ is small and neglected here [11]. A larger cubical expansion coefficient indicates a larger temperature dependency of the fluid density. Figure A-3 shows the cubical expansion coefficient as a function of temperature for both the used oil and water.

The cubical expansion coefficient increases with increasing temperature for both the oil and water. The expansion of water at temperatures just above 0°C and below is confirmed by the negative cubical expansion coefficient for water in this temperature range.

The oil data shown in these plots was acquired from test data supplied by the manufacturer see appendix F. The water data shown in these plots was acquired from the papers A. Bahadori and R.A. Fine [17, 18].

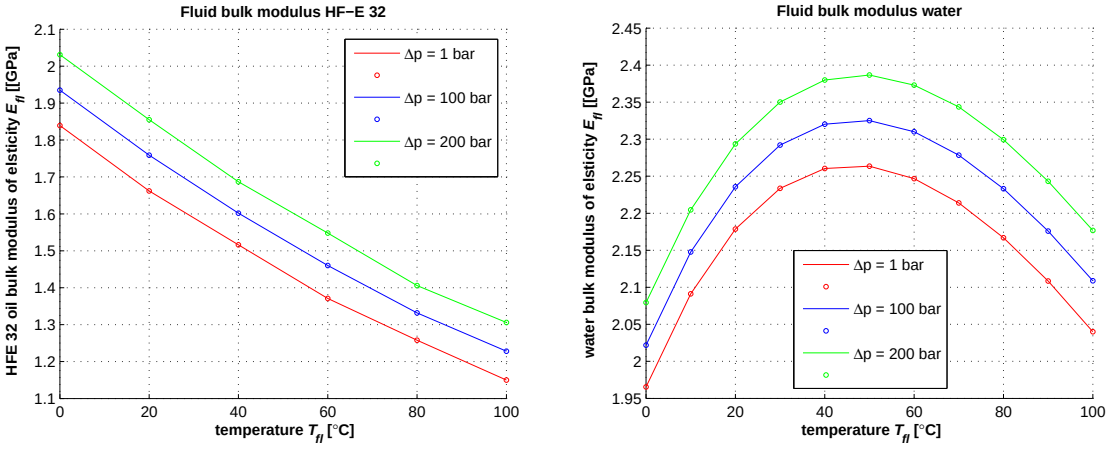


(a) (b)

**Figure A-2:** Bulk modulus of the used oil and water as function of temperature and pressure

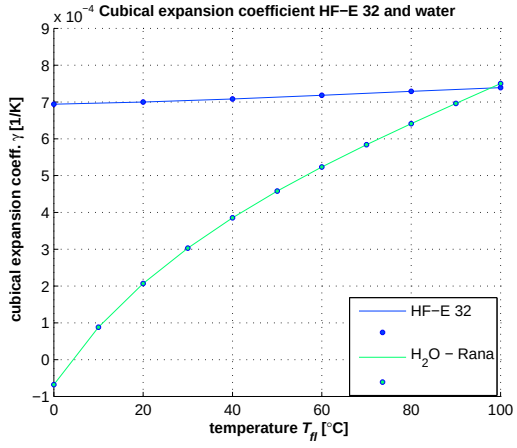


**Figure A-3:** Cubical expansion coefficient of water and oil as function of temperature

With the bulk modulus and cubical expansion coefficient known the density of the fluid is determined by equation A-18. The density as function of pressure and temperature for both the used oil and water are shown in contour plots in figure A-4.

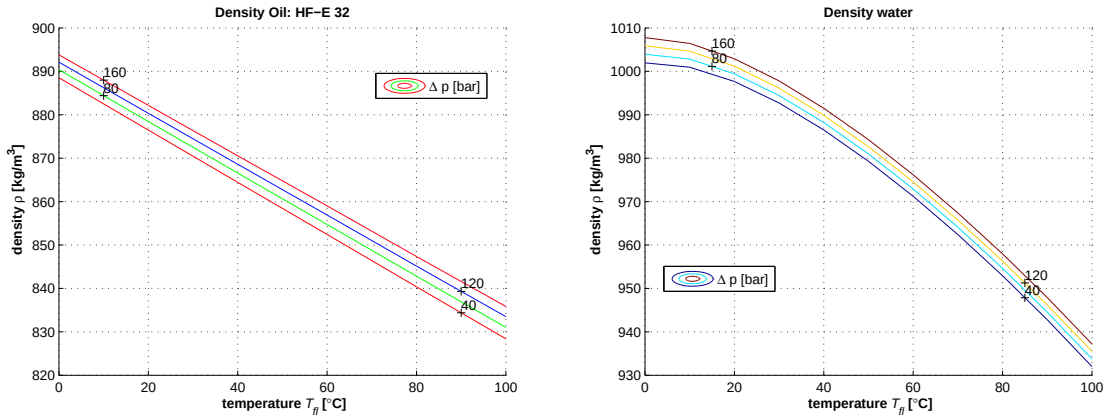


(a) (b)

**Figure A-4:** Contour plot of used oil and water density as function of temperature and pressure

The density increases with increasing pressure and decreasing temperature, for both oil and water as is seen in figure A-4. The plots also show that the temperature influence on the water and oil density is much larger than the pressure influence. However, the fluid bulk modulus can be reduced significantly by entrained air in the system and or elasticity of the hose. The influence of this on the density is taken into account by using the so called effective bulk modulus $E_e$ in the density equation of state, see equation A-18. The influence of air on the effective bulk modulus is in general the most significant [2]. The combined bulk modulus of the fluid and the entrained air $E_m$ is determined by equation A-21. Here $\alpha$ is the relative amount of air volume divided by the total volume at the start of the compression. The derivation of this equation is given in appendix G.

$$E_m = \frac{(1-\alpha)\left(1+\left(\frac{m_E p}{E_0}\right)^{-\frac{1}{m_E}}\right)+\alpha\left(\frac{p_0}{p}\right)^{\frac{1}{n}}}{\frac{1}{E_e}(1-\alpha)\left(1+\frac{m_E p}{E_0}\right)^{-\left(\frac{m+1}{m}\right)}+\frac{\alpha}{np_0}\left(\frac{p_0}{p}\right)^{\frac{n+1}{n}}} \tag{A-21}$$

The combined bulk modulus as function of pressure and air percentage is shown for both the used oil and water in figures A-5 and A-6 respectively.

Typical value of entrained air in fluid power transmissions systems is around 5% [2]. As seen in figures A-5 and A-6, this has a large influence on the effective bulk modulus especially at low pressures.

The effective bulk modulus $E_e$ is then determined by [8]:

$$\frac{1}{E_e} = \frac{1}{E_h} + \frac{1}{E_m} \tag{A-22}$$

The hose bulk modulus Eh is determined form the manufacturers test data. For the hoses used, the bulk modulus is 27.04GPa, see appendix H.

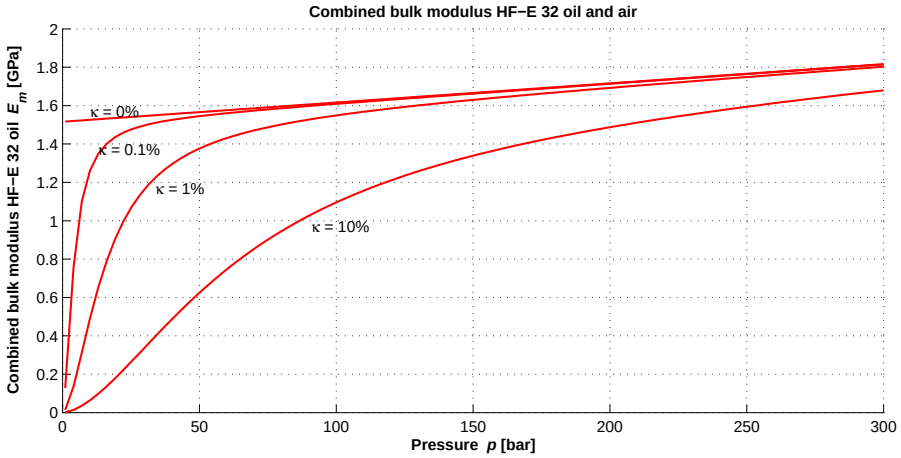


**Figure A-5:** Combined bulk modulus of oil as function of % air entrained and pressure

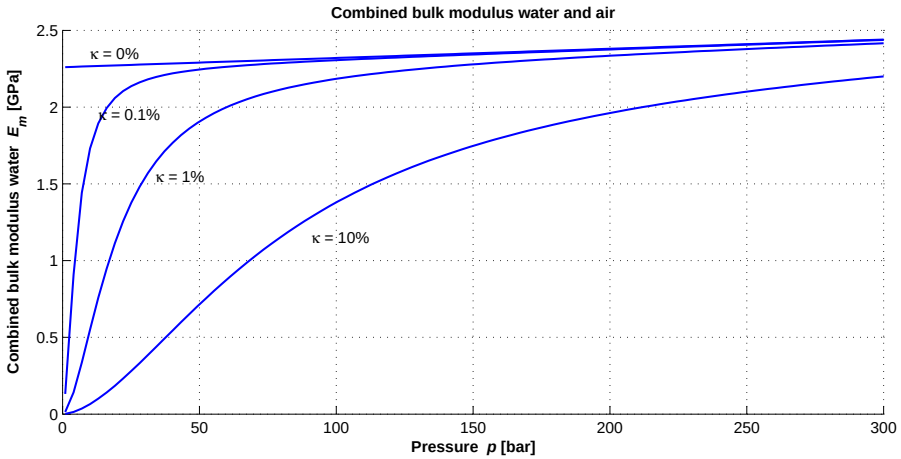


**Figure A-6:** Combined bulk modulus of water as function of % air entrained and pressure

The kinematic viscosity of the used oil and water as function of temperature is shown in figure A-7. The change in kinematic viscosity due to pressure change is insignificant up to pressures of 200 bar, and will therefore be neglected [11]. The oil data was acquired from test data supplied by the manufacturer see appendix I. The water data was acquired from the book Fluid Mechanics [11].

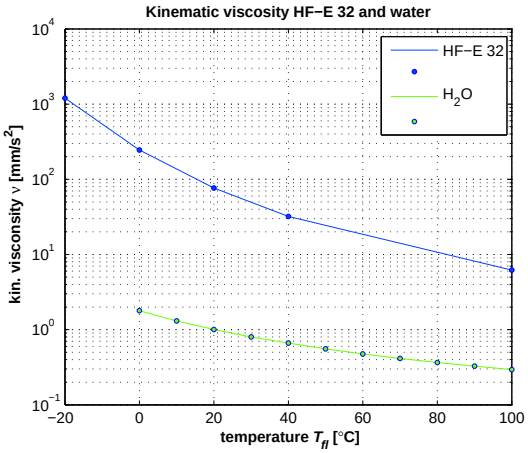


**Figure A-7:** Kinematic viscosity of oil and water as function of temperature

The temperature has a large influence on the viscosity of the used oil, especially in the region up to 500C as is seen in figure A-7. The temperature influence on the water viscosity is much smaller. The kinematic viscosity is related to the dynamic viscosity by:

$$\nu = \frac{\mu}{\rho} \tag{A-23}$$

In general a larger viscosity of the fluid results in more frictional losses. All the equations to determine the required fluid properties for the fixed control volume analysis are now known.

# Appendix B

# Hydraulic Diagram of the Detailed Design

This appendix shows the hydraulic diagram of the detailed design and the final constructed demonstration set-up including a legend for all the numbered components in the diagram.

| **Electrical components** | |
|---|---|
| E-1. | Grid |
| E-2. | Switch cabinet with frequency converter Emotron |
| E-3. | EMC protected cable |
| E-4. | Electric induction motor MEZ Frenzstat |
| E-5. | Switch cabinet with Vector frequency converter |
| E-6. | EMC protected cable |
| E-7. | Electric induction motor Vector |
| E-8. | Synchronous generator |
| E-9. | Electrical controllable load |

| **Oil hydraulic components** | |
|---|---|
| OH-1. | Hydraulic oil pump Bosch Rexroth |
| OH-2. | Pressure relief valve direct operated |
| OH-3. | Valve for breaking purpose, electrical controlled directional valve |
| OH-4. | Hydraulic oil motor Bosch Rexroth |
| OH-5. | Pressure control valve for boost/cooling system |
| OH-6. | Hydraulic oil reservoir |
| OH-7. | Boost pump |
| OH-8. | Non return valve |
| OH-9. | Manual valve |
| OH-10. | Non return valve |
| OH-11. | Non return valve pre-tensioned |
| OH-12. | Filter in the boost/cooling system |
| OH-13. | Gearbox |

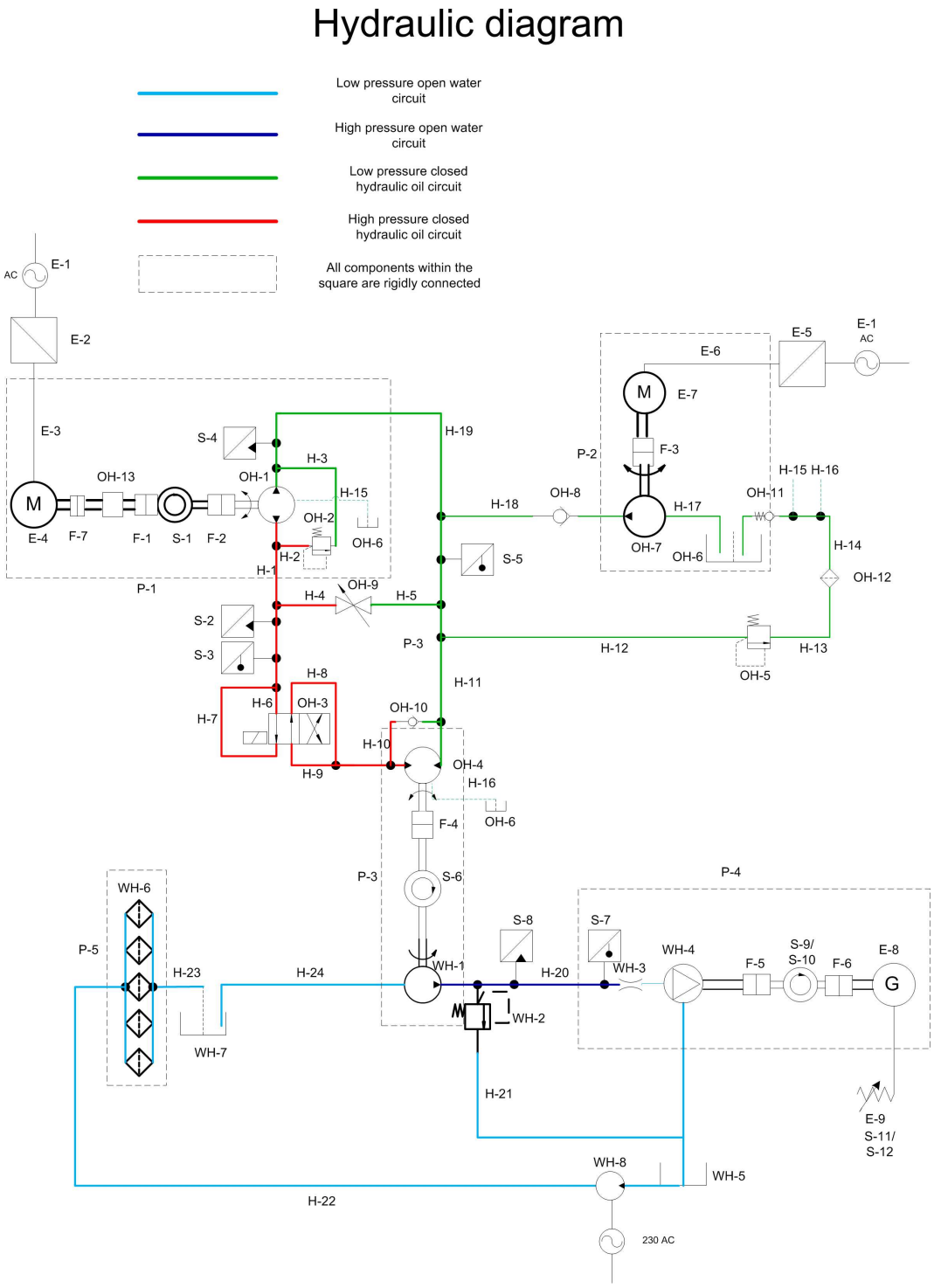


**Figure B-1:** Hydraulic diagram of the final transmission design. E = electrical component, F = flexible coupling, H = hose, OH = component of the hydraulic oil circuit, WH = component of the water circuit, S = sensor, P = platform

| **Water hydraulics components** | |
|---|---|
| WH-1. | Water pump |
| WH-2. | Pressure relief valve |
| WH-3. | Nozzle System |
| WH-4. | Pelton turbine |
| WH-5. | Large water reservoir |
| WH-6. | 5 water filters |
| WH-7. | Clean closed water reservoir |
| WH-8. | Submerged pump (to get sufficient pressure at the filters) |

| **Flexible couplings components** | |
|---|---|
| F-1. | Flexible coupling, gearbox to torque sensor |
| F-2. | Flexible coupling, torque sensor to pump |
| F-3. | Flexible coupling between boost pump and electric motor |
| F-4. | Flexible coupling between hydraulic motor and water pump |
| F-5. | Flexible coupling between Pelton and torque sensor |
| F-6. | Flexible coupling between torque sensor and generator |
| F-7. | Flexible coupling, motor to gearbox |

| **Sensor Components** | |
|---|---|
| S-1. | Torque and rpm sensor NCTE |
| S-2. | Pressure sensor AE-sensors |
| S-3. | Temperature sensor AE-sensors |
| S-4. | Pressure sensor AE-sensors |
| S-5. | Temperature sensor AE-sensors |
| S-6. | RPM sensor |
| S-7. | Temperature sensor AE-sensors |
| S-8. | Pressure sensor AE-sensors |
| S-9. | Torque sensor NCTE |
| S-10. | RPM sensor |
| S-11. | Voltage sensor at electric load |
| S-12. | Current sensor at electric load |

| **Platforms** | |
|---|---|
| P-1. | Platform 1: for electric motor and oil pump |
| P-2. | Platform for boost/cooling system |
| P-3. | Platform of hydraulic motor and water pump |
| P-4. | Pelton and generator platform |
| P-5. | Filter platform |

| **Hoses** | |
|---|---|
| H-1. | High pressure flexible hose between platform 1 and 2 (10m, 3/4 inch) |
| H-2. | High pressure flexible hose input pressure relief valve ( 1/2 inch) |
| H-3. | Low pressure flexible hose output pressure relief valve (1/2inch) |
| H-4. | High pressure flexible hose input manual start-up valve (1/2 inch) |
| H-5. | Low pressure flexible hose output manual start up valve (1/2 inch) |
| H-6. | High pressure flexible hose input break valve port P(3/4 inch) |
| H-7. | High pressure flexible hose input break valve port A(3/4 inch) |
| H-8. | High pressure flexible hose output break valve port T(3/4 inch) |
| H-9. | High pressure flexible hose output break valve port B(3/4 inch) |
| H-10. | Low pressure flexible hose output non return valve motor (1/2 inch) |
| H-11. | Low pressure flexible hose output hydraulic motor (1 inch) |
| H-12. | Low pressure flexible hose input boost system (1/2 inch) |
| H-13. | Low pressure flexible hose input filter (1/2 inch) |
| H-14. | Low pressure flexible hose output filter (1/2 inch) |
| H-15. | Low pressure flexible hose drain hydraulic pump (1/2 inch) |
| H-16. | Low pressure flexible hose drain hydraulic motor (1/2 inch) |
| H-17. | Low pressure flexible hose input boost pump (1/2 inch) |
| H-18. | Low pressure flexible hose output boost pump (1/2 inch) |
| H-19. | Low pressure flexible hose input hydraulic pump (1 inch, 10 m) |
| H-20. | High pressure flexible output water pump (1 inch, 10 m) |
| H-21. | Low pressure flexible output pressure relief valve |
| H-22. | Low pressure flexible input filters |
| H-23. | Low pressure flexible output filters |
| H-24. | Low pressure flexible input water pump |

# Appendix C

# Bond Graph Modeling Language

In this appendix a brief explanation on the used Bond Graph modelling language is given. This language is very suitable to model and analyze the dynamic response and natural frequencies of physical systems [13]. A detailed explanation on the Bond Graph language is given in "Modeling, Simulation and Analysis of Dynamic Systems" by E. Pedersen [13].

Interacting physical systems transmit power between each other. A uniform classification of variables associated with power and energy is used in the bond graph language. Were the same variables are used for different physical domains. These variables are also called the generalized variables. These generalized variables are used to define a small number of ideal elements that make it possible to approximate real physical systems by lumped parameter models of physical systems. The basic elements are connected with the so called power bonds. These power bonds transmit power (energy flow) instantaneously and without losses between the basic elements.

First the generalized variables are discussed. Then a description of the basic elements is given. Finally a procedure to model a complete physical system from these basic elements is explained briefly.

## C-1 Generalized Variables

As mentioned before interacting physical system transmit power between each other. This power is described by two variables the so called power variables. These variables are selected such that the product of the variables is power. These generalized power variables are called effort (e) and flow (f). The power bonds, that transmit the power between the elements, always transmit these variables. The product of the variables effort and flow is power. The positive direction of energy flow is indicated by the half arrow. One of the variables is the input and the other the output. this is indicated by the position of the vertical stripe, this vertical stripe indicates the direction of the effort, see figure C-1.

$$P(t) = e(t)\, f_b(t) \tag{C-1}$$

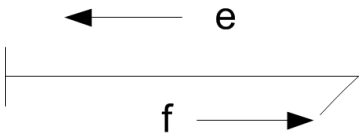


**Figure C-1:** Power bond

Physical systems are capable of storing energy. This is also modeled by these basic elements that are described in the next section. The variables that describe the energy storage are called the generalized energy variables. The time integral of power is energy. The two energy variables are generalized momentum and displacement. The generalized momentum variable is the time integrand of the effort:

$$M = \int_0^t e\,(t)\,dt + M\,(0) \tag{C-2}$$

The generalized displacement variable is the time integrant of the flow:

$$q_b = \int_0^t f_b\,(t)\,dt + q\,(0) \tag{C-3}$$

The power and energy variables for 3 physical domains are shown in table C-1.

| Energy domain | Effort | Flow | Momentum |
|---|---|---|---|
| Mechanical Translational | Force [N] | Velocity [m/s] | Linear momentum [Ns] |
| Mechanical rotational | Torque [Nm] | Angular velocity [rad/s] | Angular momentum [Nms] |
| Hydraulic | Pressure [Pa] | Volume flow [m3/s] | Pressure momentum [Pas] |

**Table C-1:** Identification of variables for different domains

## C-2 Basic Bond Graph Elements

The bond graph language consists of nine basic elements with which physical systems are represented. The basic ideal elements represent all the ways a system can process energy. The way a system can process energy are energy supply, storage, dissipation, conversion and transduction [13].

First the basic elements for energy supply are discussed. There are twp basic elements for energy supply, these are the source of effort or source of flow. The power that a source delivers is from an external supply outside the systems control volume. The source of effort $Se$ is an idealized source where the effort is prescribed as a function of time independent of the systems flow, see figure C-2. The source of flow Sf is an idealized source where the flow is prescribed as a function of time independent of the systems effort, see figure C-2. The sign convention for both energy sources is energy flow outwards. Although not often used power can flow into the energy source, due to the sign convention this will then result in a negative energy flow.


**Figure C-2:** Energy supply elements

The basic elements that are able to store energy are the inertia and the capacitor elements. Both elements are ideal meaning that they are able to store energy without losses. Systems are able to store energy in 2 forms being potential energy and kinetic energy. Kinetic energy storage is modeled by the inertia element, see figure C-3. The energy stored by an inertia element is described by a relation between a generalized momentum and a flow.

$$M = \Phi_I \left( f_b \right) \tag{C-4}$$

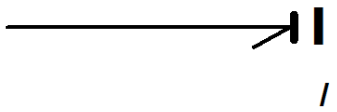


**Figure C-3:** Inertia element

In the bond graph terminology this is indicated by an $I$ element. In the linear case the constitutive relation is given, with $I$ as the constant inertia parameter.

$$M = I f_b \tag{C-5}$$

The sign convention is that the arrow is pointed towards the $I$ element, thus positive power value means that energy flows into the storage element. Potential energy storage is modeled by a capacitor element, see figure C-4. This form of energy storage is described by a relation between a generalized effort and displacement.

$$q_b = \Phi_C \left( e \right) \tag{C-6}$$

In the bond graph terminology this is indicated by a C element. In the linear case the

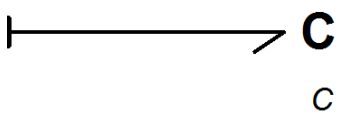


**Figure C-4:** Capacitor element

constitutive relation is given, with $C$ as the constant capacitance parameter.

$$q_b = C_e \tag{C-7}$$

Also here the sign convention is that the arrow point towards the C element. Thus positive power value means that energy flows into the storage element.

The basic element that takes care of energy dissipation is the resistor element. Off course energy is never really lost. It is only converted into a form that is not desired and the energy that is transformed to this form is then indicated as a loss or as dissipated energy. The only element that can model energy dissipation is this resistor element, see figure C-5. The energy dissipated by this resistor element is described by a relation between the generalized effort and flow variable.

$$e = \Phi_R\left(f_b\right) \tag{C-8}$$

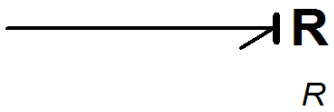


**Figure C-5:** Resistor element

In the bond graph terminology this is indicated by an R element. In the linear case the relation is given, with R as the constant resistance parameter.

$$e = Rf_b \tag{C-9}$$

Also for the R elements the sign convention is that the arrow points towards the R element. Thus positive power value means that energy is dissipated from the system.

There are two elements that model energy conversion. These are mainly used to convert energy from one domain to another domain. These elements do not store or dissipate energy they transmit power instantaneously. Therefore they have 2 ports, one power input and a power output. The elements are ideal, meaning that they convert power without any losses. Thus the power at input is equal to the output power at all times. The first energy conversion element is the transformer, see figure C-6. This element is modeled by two relations:

$$e_1 = me_2 \tag{C-10}$$

$$mf_{b1} = f_{b2} \tag{C-11}$$

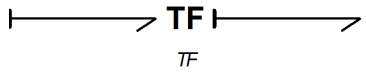


**Figure C-6:** Transformer element

A transformer is an element which transforms the effort on one port into an effort on the other port, where the magnitude of the effort depends on the modulus m. The flows are also directly related to each other as is shown in equation C-11. The transformer element is indicated by TF in a bond graph model. The sign convention is that one of the arrows is directed to the transformer element and the other arrow out of the element. The other conversion element is a gyrator, see figure C-7. This element is modeled by 2 relations:

$$e_1 = r_1 f_{b2} \tag{C-12}$$
$$r f_{b1} = e_2 \tag{C-13}$$

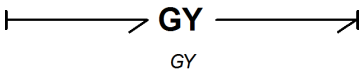


**Figure C-7:** Gyrator element

A gyrator is an element that transforms an effort on one port into a flow on the other port, where the magnitude depends on the gyrator modulus $r$, see equations C-12 and C-13. The gyrator element is indicated by $GY$ in a bond graph model. The sign convention is the same as for the transformer.

To be able to model a physical system there are an additional two elements required that can interconnect all the previous mentioned elements into a model that approximates a physical system. These are the junction elements. These elements only transmit energy. Again these are ideal elements thus no losses occur. The elements can have as many power bonds connected to them as is required, but the instantaneous power in must be equal to the instantaneous power out. The 0-junction element relations are:

$$e_1 = e_2 = e_3 \tag{C-14}$$
$$f_{b1} + f_{b2} + f_{b3} = 0 \tag{C-15}$$

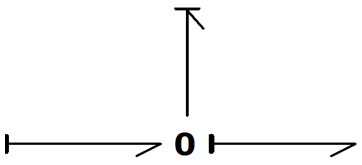


**Figure C-8:** 0-junction element

This means that the effort on all bonds are equal to each other and the sum of the flows is zero. In an electric system the 0-junction represent KirchofsŠs current law. The 1-junction element relations are:

$$f_{b1} = f_{b2} = f_{b3} \tag{C-16}$$
$$e_1 + e_2 + e_3 = 0 \tag{C-17}$$

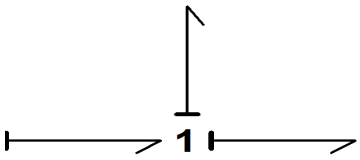


**Figure C-9:** 1-junction element

This means that the flows on all bonds are equal to each other and the sum of the efforts is zero. In an electric system the 1-junction represent Kirchofs voltage law.

All basic elements have now been discussed briefly. The bond graph elements and the relations are summarized in figure C-10.

## C-3 Modeling Procedure of a Physical System with the Basic Elements

The fluid power transmission contains systems operating in the mechanical domain and the hydraulic domain. The modeling procedures for systems in these energy domains is briefly described in this section. There are modeling procedures for other energy domains then the mechanical and hydraulic domains, but these will not be described here. First the modeling procedure for a physical system in the mechanical domain is explained briefly in this section, a more detailed explanation is given in section 3.2 of [13]. Then a brief explanation of the modeling procedure for a physical system in the hydraulic domain with the basic elements is given, a more detailed explanation is given in section 3.7 of [13]. Finally a brief explanation is given on how to connect the models in the mechanical and hydraulic domain to each other into one model.

Modeling procedure for a physical system in the mechanical domain:

1. Indicate each velocity of the physical system by a 1-junction.
2. When these velocities contain an inertia element, connect an inertia element to the one junctions.
3. When there is a relative velocity between two 1-junctions connect them to each other with one 0-junction in between. If present connect resistor and capacitor elements to the 0-junction.
4. After all the elements of the physical system are connected to each other with the above procedure. All 1-junctions with zero velocity and there connected elements can be removed.
5. Assign power direction to the elements by applying the sign conventions for each element.
6. Last step is to simplify the model replacing the 2-port 0 and 1-junctions with through power bonds.

| Bond graph element | Constitutive relations |
|---|---|
| 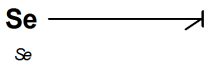 | $e=e(t)$ |
| 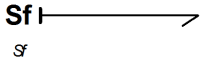 | $f=f(t)$ |
|  | $M=\Phi_I(f)$ |
| 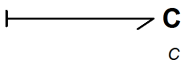 | $F=\Phi_c(e)$ |
| 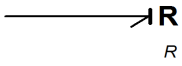 | $e=\Phi_R(f)$ |
| 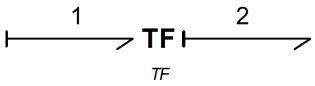 | $e_1=e_2m$<br>$f_1m=f_2$ |
| 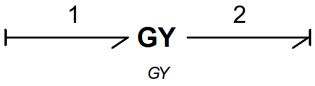 | $e_1=f_2r$<br>$e_2=f_1r$ |
| 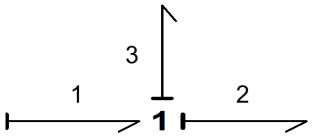 | $f_1=f_2=f_3$<br>$e_1+e_2+e_3=0$ |
| 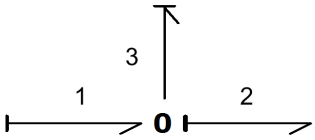 | $e_1=e_2=e_3$<br>$f_1+f_2+f_3=0$ |

**Figure C-10:** Legend of basic bond graph elements [13]

Modelling procedure for a physical system in the hydraulic domain:

1. Indicate each pressure in the system by a 0-junction.
2. The flow between 2 pressures is modeled by a 1 junction connected between the two 0-junctions. The present energy storage and dissipating elements in the physical systems are now connected to the 0 and 1-junctions.
3. Connect the present pressure and flow sources to the appropriate 0 and 1-junctions.
4. Remove all 0-junctions that represent atmospheric pressure and there connected elements.
5. Assign power direction to the elements by applying the sign conventions for each element.
6. Last step is to simplify the model replacing the 2-port 0 and 1-junctions through power bonds.

The models of a physical systems in mechanical and hydraulic domains can be coupled to each other by the energy conversion elements, thus the transformer or gyrator element.

When, the models of all the sub systems in the fluid power transmission are connected and the equations of the elements in the model are known the final system equations can be derived. This can be done manually an explanation on the procedure of how to do this is given in chapter 4 of [13]. This is very time consuming procedure especially when elements are added or removed throughout the modeling process. The final system equations can also be derived by a software program. The model and the elements equations are defined by the model user. The program will then derive the final system equations. A great advantage of this is that it is easy to add or remove elements and thus easy to analyze the influence of certain elements on the complete model. For the modeling procedure of the fluid power transmission for this thesis the software program called 20-Sim was used.

# Appendix D

# Procedure used for the Model Modifications

## D-1 Brief Explanation of the Procedure

The laboratory demonstration set-up with the exact locations of the sensors is shown in a block diagram in figure D-1. This block diagram visualizes the energy conversion steps of the transmission and the location of the sensors indicated by red letters.

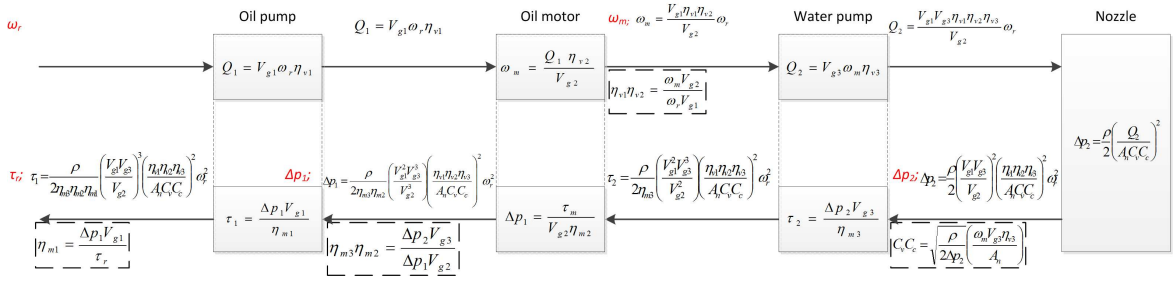


**Figure D-1:** Block diagram of demonstration set-up. The measured values are indicated with red letters

This block diagram is used to identify the efficiencies between each pair of consecutive sensors. First the measured values at each sensor are compared to the original model. The equations in figure D-1 are derived by using the equations explained in section A-4 and are indicated in the block diagram with boxes. With these equations and the measured values the actual efficiency between each pair of sensors is derived. A comparison is then made between the original predicted efficiencies and the actual efficiencies derived from the measurements. The final step is then to define new equations that describe the measured efficiencies. This procedure is executed for three different nozzles with different nozzle diameters. In the modified model all the efficiencies are calculated as a function of the rotational speed of the pump $\omega_r$ and the nozzle diameter. The advantage of this is that it greatly simplifies the model calculations

because these properties are known at the start and do not have to be determined with iterations in a loop. A disadvantage is that the determined equations for the efficiencies in the model are only valid for one specific nozzle diameter. Meaning that the procedure described here has to be executed for every new nozzle diameter.

The procedure of the model modifications is the same for all nozzles however the results are slightly different. In this appendix only the results of the model modifications for the 4.24 mm nozzle diameter are discussed.

## D-2 Comparison and Model Modifications of $\eta_{m1}$ and $\eta_{m2}$

The controllable input of the demonstration set-up is the rotational speed of the hydraulic oil pump $\omega_r$. The wind turbine rotor is removed in the simulation model so that the input of the model is also $\omega_r$. The input is measured during the experiments with a pulse sensor. The next sensor is the rotational speed sensor of the oil motor and water pump $\omega_m$, which is also a pulse sensor. Between these two sensors the mechanical energy at the input is converted into hydraulic energy and back into mechanical energy at the oil motor. As shown in the block diagram two efficiencies $\eta_{m1}$ and $\eta_{m2}$ are associated with these energy conversion steps, this results in the following equation:

$$\eta_{v1}\eta_{v2} = \frac{\omega_m}{\omega_{mid}} = \frac{\omega_m V_{g2}}{\omega_r V_{g1}} \tag{D-1}$$

The measured and predicted rotational speed of the oil motor $\omega_m$ as function of the input $\omega_r$ is shown in figure D-2. With equation D-1 the combined efficiency $\eta_{m1}$ and $\eta_{m2}$ between the two sensors is derived and also shown in figure D-2.

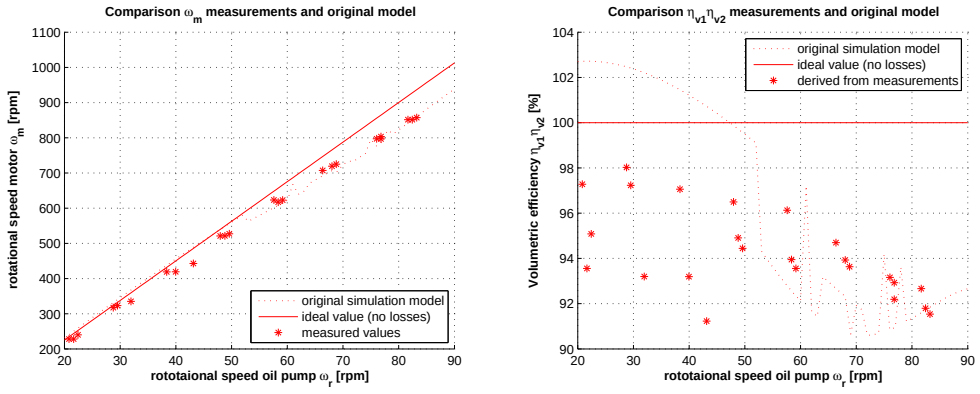


**Figure D-2:** Comparison of rotational speed $\omega_m$ and the combined efficiency $\eta_{m1}\eta_{m2}$

The original model gives a $\omega_m$ that is in reasonable good agreement with the measured value. However, the trend line of the original model is not smooth. This has to do with the look up tables used for the volumetric efficiency in the original model. Extrapolation from the oil pump efficiency look up table is required because of the low $\omega_r$. Extrapolation from this lookup table is unreliable. Due to the extrapolation from the lookup table the efficiencies predicted by the model are larger than 100% below an input of 50rpm. This is of course

impossible. And also identifies the need for modification of the efficiency equations used in the model. The spread of the measured efficiencies between 20 to 60rpm input is quite large between 98 and 91%, indicating that the values derived from measurements are not very consistent in this region. Above 60 rpm input the efficiency derived from measurements is more consistent as is also indicated by the smaller spread.

With the available sensors in the transmission it is only possible to derive the product of the volumetric efficiency of the oil pump and motor combined, see figure D-2. There is no way that the volumetric efficiencies $\eta_{m1}$ and $\eta_{m2}$ can be derived separately from the measurements. Therefore the volumetric efficiency that looks most realistic is chosen to be kept equal to the predicted values of the original model. The other volumetric efficiency equation is then modified such that the product of the efficiencies equals the derived efficiency from the measurements. The volumetric efficiencies of the oil pump and motor predicted by the original model are shown in figure D-3. This graph shows that the volumetric efficiency of the oil motor predicted by the original model is realistic. The volumetric efficiency of the oil pump is impossible and unrealistic, with values above 100%. Therefore, the oil pump volumetric efficiency is chosen to be modified.

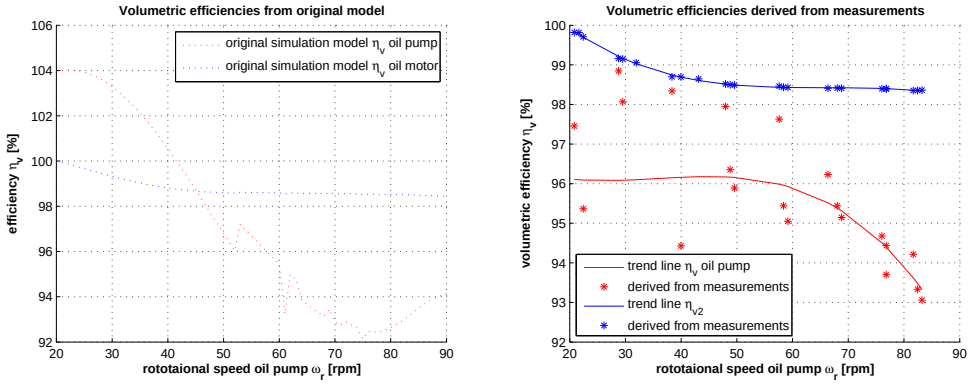


**Figure D-3:** Original volumetric efficiencies $\eta_{m1}$ and $\eta_{m2}$ predicted by the original model. $\eta_{m1}$ and $\eta_{m2}$ derived from measurements

Trend lines are fitted through the derived data from measurements, see figure D-3. The equation of these trend lines are used in the modified model.

$$\eta_{v1} = -2.94 \cdot 10^{-7}\omega_r^3 + 3.14 \cdot 10^{-5}\omega_r^2 - 1.0 \cdot 10^{-3}\omega_r + 0.972 \quad \text{(D-2)}$$

$$\eta_{v2} = -1.57 \cdot 10^{-7}\omega_r^3 + 3.09 \cdot 10^{-5}\omega_r^2 - 2.0 \cdot 10^{-3}\omega_r + 1.029 \quad \text{(D-3)}$$

Both efficiencies are only a function of $\omega_r$ in the modified model. It must be kept in mind that these equations are only valid at the specified nozzle diameter of 4.24 mm. If the nozzle diameter changes the pressures in the oil and water circuit changes, this influences the efficiencies.

## D-3 Comparison and Model Modifications of $\eta_{m3}$ and $C_v$

The next sensor is the sensor that measures the pressure in the water circuit $\Delta p_2$, see the block diagram in figure D-1. Between the sensors for $\omega_m$ and $\Delta p_2$ the energy is converted

from mechanical into hydraulic energy at the water pump and from hydraulic potential energy into hydraulic kinetic energy at the nozzle. The measured and predicted pressure in the water circuit $\Delta p_2$ as function of the input $\omega_r$ is shown in figure D-4.

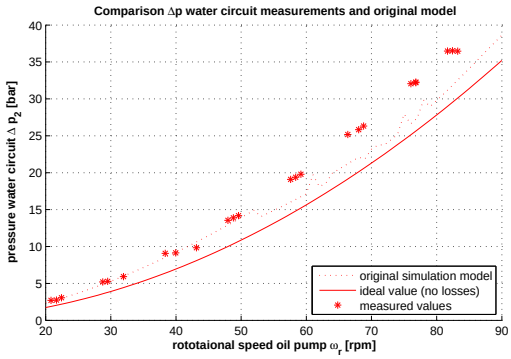


**Figure D-4:** Comparison of pressure in the water circuit $\Delta p_2$

The measurements show to be in reasonable good agreement with the original model, especially at low input $\omega_r$. However also here the trend of the original model is not smooth. This again has to do with the extrapolation from the efficiency look up tables. Again the choice is made to modify the original model so that the predicted values of the model will be closer to the measured values.

For each of the two energy conversion steps losses occur. These losses are determined by the volumetric efficiency at the water pump $\eta_{m3}$ and the efficiency at the nozzle. The efficiency at the nozzle is determined by the velocity coefficient $C_v$. Starting with the equation for $\Delta p_2$ in figure D-1 and filling in for the volume flow and rewriting this for the velocity coefficient $C_v$ and contraction coefficient $C_c$ gives:

$$C_v C_c = \sqrt{\frac{\rho}{2\Delta p_2}} \left( \frac{\omega_m V_{g3} \eta_{v3}}{A_n} \right)^2 \tag{D-4}$$

The values $C_v$, $C_c$ and $\eta_{m3}$ cannot be derived separately from measurements. Therefore two of the values need to be assumed. The manufacturer of the water pump supplied some experimental data, see appendix J. Based on this information the volumetric efficiency of the water pump $\eta_{m3}$ is assumed to be constant at 99.5%. A constant value has been chosen, for ease of calculation and because there was no data available at low rotational speed of the pump. The contraction coefficient was assumed at 1.0. This overestimates the nozzle losses as explained in section 6-2-2. With these assumptions the velocity coefficient $C_v$ is derived with equation D-4, such that the losses in these two conversion steps agree with the measured losses. In figure D-5 the predicted values by the original model and derived values from measurements for $\eta_{m3}$ and $C_v$ are shown.

The velocity coefficient predicted by the model is a lot larger than actual velocity coefficient. This mean that the actual efficiency at the nozzle is a lot lower than predicted by the original model. The spread of the derived values from measurements are small indicating these measurements were consistent. The equations of the fitted trend lines are used in the modified

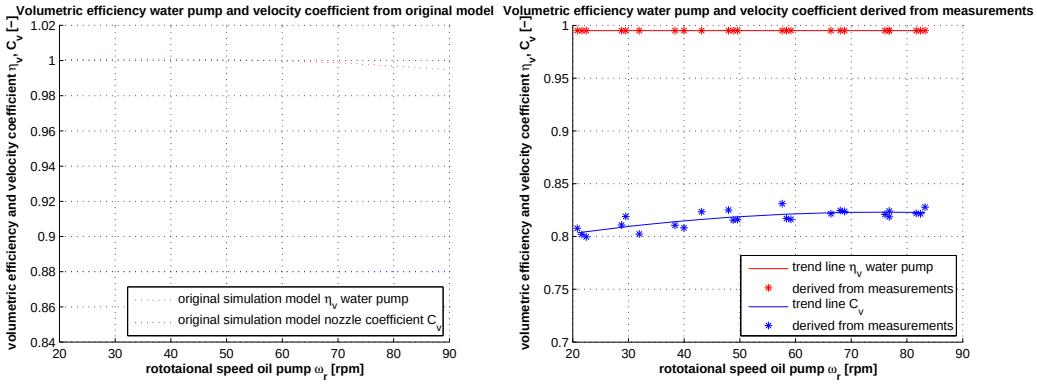


**Figure D-5:** Volumetric efficiency $\eta_{m3}$ and velocity coefficient Cv predicted by the original model and derived from measurements

model.

$$\eta_{v3} = 0.995 \tag{D-5}$$

$$C_v = -6.61 \cdot 10^{-6}\omega_r^2 + 9.96 \cdot 10^{-4}\omega_r + 0.786 \tag{D-6}$$

Both $\eta_{m3}$ and Cv are again only a function of $\omega_r$ in the modified model. This also means that these equations are only valid for the nozzle diameter of 4.24mm.

## D-4 Comparison and Model Modifications of $\eta_{m3}$ and $\eta_{m2}$

The next sensor in the block diagram of figure D-1 is the pressure sensor of the oil circuit. Between the pressure sensor of the water circuit $\Delta p_2$ and the pressure of the oil circuit $\Delta p_1$, the hydraulic energy is converted to mechanical and back to hydraulic energy at sensor $\Delta p_1$. The losses associated with these two conversion steps are described by the mechanical efficiency of the water pump $\eta_{m3}$ and oil motor $\eta_{m2}$. With the measured values of $\Delta p_2$ and $\Delta p_1$ the combined efficiency of $\eta_{m2}$ and $\eta_{m3}$ is derived, see figure D-1.

$$\eta_{m2}\eta_{m3} = \frac{\Delta p_2 V_{g3}}{\Delta p_1 V_{g2}} \tag{D-7}$$

The predicted and the measured values for the pressure in the oil circuit $\Delta p_1$ are shown in figure D-6. With equation D-7 the combined efficiency $\eta_{m2}$ and $\eta_{m3}$ between the two sensors is derived and also shown in figure D-6.

The predicted values for $\Delta p_1$ by the original model are in reasonable agreement with the measured values. However the trend line of the original model is again not smooth this is again caused by the extrapolation of the oil pump efficiency lookup tables in the model. The predicted combined mechanical efficiency $\eta_{m2}$ and $\eta_{m3}$ of the original model shows a large difference with the derived values from measurements at low $\omega_r$. Especially the overestimated combined mechanical efficiency $\eta_{m2}$ and $\eta_{m3}$ at low $\omega_r$ identifies the need for model modifications for these efficiencies. The spread of the derived combined mechanical efficiency $\eta_{m2}$ and $\eta_{m3}$ from measurements is small, indicating consistent measurements.

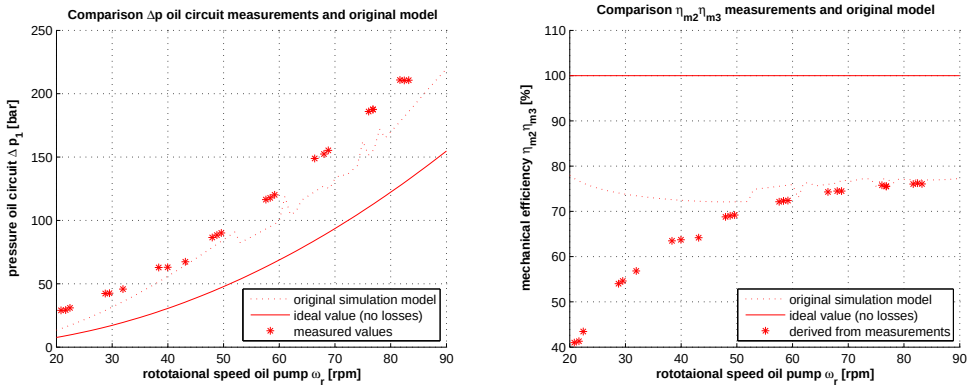


**Figure D-6:** Comparison of oil circuit pressure $\Delta p_1$ and the combined efficiency $\eta_{m2}\eta_{m3}$

The mechanical efficiencies $\eta_{m2}$ and $\eta_{m3}$ cannot be derived separately from the measurements. An overestimated mechanical efficiency of the water pump $\eta_{m3}$ is expected to be the cause of this difference between the predicted and the measured combined efficiency. Reason for this is that the supplied test data for the water pump did not give any values for the mechanical efficiency at low rotational speeds $\omega_m$, see appendix J. Therefore the choice is made to modify the mechanical efficiency for the water pump such that the combined mechanical efficiency $\eta_{m2}$ and $\eta_{m3}$ is equal to the derived values from measurements. The predicted efficiencies by the original model and the modified efficiencies are shown in figure D-7. This figure also shows that the predicted water pump mechanical efficiency in the original model results in impossible values above 100% at low $\omega_r$. The limited available test data at low rotational speeds made extrapolation from the water pump mechanical efficiency look up table necessary. This caused the unreliable and impossible values for the mechanical efficiency of the water pump.

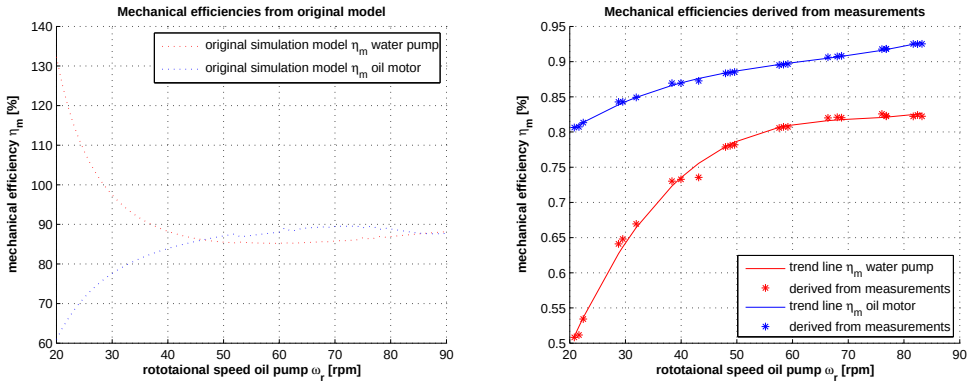


**Figure D-7:** Mechanical efficiencies $\eta_{m2}$ and $\eta_{m3}$ predicted by the original model and derived from measurements

Trend lines are fitted through the derived data from measurements, see figure D-7. The equation of these trend lines are used in the modified model.

$$\eta_{m2} = 7.00 \cdot 10^{-7}\omega_r^3 - 1.33 \cdot 10^{-4}\omega_r^2 + 9.4 \cdot 10^{-3}\omega_r + 0.663 \quad \text{(D-8)}$$

$$\eta_{m3} = 2.16 \cdot 10^{-6}\omega_r^3 - 4.66 \cdot 10^{-4}\omega_r^2 + 3.4 \cdot 10^{-2}\omega_r - 0.015 \quad \text{(D-9)}$$

Both efficiencies are then only a function of $\omega_r$ in the modified model. This also means that these equations are only valid for the nozzle diameter of 4.24mm.

## D-5 Comparison and Model Modifications of $\eta_{m1}$

The next and last sensor in the block diagram of figure D-1 is the torque sensor $\tau_1$ at the oil pump. Between the pressure sensor of the oil circuit $\Delta p_1$ and the torque sensor at the oil pump $\tau_1$, the hydraulic energy is converted into mechanical energy at sensor $\tau_1$. The losses associated with this conversion step is described by the mechanical efficiency of the oil pump $\eta_{m1}$. With the measured values of $\Delta p_1$ and $\tau_1$ the mechanical efficiency of the oil pump $\eta_{m1}$ is derived, see figure D-1.

$$\eta_{m1} = \frac{\Delta p_1 V_{g1}}{\tau_1} \tag{D-10}$$

The predicted and the measured values for the torque at the oil pump $\tau_1$ are shown in figure D-8. With equation D-10 the mechanical efficiency $\eta_{m1}$ between the two sensors is derived and also shown in figure D-8.

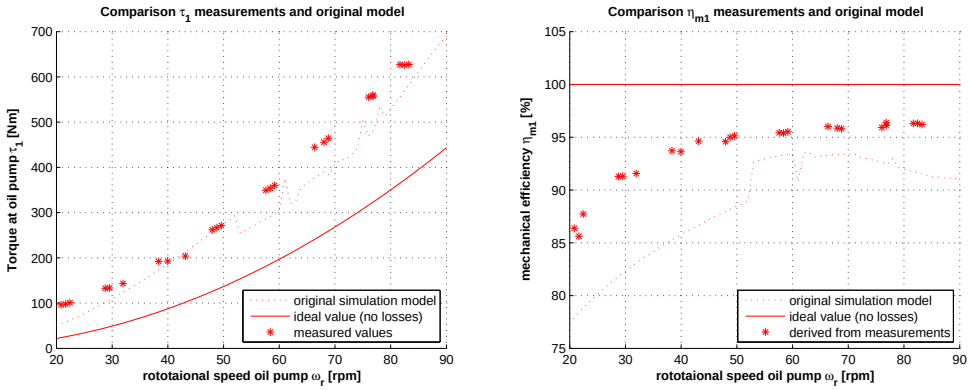


**Figure D-8:** Comparison of torque at the oil pump $\tau_1$ and the mechanical efficiency $\eta_{m1}$

The predicted values for $\tau_1$ by the original model are in reasonable agreement with the measured values. However the trend line of the original model is again not smooth this is again caused by the extrapolation of the oil pump efficiency lookup tables in the model. The predicted mechanical efficiency $\eta_{m1}$ of the original model shows a significant difference with the derived values from measurements. The under estimated predicted values for $\eta_{m1}$ identify the need to modify the equation for the mechanical efficiency $\eta_{m1}$. With equation D-10 the mechanical efficiency of the oil pump $\eta_{m1}$ is derived and shown in figure D-9.

A trend line is fitted through the derived values of $\eta_{m1}$ from measurements, see figure D-9. The equation of this trend line is used in the modified model.

$$\eta_{m1} = 1.10 \cdot 10^{-6}\omega_r^3 - 2.13 \cdot 10^{-4}\omega_r^2 + 1.38 \cdot 10^{-2}\omega_r + 0.659 \tag{D-11}$$

This efficiency is then only a function of $\omega_r$ in the modified model. This also means that this equation is only valid for the nozzle diameter of 4.24mm.

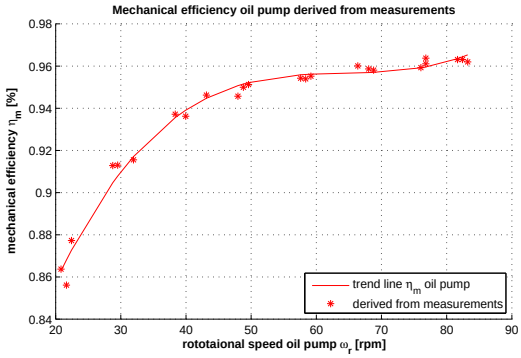


**Figure D-9:** Mechanical efficiency $\eta_{m1}$ derived from measurements

# Appendix E

# Pulse and Frequency Sensor at the Oil Pump

In the transmission setup in the laboratory there are two sensor from which the rotational speed of the oil pump can be derived. The sensors that measures the rotational speed directly is the pulse sensor. The working principle of the pulse sensor is that it counts the number of rotations in a certain defined timespan. When the timespan is set at 2 seconds for example the sensor reads the average rotational speed of the past two seconds, it does not read the real time rotational speed. The readings of this sensor are only useful for steady state experiments and not for dynamic experiments. For the dynamic experiments the analogue electric frequency sensor $\omega_e$ is used instead of the pulse sensor. This sensor measures the frequency of the electric current in the asynchronous motor that drives the transmission. From this sensor the real time rotational speed of the pump $\omega_r$ is determined fairly accurately. However, between the electric frequency of the current $\omega_e$ and the rotational speed of the rotor in the electric motor exists some slip. The slip increases with increasing torque. The result of this slip is a slightly higher measured rotational speed than the actual rotational speed of the oil pump. At maximum torque and pressures in the transmission the difference between the pulse sensor and the electric frequency sensor was measured at 4%, see figure E-1. The difference between the sensors was measured for both a high torque and low torque conditions. All measurements were taken at steady state condition.

The most suitable sensor for the rotational speed of the oil pump during dynamic experiments is thus the electric frequency sensor $\omega_e$. However keep in mind that the error is up to 4% at a high torque.

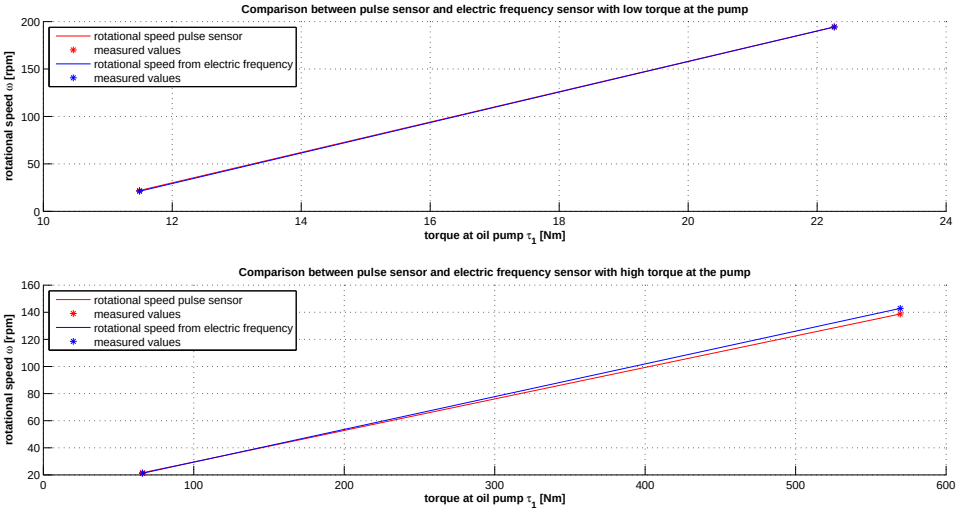


**Figure E-1:** Comparison of the rotational speed of the oil pump between the pulse sensor and frequency sensor at steady state conditions

# Appendix F

# Difference in Linearization Results between 20-Sim and Simulink

The Bode plots of the original model linearized in the 20-Sim program and the Bode plot of the original model linearized in Simulink are shown in figure F-1. The models have exactly the same inertia and capacitance elements. The resistances in the transmission are modeled exactly the same. The models linearized in Simulink and 20-Sim are thus exactly the same. The models are linearized at the same operational point at a rotor torque of 600Nm.

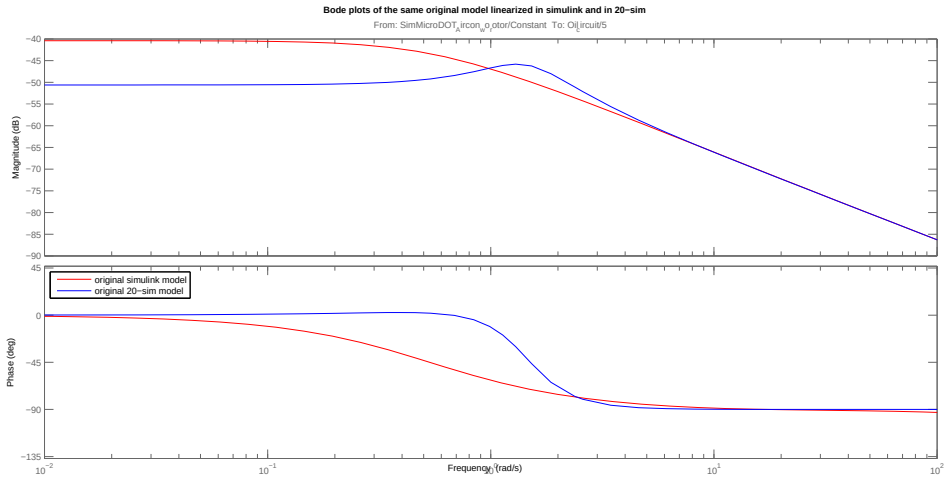


**Figure F-1:** Bode plots of the original transmission models including rotor, linearized in 20-Sim and Simulink at an operation point of 600Nm rotor torque

In theory both programs should give an exact same Bode plot. However there is a difference in magnitude between the two models at low frequency and the model linearized in Simulink is more damped than the model linearized in 20-Sim. Above a frequency of 5rad/s the Bode

plots are exactly the same. Where the difference in the low frequency range and in the damping ratio comes from was not found. However it is thought that the differences are caused by the different linearization methods of the software programs. The results of the linearizations are especially sensitive for the linearization method in the low frequency region, which is the case here. Further research is required to find the cause of the difference between the Bode plots of the models.

# Appendix G

# Derivation of the Effective Bulk Modulus

The fluid bulk modulus can be reduced significantly by entrained air in the system and or elasticity of the hose. The influence of the air on the density is taken into account by using the combined bulk modulus $E_m$ of the fluid and the entrained air in the density equation of state, equation A-18. The equation for the combined bulk modulus is [2]:

$$E_m = -\frac{V_{fl} + V_{air}}{\frac{dV_{fl}}{dp} + \frac{dv_{air}}{dp}} \tag{G-1}$$

The equation for the bulk modulus of the fluid alone is [2]:

$$E_{fl} = \frac{1}{\beta_{fl}} = -V_{fl,0}\left(\frac{dp}{dV_{fl}}\right)_T \tag{G-2}$$

The bulk modulus for oil and water is linearly dependent on the pressure up to pressure of approximately 700bar [2]. The fluid bulk modulus is then approximated by the following equation:

$$E_{fl} = E_0 + m_E p \tag{G-3}$$

With the equations G-2 and G-3 the fluid terms in equation G-1 are derived. Rewriting equation G-2 and integrating both sides gives:

$$\frac{1}{E_0}\int_{p_0}^{p} \frac{dp}{1 + \frac{m_E p}{E_0}} = \int_{V_{fl}}^{V_{fl,0}} -\frac{dV_{fl}}{v_{fl}} \tag{G-4}$$

Assuming a $p_0 = 0$, this gives:

$$\frac{1}{m} \ln \left(1 + \frac{m_E p}{E_0}\right) = -\ln V_{fl,0} + \ln V_{fl} \tag{G-5}$$

$$\ln \left(1 + \frac{m_E p}{E_0}\right)^{-\frac{1}{m_E}} = \ln \left(\frac{V_{fl}}{V_{fl,0}}\right) \tag{G-6}$$

$$V_{fl} = V_{fl,0} \left(1 + \frac{m_E p}{E_0}\right)^{-\frac{1}{m_E}} \tag{G-7}$$

The derivative of the fluid volume $dV_{fl}/dp$ is:

$$\frac{V_{fl}}{dp} = -\frac{V_{fl,0}}{E_0} \left(1 + \frac{m_E p}{E_0}\right)^{-\frac{1+m_E}{m_E}} \tag{G-8}$$

The entrained air is assumed to be an ideal gas that is compressed adiabatically ($n = 1.4$). This gives the following equation:

$$p V_{air}^n = p_0 V_{air,0}^n \tag{G-9}$$

From equation G-9 the air volume is determined:

$$V_{air} = \left(\frac{p_0}{p}\right)^{\frac{1}{n}} V_{air,0} \tag{G-10}$$

The derivative of the air volume $dV_{air}/dp$ is:

$$\frac{V_{air}}{dp} = -\frac{V_{air,0}}{n p_0} \left(\frac{p_0}{p}\right)^{\frac{n+1}{n}} \tag{G-11}$$

Filling in equations G-7, G-8, G-10 and G-11 into G-1 gives the final result for the combined bulk modulus of a fluid and air:

$$E_m = \frac{(1-\alpha)\left(1 + \left(\frac{m_E p}{E_0}\right)^{-\frac{1}{m_E}}\right) + \alpha \left(\frac{p_0}{p}\right)^{\frac{1}{n}}}{\frac{1}{E_e}(1-\alpha)\left(1 + \frac{m_E p}{E_0}\right)^{-\left(\frac{m+1}{m}\right)} + \frac{\alpha}{n p_0}\left(\frac{p_0}{p}\right)^{\frac{n+1}{n}}} \tag{G-12}$$

Where $\alpha$ is the relative amount of volume by air divided by the total fluid volume at the start before compression.

$$\alpha = \frac{V_{air,0}}{V_{air,0} + V_{fl,0}} \tag{G-13}$$

# Appendix H

# Volumetric Expansion Data Hose

The expansion data of the hoses used in the transmission are given in this appendix.

| | HOSE TRACTOR/2K | |
|---|---|---|
| | PRESSURE (bar) | VOLUMETRIC EXPANSION ($cm^3/m$) |
| DN 5 | 50 | 0,40 |
| | 415 | 1,85 |
| | 900 | 3,40 |
| DN 6 | 50 | 0,75 |
| | 400 | 2,40 |
| | 900 | 4,70 |
| DN 8 | 50 | 0,80 |
| | 350 | 3,05 |
| | 700 | 6,15 |
| DN 10 | 50 | 0,85 |
| | 330 | 3,20 |
| | 700 | 6,80 |
| DN 12 | 50 | 1,50 |
| | 275 | 4,85 |
| | 700 | 11,20 |
| DN 16 | 50 | 2,20 |
| | 250 | 7,15 |
| | 600 | 15,70 |
| DN 19 | 50 | 2,50 |
| | 215 | 8,20 |
| | 500 | 18,00 |
| DN 25 | 20 | 1,40 |
| | 165 | 11,95 |
| | 400 | 29,00 |

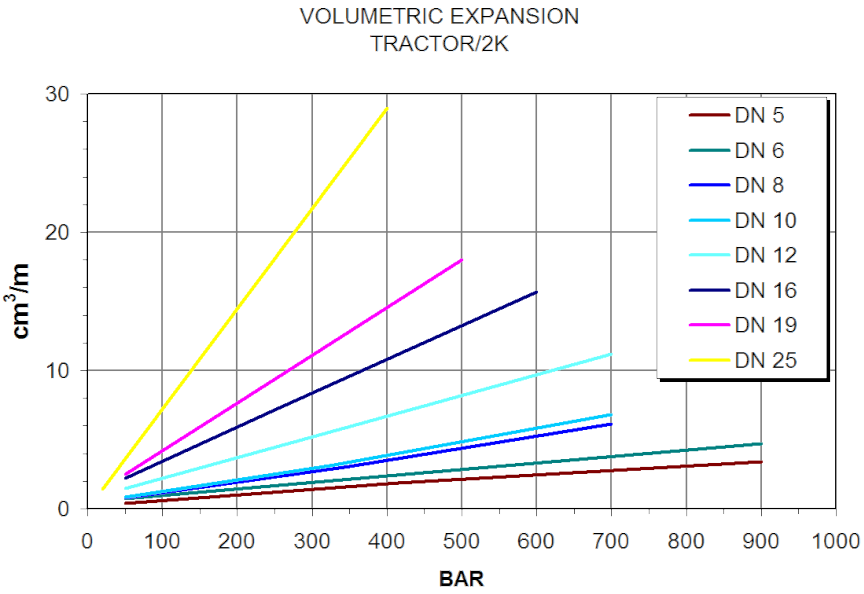


**Figure H-1:** Hose expansion data form manufacturer Manulli

# Appendix I

# Fluid Properties Biodegradable Oil HF-E 32

The fluid properties of the used oil HF-E 32 are derived with the tables and graphs of this appendix.

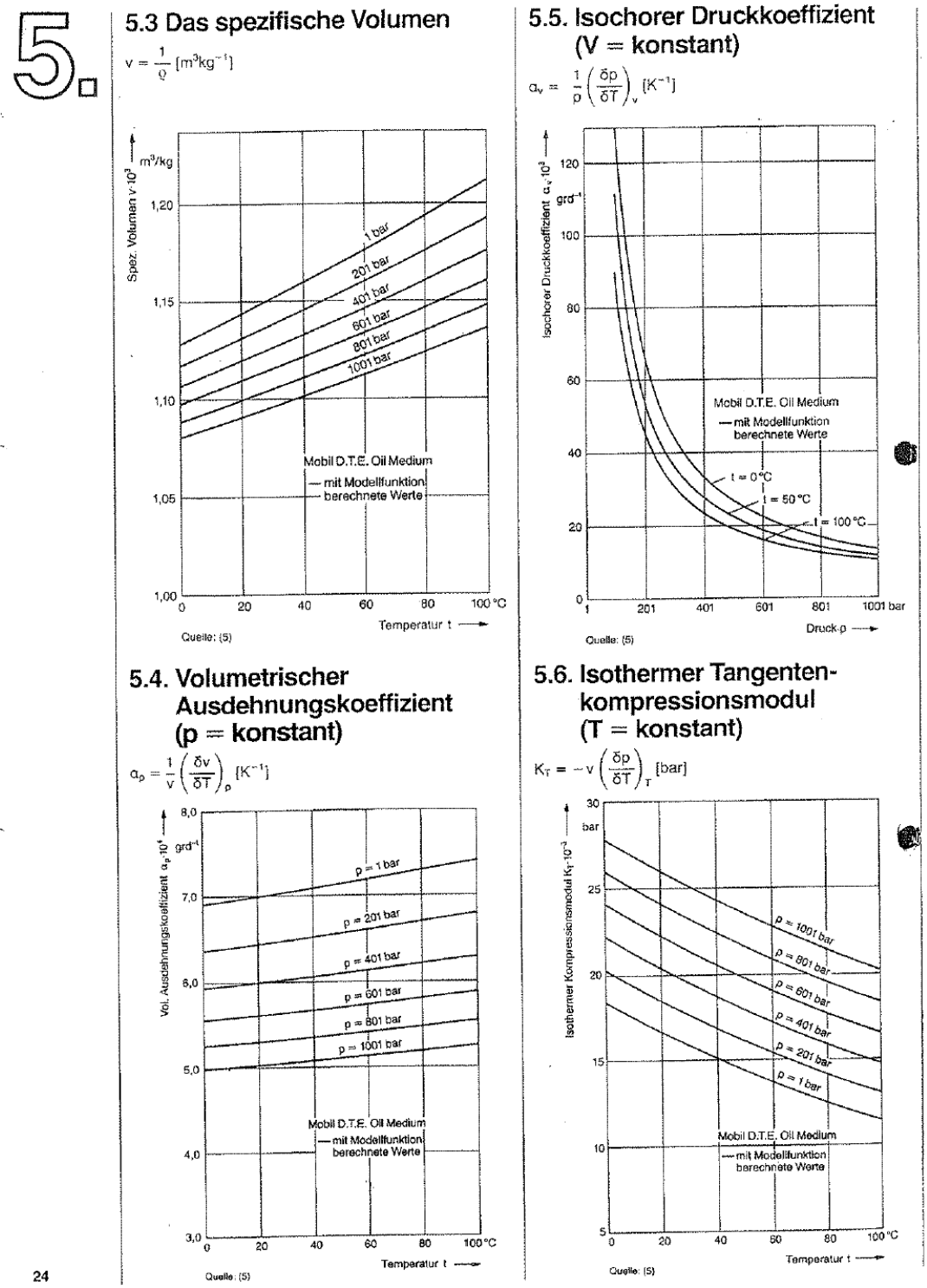


**Figure I-1:** Fluid property graphs of hydraulic oil HF-E 32

Tabelle1

**Kin.Viskosität (Vk)** [mm2 / s ]

| Temperatur | Shell Naturelle HFE 32 |
|---|---|
| -20 | 1202 |
| 0 | 245 |
| 20 | 76.6 |
| 40 | 32 |
| 100 | 6.2 |
| 150 | 2.8 |
| 200 | 1.62 |
| 250 | |
| 280 | |
| 300 | |
| 310 | |
| 340 | |

**Dichte (ρ)** [kg/m3]
ρx=ρ15-a(Tx-15) a~0,65

Konstant (a)= 0.65

| Temperatur | Shell Naturelle HFE 32 |
|---|---|
| ρ @ 15°C = | 917 |
| -20 | 940 |
| 0 | 927 |
| 20 | 914 |
| 40 | 901 |
| 100 | 862 |
| 150 | 829 |
| 200 | 797 |
| 250 | 764 |
| 280 | 745 |
| 300 | 732 |
| 310 | 725 |
| 340 | 706 |

**Spezifische Wärmekapazität (c)** [kJ/kg.K]
c=(0,402+0,00081xT)/ρ15 (wurzel)) x 4,187

| Temperatur | Shell Naturelle HFE 32 |
|---|---|
| -20 | 1.687 |
| 0 | 1.758 |
| 20 | 1.829 |
| 40 | 1.899 |
| 100 | 2.112 |
| 150 | 2.289 |
| 200 | 2.466 |
| 250 | 2.643 |
| 280 | 2.749 |
| 300 | 2.820 |
| 310 | 2.856 |
| 340 | 2.962 |

**Wärmeleitfähigkeit (l-lambda)**
l =( 0,101 - 0,000054 x T ) / d15 [kcal/m h K]
Umrechnung [kcal/m h K ] x 1.163 = [W / m K]
x 4,187 = [kJ / m h K]

Umr.faktor 1.163
4.187

| Temperatur | Shell Naturelle HFE 32 [W / m K] |
|---|---|
| -20 | 0.129 |
| 0 | 0.128 |
| 20 | 0.127 |
| 40 | 0.125 |
| 100 | 0.121 |
| 150 | 0.118 |
| 200 | 0.114 |
| 250 | 0.111 |
| 280 | 0.109 |
| 300 | 0.108 |
| 310 | 0.107 |
| 340 | 0.105 |

**Figure I-2:** Tables with the fluid property data of hydraulic oil HF-E 32

# Appendix J

# Water Pump Efficiency Manufacturer Data

The test data of the water pump is shown in this appendix. The only available test data was at 1500 rpm.

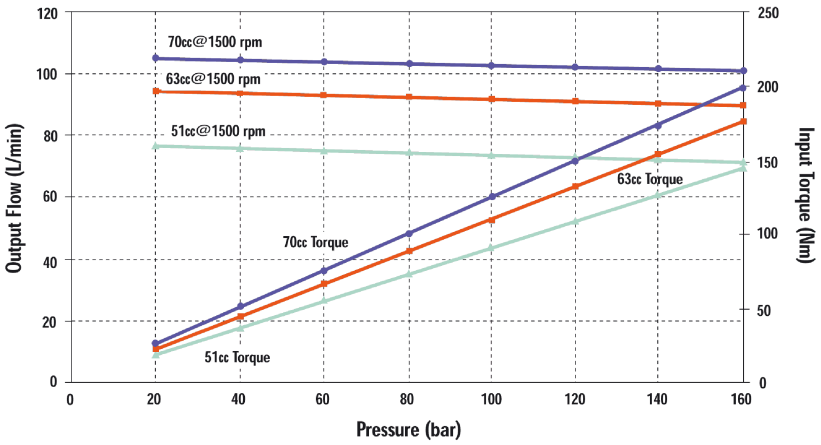


**Figure J-1:** Graph of the test data of the water pump at 1500 rpm, made available by Hydroton

From this graph supplied by the manufacturer the volumetric and mechanical efficiency is derived at 1500 rpm and a varying pressure.

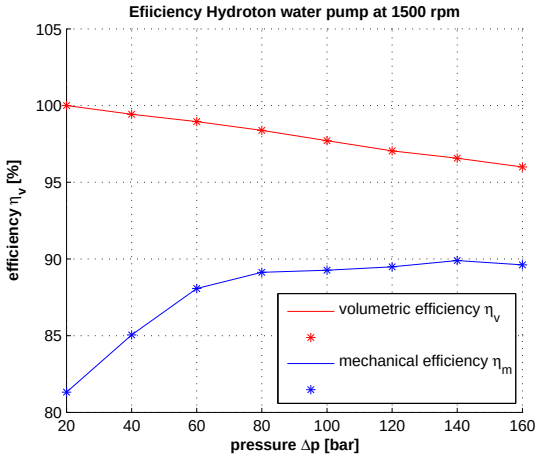


**Figure J-2:** Volumetric and mechanical efficiency as function of pressure at a constant 1500 rpm

# Glossary

## List of acronyms

| | |
|---|---|
| **DOT** | Delft Offshore Turbine |
| **ECN** | Energy research centre of The Netherlands |
| **DUWIND** | Delft University Wind Energy Research Institute |
| **CFD** | Computational Fluid Dynamics |

## List of symbols

| | | |
|---|---|---|
| $\alpha$ | Relative air volume at start compression | [-] |
| $\beta_e$ | Effective compressibility modulus | [$Pa^{-1}$] |
| $\beta_{fl}$ | Fluid compressibility modulus | [$Pa^{-1}$] |
| $\Delta p$ | Pressure difference | [Pa] |
| $\Delta p_f$ | Pressure loss due to fluid resistance | [Pa] |
| $\Delta p_{ft}$ | Total pressure loss due to fluid resistance | [Pa] |
| $\Delta p_1$ | Pressure difference oil circuit | [Pa] |
| $\Delta p_2$ | Pressure difference water circuit | [Pa] |
| $\gamma$ | Cubical expansion coefficient | [1/K] |
| $\varepsilon$ | Correction factor fluid inertia | [-] |
| $\eta_m$ | Mechanical efficiency | [-] |
| $\eta_{m1}$ | Mechanical efficiency oil pump | [-] |
| $\eta_{m2}$ | Mechanical efficiency oil motor | [-] |
| $\eta_{m3}$ | Mechanical efficiency water pump | [-] |
| $\eta_t$ | Total efficiency | [-] |
| $\eta_v$ | Volumetric efficiency | [-] |
| $\eta_{v1}$ | Volumetric efficiency oil pump | [-] |
| $\eta_{v2}$ | Volumetric efficiency oil motor | [-] |
| $\eta_{v3}$ | Volumetric efficiency water pump | [-] |
| $\lambda$ | Tip speed ratio rotor | [-] |
| $\lambda_{opt}$ | Optimal tip speed ratio rotor | [-] |

| | | |
|---|---|---|
| $\mu$ | Dynamic viscosity | [Pas] |
| $\nu$ | Kinematic viscosity | [$m^2$/s] |
| $\rho$ | Density water | [kg/$m^3$] |
| $\rho_a$ | Density air | [kg/$m^3$] |
| $\rho_0$ | Reference density | [kg/$m^3$] |
| $\tau$ | Torque | [Nm] |
| $\tau_1$ | Torque oil pump | [Nm] |
| $\tau_{ideal}$ | Ideal torque | [Nm] |
| $\tau_{lost}$ | Lost torque | [Nm] |
| $\omega$ | Rotational speed | [1/s] |
| $\omega_e$ | Rotational speed oil pump derived from elec freq | [rad/s] |
| $\omega_m$ | Rotational speed oil motor | [rad/s] |
| $\omega_n$ | Natural frequency | [rad/s] |
| $\omega_p$ | Rotational speed Pelton turbine | [rad/s] |
| $\omega_r$ | Rotational speed rotor | [rad/s] |
| $A$ | Cross section area | [$m^2$] |
| $A_{in}$ | Cross section area at inlet | [$m^2$] |
| $A_n$ | Cross section area nozzle | [$m^2$] |
| $A_{out}$ | Cross section area at outlet | [$m^2$] |
| $A_r$ | Rotor swept area | [$m^2$] |
| $B_b$ | Number of blades | [-] |
| $B_{syst}$ | Any fluid flow property (Reynolds transport theorem) | [-] |
| $C_c$ | Nozzle contraction coefficient | [-] |
| $C_d$ | Damping coefficient | [-] |
| $C_f$ | Friction coefficient | [-] |
| $C_h$ | Hydraulic capacitance | [$m^5$/N] |
| $C_m$ | Center of gravity blade | [m] |
| $C_s$ | Coefficient of slip | [-] |
| $C_{hp}$ | Pump hydraulic capacitance | [$m^5$/N] |
| $C_P$ | Power coefficient rotor | [-] |
| $C_{P,opt}$ | Optimal power coefficient rotor | [-] |
| $C_v$ | Nozzle velocity coefficient | [-] |
| $D$ | Diameter hose | [m] |
| $D_n$ | Nozzle diameter | [m] |
| $D_p$ | Pelton turbine diameter | [m] |
| $E$ | Energy | [J] |
| $E_0$ | Bulk modulus at 1 bar pressure | [Pa] |
| $E_e$ | Effective bulk modulus | [Pa] |
| $E_m$ | Combined bulk modulus of fluid and entrained air | [Pa] |
| $E_{fl}$ | Fluid bulk modulus | [Pa] |
| $E_h$ | Hose bulk modulus | [Pa] |
| $\hat{e}$ | Energy per unit mass | [J/kg] |
| $\hat{e}_{internal}$ | Internal energy per unit mass | [J/kg] |
| $\hat{e}_{kinetic}$ | Kinetic energy per unit mass | [J/kg] |
| $\hat{e}_{potential}$ | Potential energy per unit mass | [J/kg] |

| | | |
|---|---|---|
| $F$ | Force | [N] |
| $f$ | Darcy friction factor | [-] |
| $g$ | Gravity | [m/s$^2$] |
| $\hat{h}$ | Enthalpy per unit mass | [J/kg] |
| $I_f$ | Fluid inertia | [kg/m$^4$] |
| $I_{fc}$ | Corrected fluid Inertia | [kg/m$^4$] |
| $I_{hp}$ | Pump hydraulic inertia | [kg/m$^4$] |
| $J$ | Rotor rotational inertia | [kgm$^2$] |
| $J_p$ | Pump rotational inertia | [kgm$^2$] |
| $J_{shaft}$ | Shaft rotor rotational inertia | [kgm$^2$] |
| $K$ | Total loss due to fluid flow obstructions | [-] |
| $l$ | Length hose | [m] |
| $n$ | Adiabatic exponent | [-] |
| $m$ | Mass | [kg] |
| $m_{blade}$ | Mass blade | [kg] |
| $m_E$ | Bulk modulus gain coefficient | [Pa$^{-1}$] |
| $P$ | Power | [W] |
| $P_{rotor}$ | Rotor power | [W] |
| $P_{rotor,rated}$ | Rotor power at rated wind speed | [W] |
| $p$ | Pressure | [Pa] |
| $p_1$ | Pressure in high pressure oil line | [Pa] |
| $p_2$ | Pressure in high pressure water line | [Pa] |
| $p_3$ | Pressure in low pressure oil line | [Pa] |
| $p_{in}$ | Pressure at inlet | [Pa] |
| $p_{out}$ | Pressure at outlet | [Pa] |
| $Q$ | Volume flow | [m$^3$/s] |
| $Q_h$ | Heat | [J] |
| $Q_{ideal}$ | Ideal volume flow pump | [m$^3$/s] |
| $Q_{in}$ | Volume flow at inlet | [m$^3$/s] |
| $Q_{lost}$ | Lost volume flow pump | [m$^3$/s] |
| $Q_{out}$ | Volume flow at outlet | [m$^3$/s] |
| $R$ | Rotor radius | [m] |
| $R_{ed}$ | Reynolds number | [-] |
| $R_h$ | Outer radius hose | [m] |
| $R_{fh}$ | Hydraulic resistance element | [kg/sm$^4$] |
| $R_{mv}$ | Volumetric motor resistance | [sm$^4$/kg] |
| $R_{mm1}$ | Mechanical motor resistance caused by damping coeff | [kgm$^2$/s] |
| $R_{mm2}$ | Mechanical motor resistance caused by slip coeff | [m$^3$/rad] |
| $R_{pv}$ | Volumetric pump resistance | [sm$^4$/kg] |
| $R_{pm1}$ | Mechanical pump resistance caused by damping coeff | [kgm$^2$/s] |
| $R_{pm2}$ | Mechanical pump resistance caused by slip coeff | [m$^3$/rad] |
| $r_h$ | Radius hose | [m] |
| $T$ | Temperature | [K] |
| $T_1$ | Temperature in high pressure oil line | [K] |
| $T_2$ | Temperature in high pressure water line | [K] |
| $T_1$ | Temperature in low pressure oil line | [K] |

| | | |
|---|---|---|
| $t$ | Time | [s] |
| $U$ | Average fluid velocity | [m/s] |
| $U_a$ | Wind velocity | [m/s] |
| $U_{jet}$ | Jet velocity | [m/s] |
| $U_n$ | Average velocity normal to control surface | [m/s] |
| $U_{rated}$ | Rated wind speed | [m/s] |
| $u$ | Velocity | [m/s] |
| $\hat{u}$ | Internal energy per unit mass | [J/kg] |
| $\hat{u}_{in}$ | Internal energy per unit mass | [J/kg] |
| $\hat{u}_{out}$ | Internal energy per unit mass | [J/kg] |
| $V$ | Volume | [$m^3$] |
| $V_{air}$ | Air volume | [$m^3$] |
| $V_{cv}$ | Control volume | [$m^3$] |
| $V_{cv_0}$ | Control volume at start point | [$m^3$] |
| $V_{fl}$ | Fluid volume | [$m^3$] |
| $V_g$ | Displacement pump/motor | [$m^3$/rad] |
| $V_{g0}$ | Pump/motor volume in cylinders before compression | [$m^3$] |
| $V_{g1}$ | Displacement oil pump | [$m^3$/rad] |
| $V_{g2}$ | Displacement oil motor | [$m^3$/rad] |
| $V_{g3}$ | Displacement water pump | [$m^3$/rad] |
| $V_0$ | Reference volume | [$m^3$] |
| $W$ | Work | [J] |
| $W_p$ | Pressure work | [J] |
| $W_s$ | Shaft work | [J] |
| $W_v$ | Viscous work | [J] |
| $z$ | height | [m] |